

THE FLOW ABOUT A SLENDER PROPELLOR-DRIVEN
BODY IN A TEMPERATURE STRATIFIED FLUID/

by

Thomas Franklin Swean, Jr.

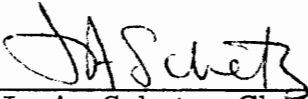
Dissertation submitted to the Graduate Faculty of the
Virginia Polytechnic Institute and State University
in partial fulfillment of the requirements for the degree of

DOCTOR OF PHILOSOPHY


in

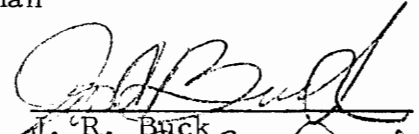
Aerospace and Ocean Engineering

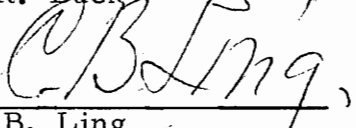
APPROVED:


J. A. Schetz, Chairman


A. K. Jakubowski


D. L. Dwoyer


J. R. Buck


C. B. Ling

April, 1977

Blacksburg, Virginia

LD
5655
V856
1977
S94
C.2

ACKNOWLEDGEMENTS

The author wishes to extend his gratitude to his advisor, Dr. Joseph A. Schetz, for his guidance and encouragement during the work described in this dissertation. Special thanks also go to Dr. Anthony K. Jakubowski, who gave much instruction and assistance during the turbulence measurements. Also acknowledged are Messrs. Wendell Brown, Harry Dawson, Frank Shelor, and Jake Frazier for their expert technical assistance with model and instrument design and development and with the testing facilities. Thanks also go to Messrs. Mike Long and Ray Walden for the drafting work contained herein, and also much gratitude is extended to Mrs. Sherry Butler for typing this manuscript. Last, but certainly not least, the author would like to thank, first, the Aerospace Department's secretary, Mrs. Pat Snider for her efforts in attending to the various special problems which arose during his graduate education and, second, his parents for their continued support.

TABLE OF CONTENTS

	Page
ACKNOWLEDGEMENTS	ii
NOMENCLATURE	v
LIST OF FIGURES	vii
I. INTRODUCTION	1
II. EXPERIMENTAL APPARATUS AND INSTRUMENTATION	6
Wind Tunnel Facility	6
Self-Propelled Model	6
Air Heating Apparatus	7
Wake Probes	9
Traverse Mount	9
Boundary Layer Probes	10
III. EXPERIMENTAL METHODS	11
Producing a Nearly Uniform Velocity, Temperature- Stratified Flow	11
Producing the Self-Propelled Condition	12
Boundary Layer Flow	12
Wake Flow	13
IV. RESULTS	18
Body Boundary Layer Measurements	18
Mean Wake Flow Measurements	20
Turbulence Measurements in The Wake	24
V. CONCLUSIONS AND RECOMMENDATIONS	29
REFERENCES	31
FIGURES	33

TABLE OF CONTENTS - CONTINUED

	Page
APPENDIX	82
VITA	106
ABSTRACT	107

NOMENCLATURE

A, B	RMS. voltage
E	D.C. voltage
f	temperature compensating term
FP	flow pitch angle
FY	flow yaw angle
K(FY)	probe coefficient for flow yaw
K(FP)	probe coefficient for flow pitch
K_i	hole coefficient
m_j	mass flow rate of jet
m_{tot}	total mass flow rate
P_B	barometric pressure
P_i	probe hole pressure
P_S	static pressure
$P_{S\infty}$	freestream static pressure
P_o	total pressure
q, Q	dynamic pressure
Re_D	Reynolds number based on model diameter
T_∞	freestream static temperature
T_i	temperature of injection
$\sqrt{T'^2}$	temperature fluctuation
u_∞	freestream velocity
u_z	axial velocity
u_j	velocity of jet

$\sqrt{u'^2}$ mean axial velocity fluctuation

$\overline{u'v'}$ radial shear stress

V_{total} total velocity

$\sqrt{v'^2}$ total velocity fluctuation

$\sqrt{v'^2}$ mean radial velocity fluctuation

X, Y, Z coordinate directions in wake

Y', Z' coordinate directions long body

ρ density

θ tangential coordinate

LIST OF FIGURES

Fig. No.		Page
1.	VPI&SU Stability Wind Tunnel	33
2.	Photographs of Model and Injector	34
3.	Model Dimensions	35
4.	Interior of the Self-Propelled Model	36
5.	Cutaway of Cylindrical Center Body	37
6.	Schematic of Test Section Arrangement	38
7.	Overall Dimensions of Injector	39
8.	Cutaway of Injector	40
9.	Heating Apparatus	41
10.	Yawhead Probe	42
11.	Pitot Rake	43
12.	Velocity and Temperature Profiles Upstream of Body	44
13.	Schematic of Coordinate Systems	45
14.	Schematic of Traverses Used for Wake Study	46
15.	Wake Coordinate System	47
16.	Sign Conventions	48
17.	Cross-Wire Probe	49
18.	Boundary Layer Velocity Profiles at Various Stations on the Body	50
19.	Temperature Profiles at Various Stations on the Body	51
20.	Flow Angularity, Mean Static Pressure, Mean Axial Velocity at $Z/D = 0.33$, $X = 0$, $\theta = 90^\circ$	52
21.	Flow Angularity, Mean Static Pressure, Mean Axial Velocity at $Z/D = 0.33$, $Y = 0$, $\theta = 0^\circ$	53

LIST OF FIGURES - CONTINUED

Fig. No.	Page
22. Flow Angularity, Mean Static Pressure, Mean Axial Velocity at $Z/D = 0.33$, $X=Y$, $\theta = 45^\circ$	54
23. Flow Angularity, Mean Static Pressure, Mean Axial Velocity at $Z/D = 1.0$, $X=0$, $\theta = 90^\circ$	55
24. Flow Angularity, Mean Static Pressure, Mean Axial Velocity at $Z/D = 1.0$, $Y=0$, $\theta = 0^\circ$	56
25. Flow Angularity, Mean Static Pressure, Mean Axial Velocity at $Z/D = 1.0$, $X=Y$, $\theta = 45^\circ$	57
26. Flow Angularity, Mean Static Pressure, Mean Axial Velocity at $Z/D = 2.0$, $X=0$, $\theta = 90^\circ$	58
27. Flow Angularity, Mean Static Pressure, Mean Axial Velocity at $Z/D = 2.0$, $Y=0$, $\theta = 0^\circ$	59
28. Flow Angularity, Mean Static Pressure, Mean Axial Velocity at $Z/D = 2.0$, $Y=X$, $\theta = 45^\circ$	60
29. Flow Angularity, Mean Static Pressure, Mean Axial Velocity at $Z/D = 3.0$, $X=0$, $\theta = 90^\circ$	61
30. Flow Angularity, Mean Static Pressure, Mean Axial Velocity at $Z/D = 3.0$, $Y=0$, $\theta = 0^\circ$	62
31. Flow Angularity, Mean Static Pressure, Mean Axial Velocity at $Z/D = 3.0$, $Y=X$, $\theta = 45^\circ$	63
32. Flow Angularity, Mean Static Pressure, Mean Axial Velocity at $Z/D = 4.0$, $X=0$, $\theta = 90^\circ$	64
33. Flow Angularity, Mean Static Pressure, Mean Axial Velocity at $Z/D = 4.0$, $Y=0$, $\theta = 0^\circ$	65
34. Flow Angularity, Mean Static Pressure, Mean Axial Velocity at $Z/D = 4.0$, $Y=X$, $\theta = 45^\circ$	66
35. Temperature Distributions in the Wake at $Z/D = 0.33$	67
36. Temperature Distributions in the Wake at $Z/D = 1.0$	68
37. Temperature Distributions in the Wake at $Z/D = 2.0$	69
38. Temperature Distributions in the Wake at $Z/D = 3.0$	70

LIST OF FIGURES - CONTINUED

Fig. No.	Page
39. Temperature Distributions in the Wake at $Z/D = 4.0$	71
40. Axial and Radial Turbulence Intensity Distributions at $Z/D = 0.33, X=0, \theta = 90^\circ$	72
41. Axial and Radial Turbulence Intensity Distributions at $Z/D = 0.33, Y=0, \theta = 0^\circ$	73
42. Axial and Radial Turbulence Intensity Distributions at $Z/D = 0.33, Y=X, \theta = 45^\circ$	74
43. Radial Shear Stress Distributions at $Z/D = 0.33$	75
44. Axial and Radial Turbulence Intensity Distribution at $Z/D = 4.0,$ $X=0, \theta = 0^\circ$	76
45. Axial and Radial Turbulence Intensity Distribution at $Z/D = 4.0,$ $Y=0, \theta = 45^\circ$	77
46. Axial and Radial Turbulence Intensity Distribution at $Z/D = 4.0,$ $Y=X, \theta = 45^\circ$	78
47. Radial Shear Stress Distributions at $Z/D = 4.0$	79
48. Temperature Fluctuation Distribution at $Z/D = 0.33$	80
49. Temperature Fluctuation Distribution at $Z/D = 4.0$	81

I. INTRODUCTION

The turbulent wake produced by a body in a fluid stream has long been a subject of interest in fluid mechanics. In more recent years, with the increased concern for maintaining the natural ecological system of checks and balances, this topic has acquired added impact. With a thorough understanding of wake development and subsequent dissipation, the problem of dispersion and control of dispersion of pollutants from aircraft and water vehicle propulsion units can better be approached. Experimental studies of the turbulent wake are also of interest for testing theories on turbulent modelling.

Unfortunately, as is evident from Table I, most of the previous experimental studies have dealt with relatively simple bodies such as circular disks, ellipsoids, spheroids, and some slender bodies. Generally these studies have been restricted to the unpropelled or "drag-body" situation. In fact, most estimates of the wake development behind self-propelled bodies have been based on the experiments of Naudascher [1] in which the momentumless condition was established with a circular disk and a central jet providing the necessary thrust to balance the drag of the disk. Later, Gran [2] investigated the momentumless wake behind a self-propelled Rankine ovoid at $Re_D \approx 6 \times 10^4$. Until recently the above were the only two self-propelled configurations which had been examined and the utility of these results are limited because of impractical body shapes or low Reynolds numbers, or both. More extensive work was published in 1974 by Swanson [3], et.al., and Chieng [4], et. al., at $Re_D \approx 6.18 \times 10^5$.

TABLE I

Summary of Subsonic, Axisymmetric Turbulent Wake Experiments

Author	Year	Ref. No.	Momentumless	Mean Flow	Turbulent Properties	Configuration
Hall and Hislop	1938	10		X		1 x 2 Cylinder
Cooper and Lutzky	1955	11		X	X	Thin Disks
Ilizarova and Pochkina	1962	12		X		6.67 x 1 Body of Revolution
Ridjanovic	1963	13	X	X	X	Circular Disk
Carmody	1964	14		X	X	Circular Disk
Wang	1965	15	X	X	X	Circular Disk
Naudascher	1965	1	X	X	X	Circular Disk
Ginevskii, Pochkina, and Ukhanova	1966	16	X	X	X	Circular Disk
Buchinskaya and Pochkina	1966	17		X		6 x 1 Ellipsoid
Chevray	1968	18		X	X	6 x 1 Spheroid
Bukreev, Kostomakha, and Lytkin	1972	19		X	X	Slender Body (8:1 Pro- longation)

TABLE I (Continued)

Summary of Subsonic, Axisymmetric Turbulent Wake Experiments

Author	Year	Ref. No.	Momentumless	Mean Flow	Turbulent Properties	Configuration
Hokenson and Schetz	1973	20		X	X	Sphere
Bukreev, Kostomakha, and Lytkin	1974	21		X	X	Sphere and Slender Body
Gran	1974	2	X	X	X	Rankine Ovoid
Swanson, Chieng et al	1974	3, 4	X	X	X	Slender Bodies
Daffan	1976	5	X	X	X	Slender Body
Schetz, et al	1976	6	X	X	X	Slender Body

These studies provide a systematic comparison of the turbulent wakes behind slender bodies with identical forebody shape by varying through the following cases: 1) Pure drag body, 2) self-propelled by axial fluid injection, 3) self-propelled with a well designed propellor. Daffan [5] extended the work of Swanson and Chieng on the propellor-driven configuration by studying the effect on the wake of a sail-type appendage to the formerly axisymmetric body and also the effect of nonzero pitch angles (0° to -2°). Schetz [6], et.al., studied the effect of replacing the single propellor by an equivalent set of side-by-side counter rotating propellers. Additionally, Schetz conducted measurements of the aero-hydrodynamic forces and movements on propellor-driven slender bodies, and boundary layer measurements on the body itself.

It is evident that the work reported in Refs. No. [3], [4], [5], and [6] has contributed greatly to the better understanding of the phenomena associated with the turbulent wakes produced by self-propelled bodies of practical configurations. The present investigation was designed to study the development of the mean wake flow using the fluid temperature as a tracer and to document the turbulent fluctuations including those of temperature. The stratification of the temperature field remains sufficiently small that bouyancy effects are negligible.

The testing was conducted in the VPI 6' x 6', subsonic wind tunnel at $Re_D \approx 2.04 \times 10^5$. The approaching mean velocity and temperature fields were measured with a pitot-static tube and a thermocouple.

Mean boundary layer measurements were made at several stations along

the body with a "rake" of small pitot tubes for the velocity field and a small thermocouple for the temperature field. The mean velocity and temperature fields in the near wake were measured with a yawhead probe and a thermocouple respectively. From the yawhead probe the flow angularity could also be determined. Measurements of axial and radial turbulence intensities, radial shear stress, and temperature fluctuations were taken using cross-wire and straight hot-wire probes.

In order to achieve a temperature stratified flow, an air injection and heating system was designed and built. The primary design criterion of the heating/injection arrangement was to produce in the wind tunnel main stream a slug of relatively high temperature air while at the same time disturbing the normal dynamic pressure field as little as possible.

This report is arranged into several major sections. First, the apparatus, models, and experimental methods are described in detail. The results are presented in separate sections, starting with the boundary layer data. The next subsections in the RESULTS section deal with the mean wake flow and finally the turbulence measurements in the near wake are reported. The results are presented in graphical and tabulated form in Appendices at the rear of this report.

II. EXPERIMENTAL APPARATUS AND INSTRUMENTATION

Wind Tunnel Facility

All tests were conducted in the VPI & SU 6' x 6' subsonic stability tunnel (Fig.No.1) at a dynamic pressure of 1.0 in. of water (approximately 68 ft/sec) corresponding to a Re_D based on diameter of 2.04×10^5 . This facility is a continuous, closed jet, single return, wind tunnel. The test section is 28 ft. long which is sufficient, with the model located near the center of the section, to allow measurements in the near wake. The airstream has a low turbulence intensity factor of 1.08. To control the tunnel velocity a Barocel Electronic Manometer is used to read dynamic pressure from a pitot-static tube mounted on the test section wall out of the wake of the model. Static free-stream pressure is measured by a Validyne digital barometer Model DB99.

Self-Propelled Model

The model considered in this investigation has an overall length of 72 in. and a maximum diameter of 6 in., giving a fineness ratio of 12:1. The model was strut mounted from the floor of the wind tunnel in the center of the test section (Fig.No. 2). The forebody is parabolic and machined from laminated layers of plexiglass. The center-body is an aluminum cylindrical tube. The tail body is also plexiglass machined into an ogival shape. The overall dimensions of the body are shown in Fig. No. (3).

The model used a 2.75 hp. DC motor to direct drive the single propellor shaft which extended thru the center of the tail section

(Fig. No. 4). A 6 in. diameter, 4 in. pitch three-bladed model airplane propeller, Tornado Model, manufactured by Griggs Bros. was used to provide sufficient thrust to obtain the self-propelled condition.

To avoid overheating in long duration experiments, the motor was enclosed by copper tubing to allow for water cooling. The water cooling was not used for the short duration test necessary to determine the required propeller speed to produce the momentumless condition since the motion of the cooling water and the connecting tubing could affect this determination. The "sail-drag" is included in determining this condition. In order to measure the drag forces on the body and subsequently measure the thrust necessary to exactly counteract these forces, a strain gage balance (Fig. No. 5) was internally mounted in the model. To power the DC motor, a Sorenson 150v, 15a power supply was used.

Air Heating Apparatus

The stratification of the approaching airstream was induced by injecting heated air at the freestream velocity upstream of the self-propelled model. A schematic of the test section arrangement including the injection and self-propelled model is shown in Fig. No. (6). For this purpose an injector was constructed with the overall dimensions shown in Fig. No. (7). The interior of the injector is shown in Fig. No. (8). Air enters the injector through the smaller 1 in. galvanized pipe and exits through 1/8 in. holes which are distributed

uniformly on the centerline along the span. Surrounding this pipe is a larger 2 in. galvanized pipe into which two rows of 1/2 in. holes are evenly distributed along the span. These holes are offset above and below the centerline by 45°. Downstream of the pipe assembly, there is a .035 in. stainless steel plate to help guide the exiting air and begin the flow straightening process. Immediately downstream of this plate, the injector is filled with 1/8 in. aluminum tubes of 1.25 in. length. These are held in place by a small box with sides and top constructed of .035 in. stainless steel. The upstream and downstream ends of the box are covered with .011 in. copper mesh. The mounting of the injector may be seen in Fig. No. (2). The basic ideas for the construction of the two-dimensional injector were obtained from Hokenson [9].

The injected air was supplied by four Ingersoll-Rand Type 90 compressors operating continuously. The compressed air fed into a Grove dome pressure regulator which controlled the mass flow rate. The heating was done electrically by 6 Plasmatron PS-20 transformers. The heating mechanism was as shown in Fig. No. (9). After leaving the regulator the air was guided into two lengths of Inconel 601 1-1/4 in. diam., 1/4 in. wall pipe. The Plasmatrons were connected to the upstream and downstream ends of the pipes thus forming a parallel electric circuit. To minimize the heat loss to the atmosphere, the entire piping system from the upstream end of the heating circuit to the injector was covered by 1-1/4 in. Kay-Lo Owens-Corning insulation.

Wake Probes

The mean flow pressure measurements in the wake were taken using a three-dimensional yawhead probe constructed by United Sensor (Fig. No. 10). The output from the pressure probe was measured on a Barocel electronic manometer and displayed on a Doris digital voltmeter. To read all five pressure points for the yawhead probe on the manometer, a Scanivalve Model W0601/IP-RT fluid switch wafer with solenoid drive was used. The mean temperature field was measured by means of an Omega SCASS-062G-6 thermocouple. The output was fed into a Consolidated Controls Type K digital indication voltmeter and read directly in °F.

The axial and radial turbulence and radial shear stress data were obtained using a cross-wire probe (TSI Model 1241T1.5). The probe was operated at an overheat ratio of 1.8 using a constant temperature anemometer module (TSI Model 1050) and a power supply and monitor (TSI Model 1051-6). Readings were taken from a DISA 55D35 RMS meter. A Model 1015C correlator and TSI Model 1076 voltmeter were also used. Temperature fluctuations in the wake were measured using a straight hot wire (TSI Model 1210). This probe was operated at a low overheat ratio of 1.05 in order to more accurately measure the temperature fluctuations.

Traverse Mount

The traverse mount had a vertical movement of 4 ft. and a horizontal movement of 11 in. Both vertical and horizontal movement was accomplished with variable speed motors which were remote-controlled from outside the test section. The probe position was monitored using

a series of potentiometers.

Boundary Layer Probes

The pitot rake (Fig.No. 11) was developed by Nerney [7] and was approximately 1.5 in. high with one static port and 24 total pressure tubes at increasing distances up the rake. This allowed for more data points in the wall region. The temperature field near the body was measured by means of an Omega SCASS-062G-6 thermocouple suspended vertically from the traverse mount. The thermocouple could then be withdrawn to any desired distance from the body.

III. EXPERIMENTAL METHODS

Producing a Nearly Uniform Velocity, Temperature-Stratified Flow

Initially, the primary consideration was to define the control settings which would allow a nearly uniform velocity distribution downstream of the injector while maintaining $(T_i - T_\infty)$ as large as possible. This was accomplished in the following sequence. The Plasmatrons were activated at the highest setting which they could safely support. The compressors were then activated and allowed to run continuously forcing the air thru the heating system and thru the injector. The tunnel was operated at the test condition of 1.0 in. H_2O dynamic pressure (approximately 68 ft/sec). The injector exit temperature was monitored by a thermocouple located .5 in. from the exit. After about 20 minutes, this temperature would stabilize, indicating the steady-state condition had been reached. At this time temperature and pressure scans were taken at a station 16 in. upstream of the submarine body. The velocity defect or overshoot was observed and appropriate adjustments were then made to the pressure regulator ahead of the heating system. By trial and error, the proper control settings were determined to be as follows: The compressors were operated continuously between 120-130 psig. The regulator was set to maintain a 60 psig. exit pressure. The large pressure difference between the incoming flow to the regulator and the exiting flow was necessary to help facilitate a constant flow through the regulator. The plasmatrons were operated at 1740a and 20v. These settings resulted in nearly uniform velocity profiles and substantial temperature nonuniformity at

the test station ahead of the submarine body. They corresponded to a U_i/U_∞ of approximately 1.3 and a $T_i - T_\infty$ of approximately 150°F. Typical velocity and temperature profiles at the station 16 in. upstream of the submarine body are shown in Fig. No. (12). Note the greatly exaggerated scale for velocity variations. Precise lateral uniformity from the injector proved to be difficult to obtain. The basic magnitudes of the velocity and temperature profiles were laterally fairly uniform but the local maximums were often at different locations along the Y-axis. This "undesigned" characteristic of the injector proved to be helpful, however, in tracing the wake flow.

Producing the Self-Propelled Condition

To determine a self-propelled configuration, a strain gage balance was internally mounted in the model (Fig.No.5). With the model mounted in the tunnel, potentiometers were used to zero the output from the balance due to the weight of the model. The injector was operated and the free-stream velocity was increased to 1.0 in. H₂O while the axial force was monitored. The propellor rpm was then increased until the axial force reading was zero. It was determined that a propellor rpm of 12987 was needed to achieve the self-propelled status. This corresponds to advance-diameter ratio $\left(\frac{U_\infty}{ND}\right)$ of 0.628.

Boundary Layer Flow

Measurements were made with the pitot rake and the thermocouple at $Z'/D = 2.67, 4.67, 6.67, 8.67, \text{ and } 10.0$. The data were reduced using the Bernoulli equation, the local pitot pressure, and the local static

temperature obtained from the thermocouple. The local static pressure was determined by lowering a small pitot-static tube to a point 0.25 in. from the body and not from the static tube on the rake. The boundary layer measurements were made on the side away from the sail. The coordinate system used for these measurements is illustrated in Fig. No. (13).

Wake Flow

The mean flow velocity as well as the flow angularity were determined using a five-port yawhead probe. This probe was calibrated over a range of flow pitch and yaw angles between -30° and $+30^\circ$ by Daffan [5].

It was decided that an adequate description of the wake could be achieved with three traverses which are shown in Fig. No. (14). The three traverses were made at downstream stations of $Z/D = 0.33, 1.0, 2.0, 3.0$ and 4.0 . The coordinate system for the wake study is illustrated in Figs. No. (13) and (15).

To obtain the mean velocity components from the pressure measurements the following equation for total pressure was used:

$$P_0 = P_S + 1/2\rho V^2 + 1/2\rho \overline{v'^2}$$

where V is the mean total velocity and $\overline{v'^2}$ is the sum of the mean fluctuations. Since $V^2 \gg \overline{v'^2}$ the $1/2\rho \overline{v'^2}$ term was neglected. The yawhead probe gave direct readings of $P_1 - P_{S_\infty}$, where P_1 is the mean total pressure and P_{S_∞} is the free-stream static pressure. Therefore since

$$P_1 = P_S + 1/2\rho V^2$$

the mean total velocity can be calculated from

$$V_{\text{TOTAL}} = \sqrt{\frac{2 [(P_1 - P_{S\infty}) - (P_S - P_{S\infty})]}{\rho}}$$

The mean axial velocity can be obtained by

$$U_Z = V \cos(\text{FP}) \cos(\text{FY})$$

where FP is the flow pitch angle and FY is the flow yaw angle. Similarly the other velocity components are given by,

$$U_X = V \cos(\text{FP}) \sin(\text{FY})$$

$$U_Y = V \sin(\text{FP})$$

To obtain the local static pressure from the yawhead probe a method described by Winternitz [8] was used. Since this method is only good for substantial flow angularity in one direction, calibration curves were used for both pitch and yaw. The flow yaw angle FY is found from the calibration probe constant

$$K_{\text{FY}} = \frac{P_3 - P_2}{P_1 - P_4}$$

for each station. Defining the hole constant as

$$K_i(\text{FY}) = \frac{P_i - P_S}{q}$$

where P_i is the hole pressure and q is the dynamic pressure, Winternitz showed that

$$q = \frac{(P_1 - P_{S\infty}) - (P_2 - P_{S\infty})}{K_1 - K_2}$$

or

$$(P_S - P_{S\infty}) = (P_2 - P_{S\infty}) - qK_2$$

Therefore

$$(P_S - P_S) = \frac{K_1 (P_2 - P_{S\infty}) - K_2 (P_1 - P_{S\infty})}{K_1 - K_2}$$

Similarly for the pitched case where the yaw angles are small

$$K_{FP} = \frac{P_4 - P_5}{P_1 - P_2}$$

and,

$$P_S - P_{S\infty} = \frac{K_1 (P_S - P_{S\infty}) - K_5 (P_1 - P_{S\infty})}{K_1 - K_5}$$

From these relations, the local static pressure could be determined when there were substantial pitch angles with small yaw angles or for large yaw angles with small pitch angles. Figure (16) is an illustration of the sign conventions used for measuring pitch and yaw.

Mean temperature measurements were taken in the wake by using a thermocouple and making the identical traverses at each downstream location behind the propellor. Temperature was read directly in °F on a digital voltmeter.

The axial and radial turbulence intensities and radial shear stress were measured at $Z/D = 0.33$ and $Z/D = 4.0$. These traverses were made at each station as was done in the mean flow study. The cross-wire probe was operated at a high overheat ratio of 1.8 in order to decrease the temperature sensitivity. Initially the probe was calibrated by orienting one of the sensors parallel to the flow direction and

subjecting the probe to two different flow conditions (motionless air and air moving at 98.4 ft/sec). The probe was then rotated 90° to align the other sensor and the process was repeated. Temperature was recorded for each situation.

Figure (17) shows the two-sensor orientation. With this arrangement the turbulence in two perpendicular directions and the directional correlation (Reynolds stress) can be measured. Assuming that the effective cooling velocity follows a sine law and that the two sensors are 45° to the mean flow, their output voltages are related by:

$$A = S_A (U + V)$$

$$B = S_B (U - V)$$

where S = proportionality constant, A and B are output voltages. If the two signals are adjusted so that $S_A = S_B = S$ (during calibration) then:

$$\sqrt{\overline{u'^2}} = \frac{f}{2S} \sqrt{(\overline{A + B})^2}$$

$$\sqrt{\overline{v'^2}} = \frac{f}{2S} \sqrt{(\overline{A - B})^2}$$

$$\overline{u'v'} = \frac{f^2}{4S^2} (\overline{A^2} - \overline{B^2})$$

where f appears as a temperature compensating factor which corrects for temperature variations. For the measurements of this experiment the calibration constants were determined as follows:

$$S = .0718$$

$$f = \sqrt{\frac{396.8 - T}{347.8}}$$

where $T = ^\circ\text{F}$.

Temperature fluctuation measurements were made using a straight-wire probe at a low overheat ratio of 1.05 to minimize velocity sensitivity and maximize temperature sensitivity. The probe was calibrated by immersing the hot wire into first an ice bath and second into boiling water. The output was adjusted so that the measured voltage was 0v at 32°F and 10v at 212°F . Output voltage varies linearly with temperature between these extremes. The probe was then mounted on the traverse and the wake traverses were repeated at $Z/D = 0.33$ and $Z/D = 4.0$.

IV. RESULTS

The experimental results obtained during this research are presented in Figs. No. (18) - (49) in the form of velocity and temperature profiles for each station examined along the body. Figures (20) - (34) are graphs of the distribution of flow angle, mean static pressure, and axial velocity for each station examined in the wake. Figures (35) - (39) are graphs of the mean temperature distribution at each of these stations. Figures (40) - (49) are graphs of the axial and radial turbulence intensity, radial shear stress, and temperature fluctuation distributions at $Z/D = 0.33$ and $Z/D = 4.0$. The results are also presented in tabular form in Tables A-1 thru A-14.

The turbulence data were not corrected for the effect of flow angularity and the mean flow data were not corrected for the effect of turbulent fluctuations. The latter approximation is valid to a high degree of accuracy due to the relatively small turbulence levels in most of the wake region. Jakubowski (23) has found in recent tests that the error induced by not correcting the data for flow angle variations is less than 7% in general for the flow angles encountered in this research. Following is a discussion of the results of the current research.

Body Boundary Layer Measurements

The boundary layer development along the body was examined in order to trace the temperature distribution in the longitudinal direction and subsequently more accurately determine the effects of the propellor on the initial flow field. In Fig. No. (18) are plotted the boundary layer velocity data, non-dimensionalized by U_∞ , for $Z'/D = 2.67, 4.67,$

6.67, 8.67, and 10.0. These data are very similar to those first reported in Ref. No. (6). They show a normal boundary layer growth with increasing downstream distance. The slope of the profiles near the wall tends to indicate a developing turbulent boundary layer. An examination of the boundary layer thickness at stations $Z'/D = 6.67$, 8.67, and 10.0 shows that $\delta(x) \sim x^{.8}$ as would be the case for a turbulent boundary layer. Turbulence measurements were not made in the boundary layer due to lack of instrumentation for that task. These data were collected with the submarine in the self-propelled mode and the effects of the propeller on the development of the boundary layer were not studied since Schetz (6) has determined that the prop has little or no effect until $Z'/D > 11$.

Figure No. (19) contains the temperature distributions near the body at streamwise stations corresponding to those of Fig. No. (18). First it should be noted that these distributions are not graphs of the thermal boundary layer but rather that the thermal boundary layer is contained within the variable temperature region. The Prandtl number, which is the connecting link between the velocity and temperature fields, is near unity for air which indicates that the velocity and temperature boundary layers should have nearly equivalent dimensions. The temperature varies over a normal distance of nearly double that of the velocity boundary layer. This is simply a result of the initial injection geometry and subsequent spreading of the jet. The development of the thermal boundary layer can be qualitatively examined by focusing attention on the region nearest the wall. Note that these profiles resemble classical insulated wall thermal boundary layers. The regions wherein

$dT/dy \approx 0$ can be seen to grow very distinctly with increasing Z'/D to the point that the size of the region at $Z'/D = 10.0$ is nearly twice that at station $Z'/D = 4.67$. This is essentially identical to the behavior of the velocity profiles of Fig. No. (18). The thickening of the overall layer is also evident in Fig. No. (19), but the growth due to the proximity of the body and the normal growth rate of the jet cannot be quantitatively separated.

Figure No. (19) also demonstrates the overall cooling of the high temperature layer with increasing streamwise distance. This energy is lost to the free stream and manifests itself as a general overall heating of the entire wind tunnel fluid. Typically during a test program lasting 30 minutes, the free stream temperature would increase by 1° to 2°F . The fact that the mass flow of the jet was very small compared to the total mass flow ($\frac{m_j}{m_{\text{tot}}} \approx .01$) and the presence of air coolers in the wind tunnel circuit kept the overall heating rate very low.

Mean Wake Flow Measurements

Figures No. (20) - (34) are graphical presentations of the mean static pressure, mean axial velocity, and flow angularity distributions in the near wake at stations $Z/D = 0.33, 1.0, 2.0, 3.0,$ and 4.0 . At each station results are presented along three distinct traverses, vertical, horizontal, and $\theta = 45^\circ$. The coordinate systems and sign conventions used are shown in Figs. No. (13) - (16).

In general from an overall examination of these data, one sees the initial momentum excess and defect regions spread in extent but decrease in magnitude with increasing Z/D . Similar behavior is exhibited by the

propellor swirl and static pressure variations. Along a vertical traverse the flow is pitched very slightly and the yaw angles are larger. The converse is true along the horizontal traverse. Maximum flow angles vary from approximately 10° at $Z/D = 0.33$ to about 5° at $Z/D = 4.0$. Results along the $\theta = 45^\circ$ traverses show that in this plane flow pitch and flow yaw are about equally present. Some small asymmetry of the results is evident. This is due to a combination of circumstances which cause the flow to deviate slightly from axisymmetric: the presence of the sail, the vertical and lateral gradients in the injected jet, and the small errors in alignment which occur in positioning the model. Basically the behavior of the flow is similar to that reported by Daffan [5]. The magnitude of the momentum excess and defect and the other associated properties of the wake structure are smaller due to the lower Reynolds number and corresponding lower propellor rpm of this study. One noticeable departure from the results of Ref. No. (5) is the appearance of another momentum defect region in the near wake. At every station there is the maximum defect in the wake center. Passing the center there is a region of momentum excess, characterized, for instance, by the axial velocity overshoot. Continuing into the outboard portion of the wake there is invariably another region of velocity defect which is smaller in both magnitude and extent. Actually this behavior is predicted by simple propellor theory and is discussed in Ref. No. (24).

Of particular interest are the results in Figs. No. (35) - (39). These are graphs of the temperature distribution in the wake at the identical stations used in obtaining the mean pressure data. At each

station the three traverses were made, first with the prop not rotating and second at the rpm necessary to achieve the self-propelled condition. In the former circumstance, the prop was rotated by hand before the traverse was made and positioned where it would not interfere with the flow.

The results at station $Z/D = 0.33$ (Fig. No. (35)) are typical of each station if viewed singly. The initial temperature distribution without the influence of the propeller can be easily seen. The vertical variation is quite pronounced with peak temperatures of approximately $16^\circ - 20^\circ$ greater than T_∞ . Ideally the temperature variation along the horizontal traverse should be zero, however variations up to 5°F are observed. This is largely due to the lateral gradients which were present initially in the injected jet and to a lesser degree due to distortion produced by the body. The local temperature maximums at each lateral location along the jet injector were very nearly the same, however, the vertical location of these maximums (i.e., the vertical temperature distribution) would vary somewhat laterally. Rotating the propeller has the effect of mixing the flow to some extent. Regions where the temperature was higher tend to decrease in temperature and vice-versa. As Z/D increases, these data indicate an overall rotation of the flow. This is most evident from the vertical and horizontal traverses of Figs. No. (35) - (39). Before activation of the propeller, the highest temperature levels in the wake of the body are located along the x-axis near $x = 1.0$ in. Examination of the temperature field with the propeller running shows that these higher levels of temperature are beginning to appear along the y-axis at $y = -1.5$ in. further downstream at $Z/D = 4.0$.

Similarly the temperature levels along the x-axis drop considerably to levels that are consistent with those that existed near $y = 1.0$ in. before prop activation.

Consider for a moment the fluid particles that existed at $x_0 = 1.0$ in. and $y_0 = 0.00$ in. at time $t = t_0$. The fluid state of those particles is determined by the data illustrated in Figs. No. (21) and (35). As has been pointed out, the temperature distributions of Figs. No. (35) - (39) tend to indicate that they have moved to $x_1 \approx 0.0$ in and $y_1 \approx -1.5$ in. during the time $t_1 - t_0$ necessary for them to negotiate 22.0 in. along the longitudinal axis. If this is in fact the case, calculations based on the mean pressure data of Figs. (21) - (35) should predict this rotation and translation. Unfortunately, the coarse "grid size" employed for the data collection prevents an exact analysis of the path of a particular streamline, but by taking the fluid state as it existed at station $Z/D = 0.33$ and assuming that all gradients of the fluid properties are zero, one can approximately predict the location of these particles at time $t_1 - t_0$. Carrying out the indicated calculations the results are,

$$U_y = -7.25 \text{ ft/sec}$$

$$U_x = -1.20 \text{ ft/sec}$$

$$t_1 - t_0 = 0.026 \text{ sec}$$

$$y_1 - y_0 = -1.5 \text{ in}$$

$$x_1 - x_0 = -0.382 \text{ in}$$

The results of the approximate calculations indicate that these particles would move in pitch more than is observed and move in yaw less than is observed. The direction of rotation is, of course, the same as that

observed (counter-clockwise looking upstream). The discrepancies between the calculations and the observed results are due to the assumption of zero gradients in the flow properties. In fact as the fluid particles move from the +x axis to the -y axis, the pitch angles become smaller and the yaw angles become larger. This would result in a fluid element moving more in yaw and less in pitch than is crudely predicted by assuming $\frac{\partial U_x}{\partial z}, \frac{\partial U_y}{\partial z} = 0$.

The propellor seems to act more as a "swirl inducer" than a "mixer" in this near wake region. This is supported by the data in that the levels of the maximum temperature observed do not fall rapidly with distance downstream. If a severe mixing action were occurring, one would expect a nearly uniform temperature to appear at these downstream locations. That this is not the case indicates that there is a more or less fixed fluid element rotation occurring. Future wake models should account for this behavior.

Turbulence Measurements in the Wake

Turbulence measurements were performed in the near wake at stations $Z/D = 0.33$ and 4.0 . At each station axial and radial turbulence intensities, radial shear stress, and temperature fluctuations were recorded. Figures No. (41) - (47) are graphs of the axial and radial turbulence intensities at these stations.

Before discussing these data a condition that existed which is detrimental to the accurate measurement with a hot-wire should be pointed out. The injected air had a small oil content which was present because of leaky compressors. Examination of the hot-wire instruments after the

tests revealed that small amounts of oil were deposited on the wires. It is probable that the electrical and thermal properties of the wires were changed somewhat by this deposit. Accordingly, the absolute levels of the reported fluctuations could be somewhat in error. Several measurements were, however, duplicated at different times and with widely varying conditions such as compressor run-time (and thus oil vapor accumulation) and the data were seen to agree within 10%. This would indicate that the error due to the oil deposit is minimal. Figures No. (40) - (42) show that the axial velocity fluctuations are high (nearly 10% of the free stream velocity) at the center of the wake. This is at variance with the data reported in Ref. No. (22) which show a minimum at this point. The fluctuations decrease rapidly followed by another peak which occurs in the vicinity of the propellor tips. This is identical to the trend of the data in the above reference. At $Z/D = 4.0$, Figs. No. (44) - (46) show generally the same distribution although the maximum intensities in the wake center have fallen to about half their former values. The axial turbulence intensity in the area of the propellor tips for the vertical traverse of Fig. No. (44) has not declined nearly so much. The radial turbulence intensity along all three traverses at $Z/D = 0.33$ has the same distribution, with the maximums at the center of wake and at the propellor tips. However, at $Z/D = 4.0$ the radial velocity fluctuation has fallen to 1 - 2% of the free stream velocity near the tips. The fluctuations along the center of the wake remain relatively high at 3 - 5%.

Figures No. (43) and (47) are graphs of the radial shear stress at stations $Z/D = 0.33$ and 4.0 respectively. During this point of the

experimental program there were equipment problems with the correlator. Consequently, there were several points at which the shear stress could not be determined. The data that were able to be obtained indicate that the highest values of the shear stress occur in the vicinity of high velocity gradients which is to be expected. The maximum values of the shear stress do not decrease greatly from $Z/D = 0.33$ to 4.0.

Figure No. (48) is a graph of the temperature fluctuation at $Z/D = 0.33$. These results show that the fluctuations are uniformly very small ($< .5\%$ of T_∞) along any traverse until the edge of the wake is approached. The temperature fluctuations in this region are a maximum of approximately 10.5% along the horizontal and $\theta = 45^\circ$ traverses and a comparatively large 14% along the vertical axis. Comparison with the data of Fig. No. (49) shows the same behavior. Maximums of $\sqrt{T'^2}/T_\infty$ are reduced to less than 10% along the horizontal and $\theta = 45^\circ$ traverses and to about 13% along the vertical traverse. Again the levels along the vertical axis in the vicinity of the propellor tips are much larger. The results in Figs. No. (35) and (39) show that the mean temperatures are higher in the vicinity of the center of the wake and much smaller at the edge. The turbulence results indicate that the maximum temperature fluctuations are occurring in a region of relatively low mean temperature gradients. This is an important result when it is considered in the light of current popular techniques used in the theoretical study of the compressible turbulent boundary layer. During the course of such a study, at some point it becomes necessary to depart from the exactness of the Navier-Stokes equations and model various terms containing the fluctuating components of density, velocity and temperature. An example of such a

term, for example, is the turbulent heat flux

$$q_i \equiv C_{pp} \overline{U_i' T'}$$

where the subscript $i = 1, 2, 3$ denotes the coordinate direction. The usual practice is to model the $\overline{U_i' T'}$ term as

$$\overline{U_i' T'} \sim - \frac{\partial T'}{\partial X_i}$$

From this model, one would expect a larger $\sqrt{T'^2} / T_\infty$ in the interior of the wake where $\frac{\partial T}{\partial y}$ is larger and comparatively smaller fluctuations in the outboard region. The experimental results of this study do not confirm such a model. There is however some indication that $\sqrt{T'^2}$ has dependence on $\frac{\partial T}{\partial X_i}$. The data of $Z/D = 0.33$ and $Z/D = 4.0$ (Figs. No. (48) and (49)) show larger fluctuations in the tip area along the y axis than in the tip areas along the $\theta = 45^\circ$ traverse and x axis. The gradients in the mean temperature are larger in the tip region along the y axis.

The question of why the temperature fluctuations are concentrated only in the tip regions is a difficult one to answer. On the surface, it is tempting to answer that the fluctuations are directly associated with the vortices which are shed at the tips. Indeed, a common assumption of blade element theory to calculate propellor performance is to assume that the circulation is constant along the blade and consequently vortices are shed only at the root and the tips. Close examination of Figs. No. (48) and (49) show that the temperature fluctuations do tend to rise at the wake center in the vicinity of the roots of the propellor blades. However, the strength of circulation does vary along a propellor

blade. In fact, it can be proved that the condition of constant circulation along the blade length is physically impossible (e.g., see Ref. No. (24)). This means that vortices are necessarily shed along the entire span so the high temperature fluctuations at the tips cannot be explained solely by vortex shedding. The tip vortices will, however, be of greater strength and correspondingly higher turbulence levels should be expected.

Another possibility is the effect of compressibility. The tip speeds associated with this experiment are approximately 400 ft/sec ($M = 0.35$). Although this is below $M = 0.5$, the value of Mach number above which compressibility effects are normally considered to be important, it is sufficiently high that some measureable compressibility effects should be expected. There is the additional possibility that the higher temperature fluctuations at the tips are the result of eddies being convected along the span of the blade and finally being shed at the tips. This would happen if the flow is separating as it moves over the airfoil surface. If this were the case, a corresponding loss of thrust should be apparent. In fact, the angular velocities which were determined experimentally to be necessary to produce the self-propelled condition are higher than was anticipated based upon the experiments of Swanson (3) and Daffan (5).

V. CONCLUSIONS AND RECOMMENDATIONS

An experimental study of the flow field produced by a self-propelled, slender body of revolution in a temperature stratified airstream has been conducted. The experiments concentrated mainly on the mean and turbulent flow in the near-wake region although mean boundary layer measurements were taken in order to establish the initial conditions immediately upstream of the propellor.

The mean flow results have shown that the temperature stratifications, as produced in this experiment, has no large, noticeable effect on the development of the mean flow in the near wake. The temperature results show that the fluid undergoes more of a rotation in this near-wake region and is mixed to a lesser extent.

The turbulence measurements strongly reinforce recent findings that the highest levels of axial turbulence intensity are to be found in the immediate vicinity of the propellor tips. Additionally the current results indicate that higher levels of turbulence than previously found are present in the wake center. These centerline fluctuations appear to decay at a faster rate than do the turbulence intensities at the outboard edge. They are possibly only a phenomenon peculiar to the near-body region. The radial turbulence intensities are also unusually high at the wake center. In fact, in this case, the magnitudes along the centerline are higher than those near the propellor tips at the most distant downstream station studied. The turbulent fluctuations in temperature quite emphatically point out the unsteadiness of the flow in the outer regions of the wake. For the conditions

of this experiment, this was a vicinity of only small to moderate gradients in mean temperature. Temperature fluctuations in the wake in areas other than the vicinity of the propellor tips are quite small.

This experimental program has pointed out the relative ease with which measurements of mean temperature and temperature fluctuations can be made. It proved to be simpler to use the straight hot-wire in the low overheat mode to measure the temperature fluctuations than to gather the velocity fluctuation data with the cross-wire. Additionally, the measurement of mean temperature data with a thermocouple is very rapid and uncomplicated. Accordingly, it is suggested that future experimental programs not hesitate to gather these data in any situation where temperature fluctuations may be an element in question, however small. The results suggest some interesting points for further study. The influence of different initial mean temperature distributions should be determined. The temperature fluctuation distribution in the vicinity of the propellor tips is quite pronounced and it would be interesting to see the effect of different initial temperature gradients and their location relative to the propellor geometry. Second, the turbulent thermal boundary layer should be considered since the incoming turbulence levels should have some effect on the wake development. Third, but only incidentally associated with the current subject area, the problem of high temperature jet injection into a co-flowing stream should be considered.

REFERENCES

1. Naudascher, E., "Flow in the Wake of a Self-Propelled Body and Related Sources of Turbulence", *Journal of Fluid Mechanics*, Vol. 22, 1965, pp. 625-656.
2. Gran, R. L., "An Experiment on the Wake of a Slender Propeller-Driven Body", TRW Report 20086-6006-RU-80.
3. Swanson, R. C., Jr., Schetz, J. A., Jakubowski, A. K., "Turbulent Wake Behind Slender Bodies Including Self-Propelled Configurations", VPI-AERO-024, 1974. (Available thru D.D.C.)
4. Chieng, C. C., Jakubowski, A. K., Schetz, J. A., "Investigation of the Turbulent Properties of the Wake Behind Self-Propelled Axisymmetric Bodies", VPI-AERO-025, 1974. (Available thru D.D.C.)
5. Daffan, E. B., "Mean Flow and Trubulence Measurements in the Wake of a Slender Propeller-Driven Body Including Effects of Pitch Angle", M.S. Thesis, 1976, Virginia Polytechnic Institute and State University, Blacksburg, Virginia.
6. Schetz, J. A., Daffan, E. B., Jakubowski, A. K., Cannon, S., Cox, R., and Dubberley, D., "Mean Flow and Turbulence Measurements in the Wake of Slender Propeller-Driven Bodies Including Effects of Pitch Angle", VPI-AERO-050, 1976.
7. Nerney, B. E., "An Experimental Study of Mass Transer Effects on Turbulent Flows Along Surfaces", M.S. Thesis, 1976, Virginia Polytechnic Institute and State University, Blacksburg, Virginia.
8. Winternitz, F. A. L., "Probe Measurements in Three-Dimensional Flow", *Aircraft Engineering*, August 1956, p. 273.
9. Hokenson, G. J., "Incompressible Free Trubulent Mixing in Axial Pressure Gradients", Ph.D. Dissertation, 1970, University of Maryland, College Park, Maryland.
10. Hall, A. A. and Hislop, G. S., "Velocity and Temperature Distributions in the Wake Behind a Heated Body of Revolution", *Proc. Comb. Phil. Soc.* 34, 1938.
11. Cooper, R. D. and Lutzky, M., "Exploratory Investigation of the Turbulent Wakes Behind Bluff Bodies", DTMB R4D Rept. No. 953, October 1955.
12. Ilizorova, L. I. and Pochkina, K. A., "Experimental Study of a Wake Behind a Body of Revolution", *Prom. Aerodynamika*, No. 23, 1962.

13. Ridjanovic, M., "Wake With Zero Change of Momentum Flux", Ph.D. Dissertation, 1963, University of Iowa, Iowa City, Iowa.
14. Carmody, Thomas, "Establishment of the Wake Behind a Disk", Journal of Basic Engineering-Transactions of the ASME, December 1964.
15. Wang, H., "Flow Behind a Point Source of Turbulence", Ph.D. Dissertation, 1963, University of Iowa, Iowa City, Iowa.
16. Ginevskii, A. S., Pochkina, K. A., and Ukhanova, L. N., "Propagation of Turbulent Jet Flow with Zero Excess Momentum", Fluid Dynamics Academy of Sciences USSR, Vol. 1, No. 6, November-December 1966, Faraday Press, Inc.
17. Buckinskaya, E. K. and Pochkina, K. A., "Investigation of Vortex Wake Behind a Body of Revolution", Prom. Aerodynamika No. 23, 1962.
18. Chevray, R., "The Turbulent Wake of a Body of Revolution", Journal of Basic Engineering-Transactions of the ASME, Series D, 1968.
19. Bukreev, V. I., Kostomakha, V. A., and Lytkin, Yu, "Axisymmetric Turbulent Wake Behind a Streamlined Body", Sibirskae, Otdeline An SSSR, Institut Gidrodinamiki, Dinamika Splashhoi Sredy, No. 10, 1972.
20. Hokenson, G. J. and Schetz, J. A., "Free Turbulent Mixing in Axial Pressure Gradients", Journal of Applied Mechanics, June 1973.
21. Bukreev, V. I., Kostomakha, V. A., and Lytkin, Yu, M., "Turbulent Energy Balance in Asixymmetric Wakes Behind Differently Shaped Bodies", Prikladnaya Mikhanika i Teknicheskaya Fizika, No. 1, 1974.
22. Schetz, J. A., Daffan, E. B., and Jakubowski, A. K., "The Turbulent Wake Behind Slender Propeller-Driven Bodies at Angle of Attack", AIAA Paper 77-133, AIAA 15th Aerospace Sciences Meeting, Los Angeles, California, January 1977.
23. Jakubowski, A. K., private communication, February 1977.
24. Durand, W. F., Aerodynamic Theory, Vol. IV, Dover Publications, Inc., New York, N.Y., Dover edition published 1963.

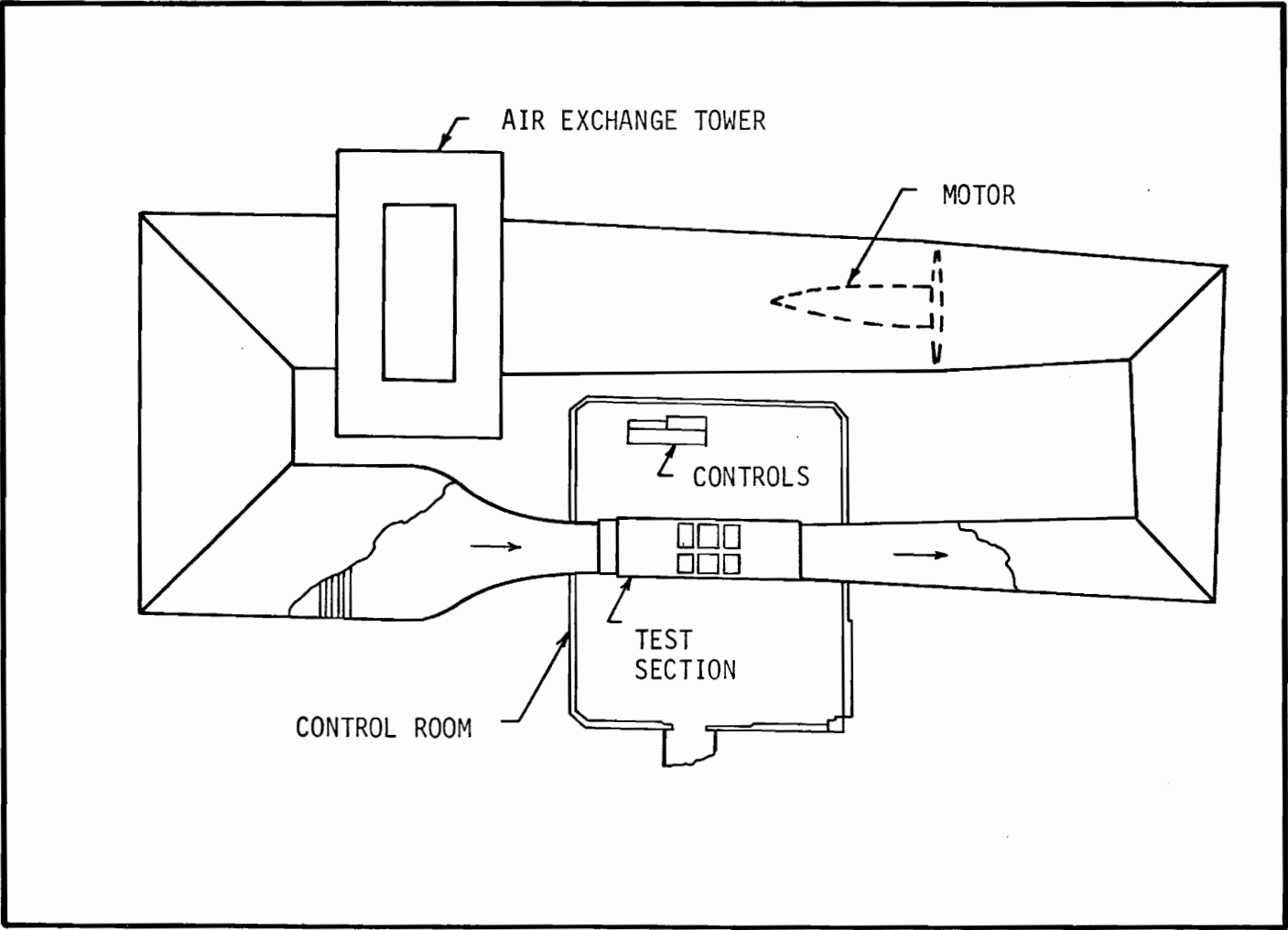


Figure 1

VPI & SU Stability Wind Tunnel

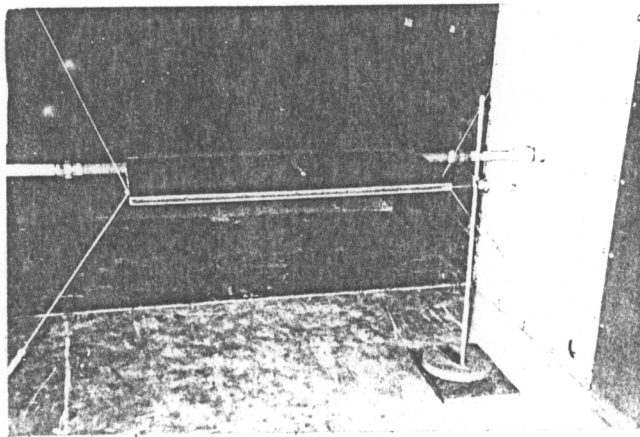
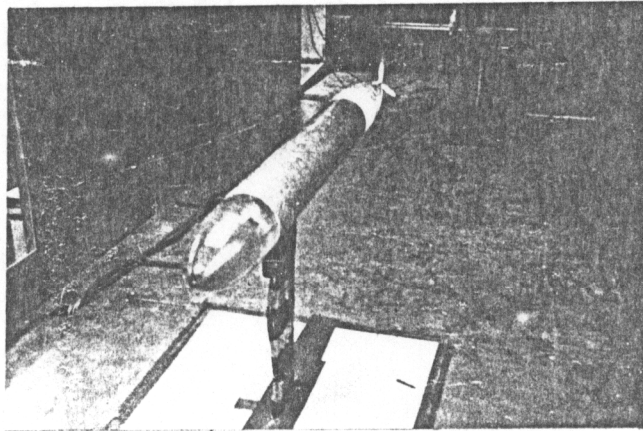
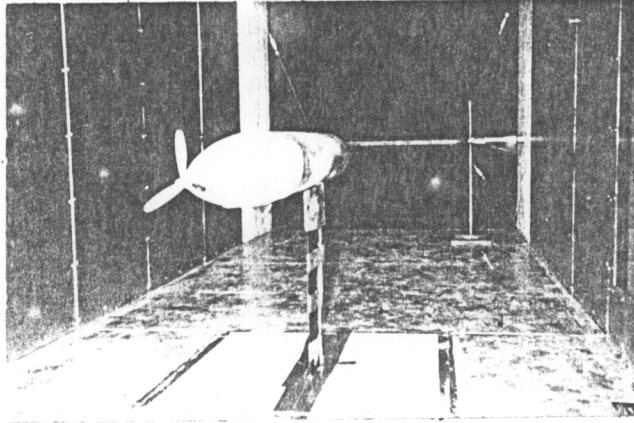


Fig. 2 Photographs of Model and Injector

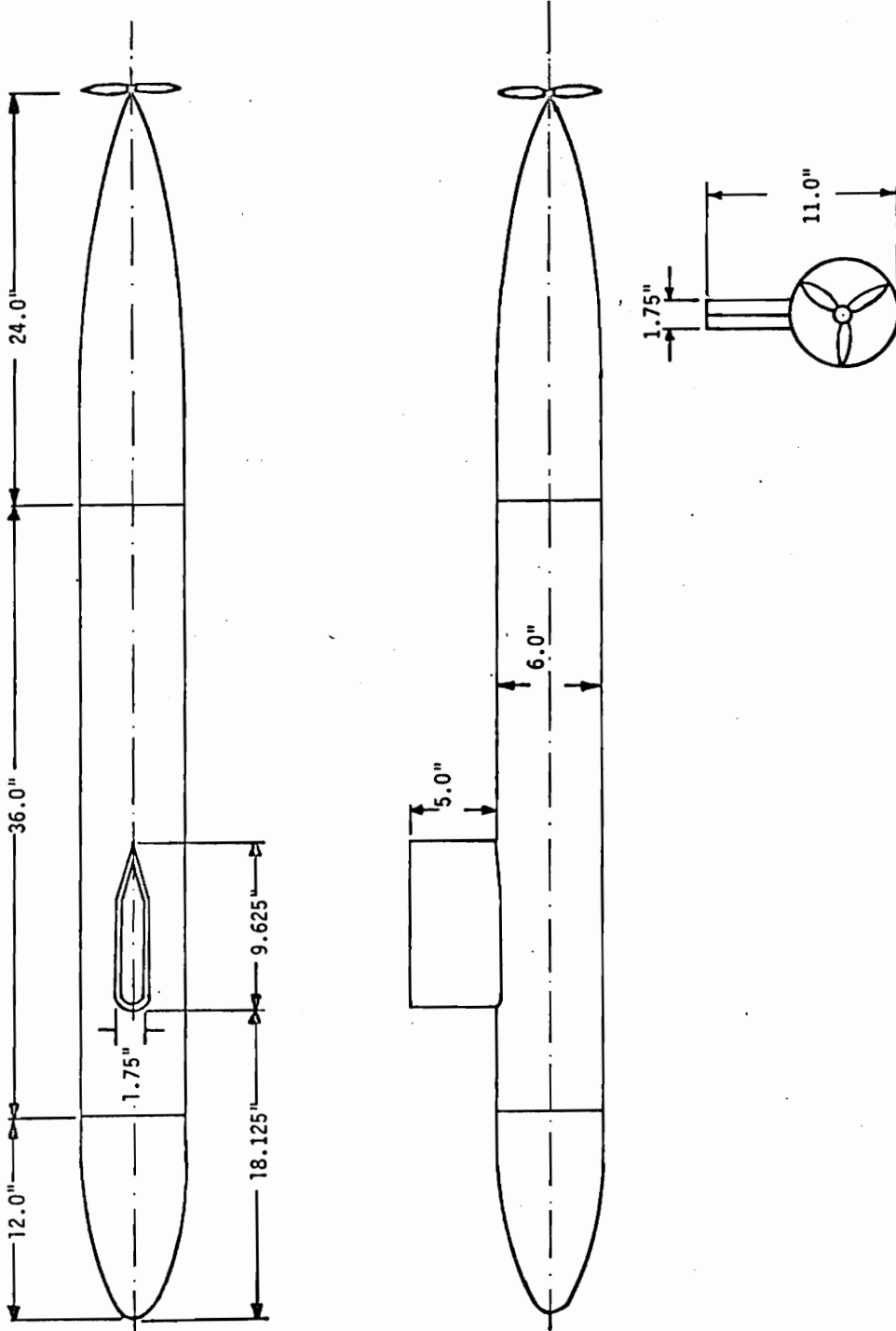


Fig. 3 Model Dimensions

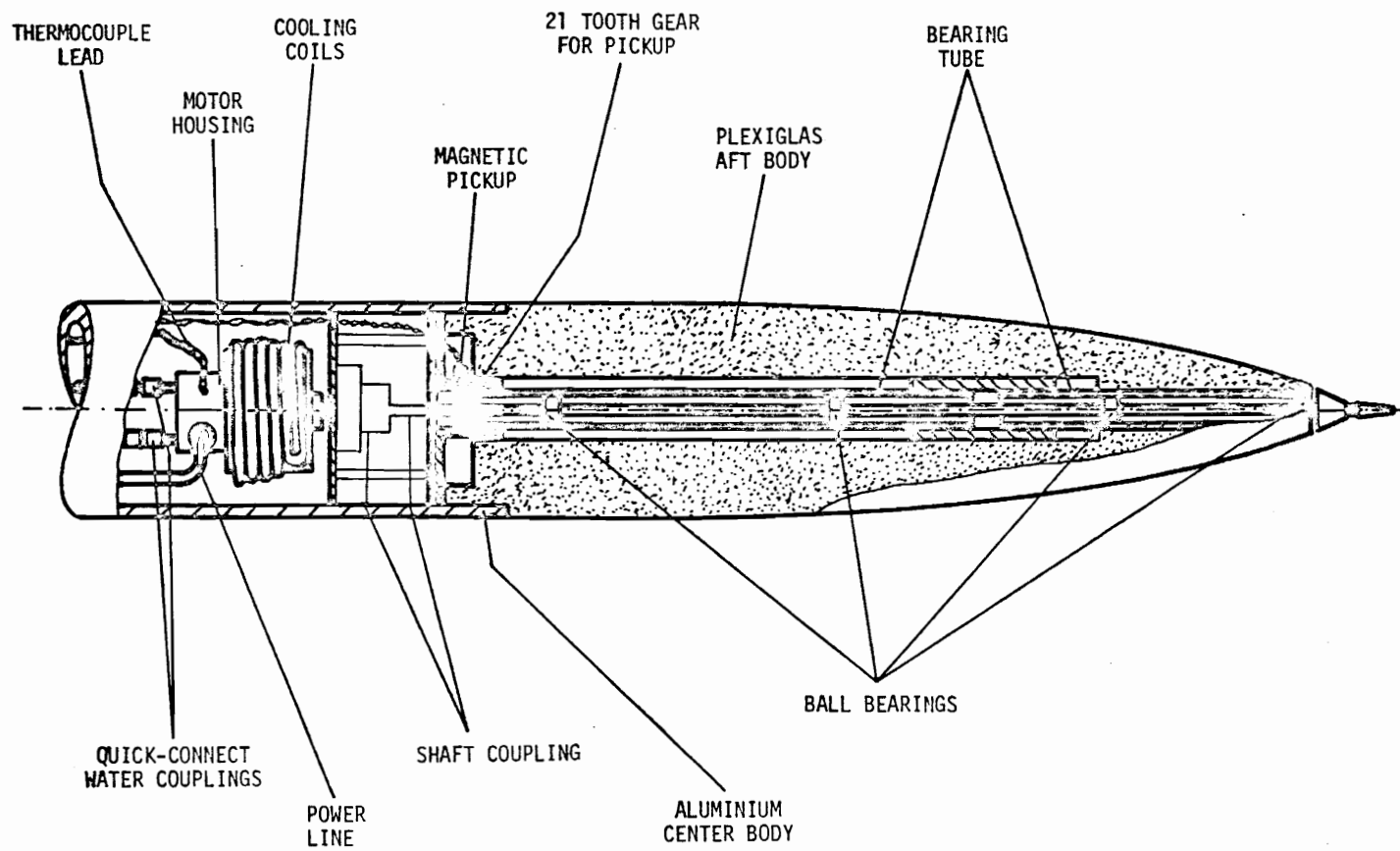


Fig. 4 Interior of Self-Propelled Model

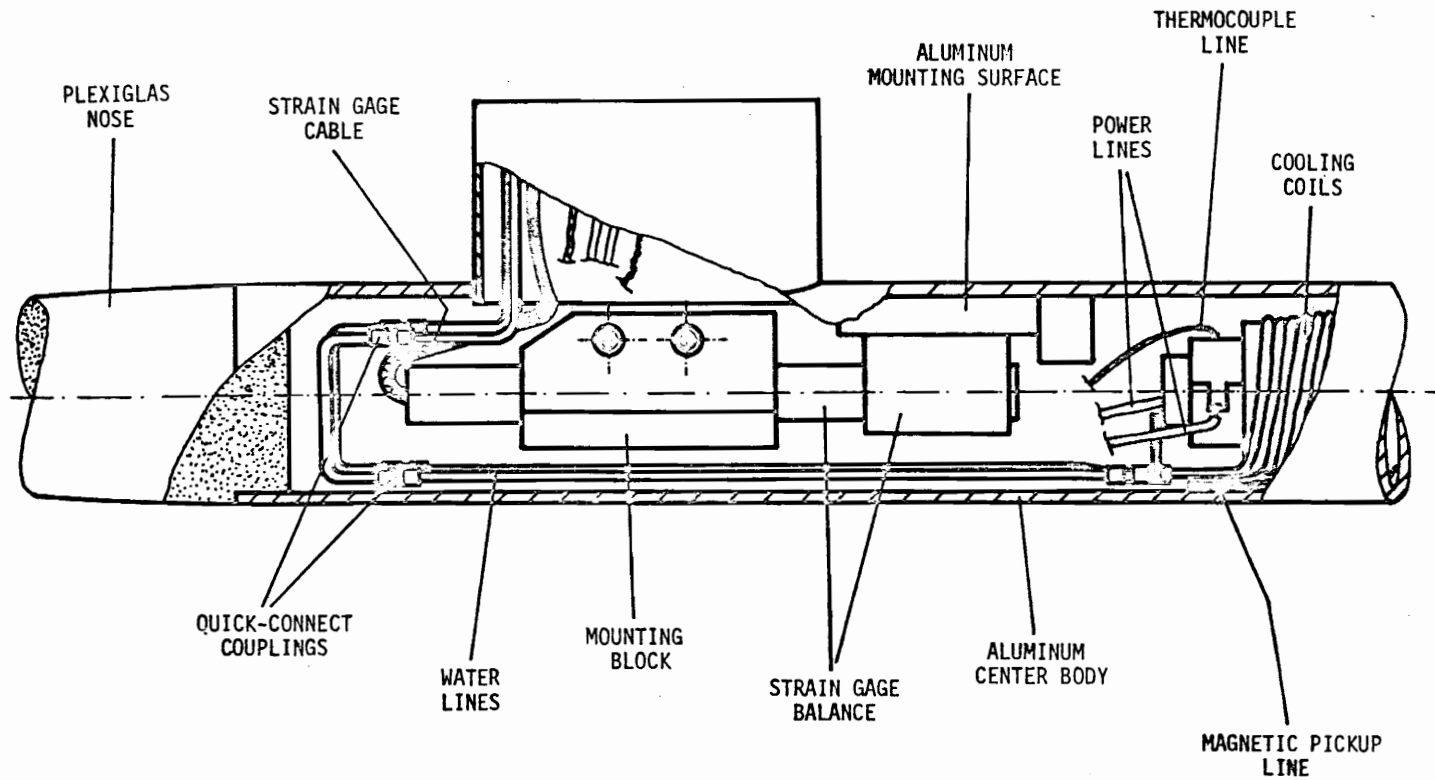


Fig. 5 Cutaway of Cylindrical Center Body
Showing Strain Gage Balance

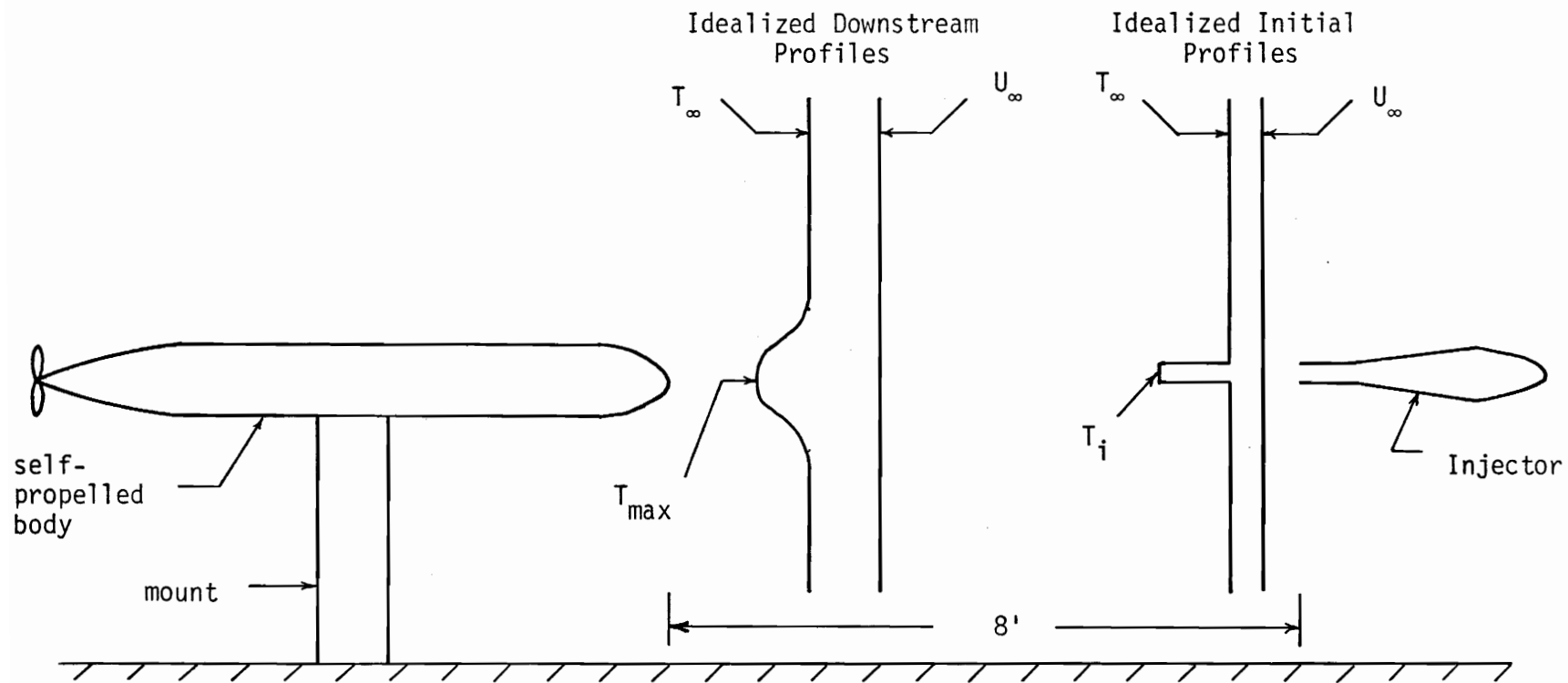


Figure 6

Schematic of Test Section Arrangement

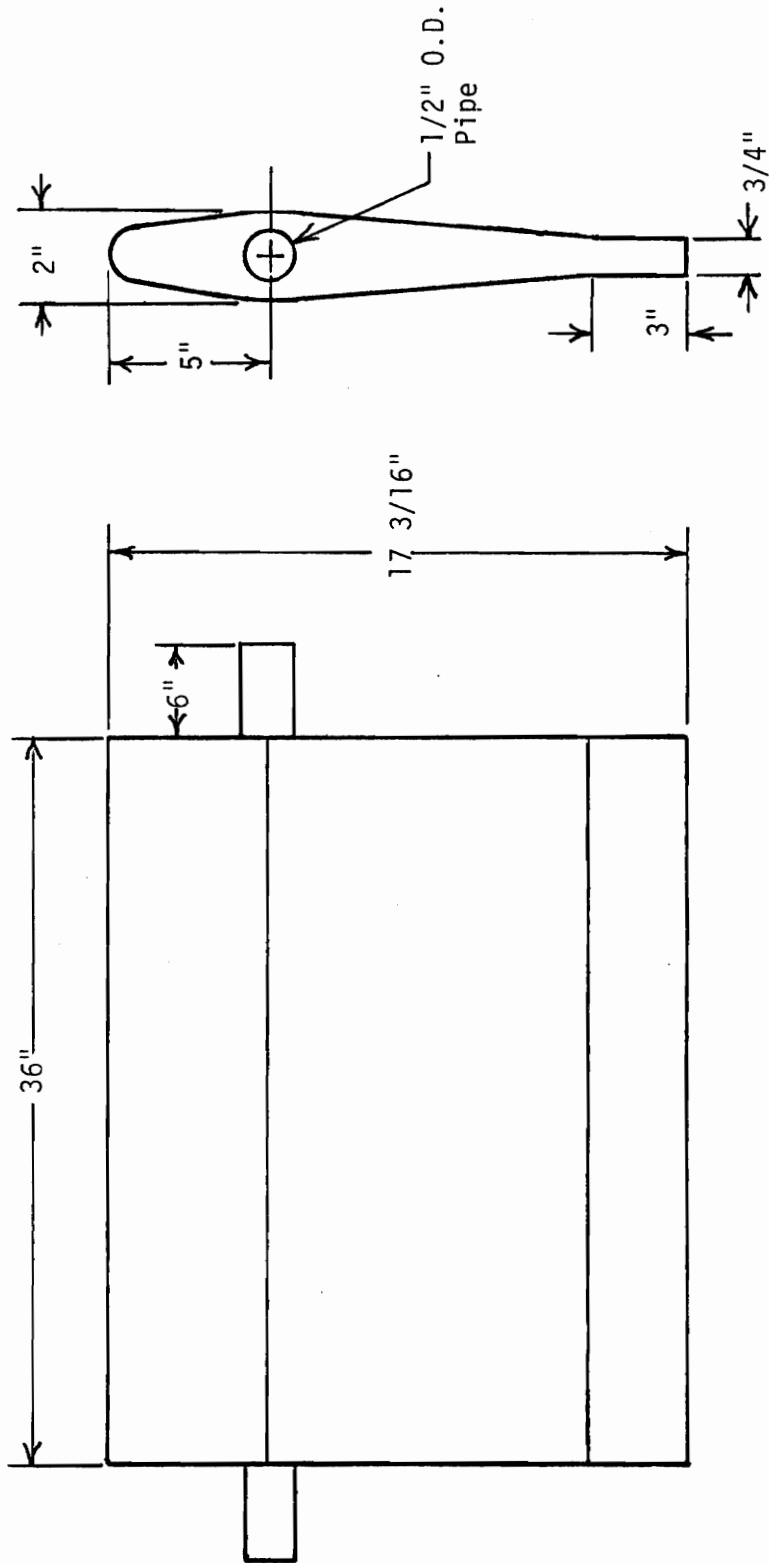


Fig. 7 Overall Dimensions of Injector

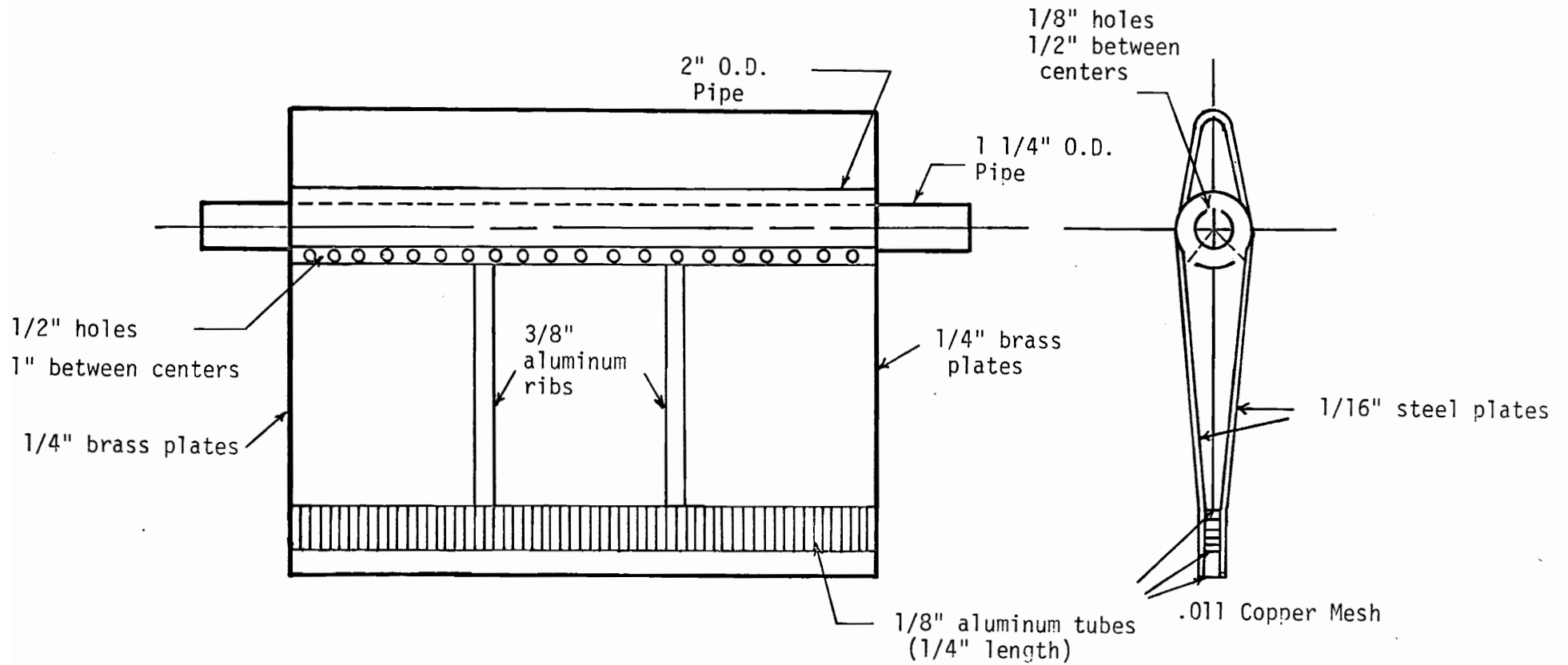
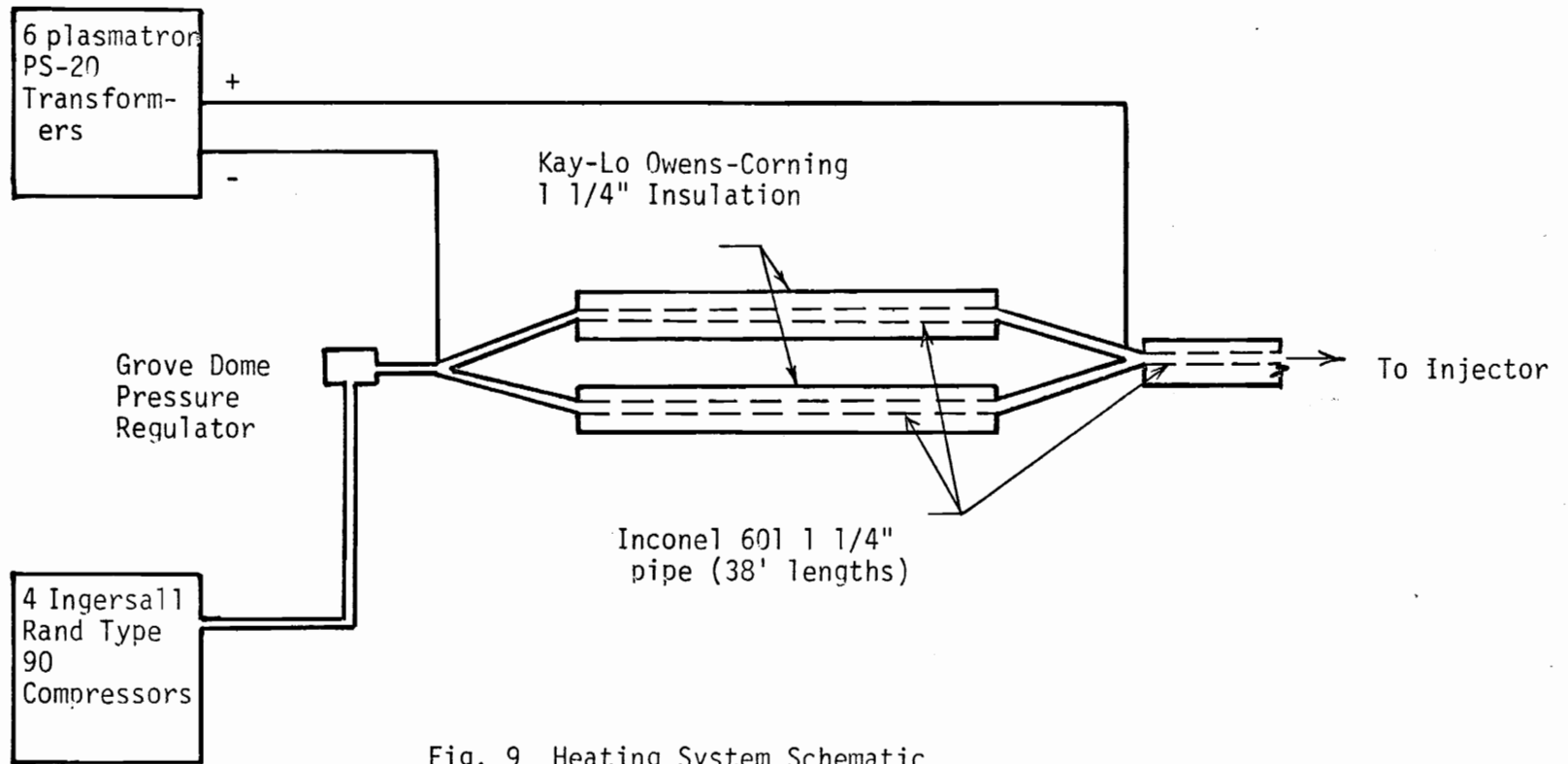


Fig. 8 Cutaway of Injector



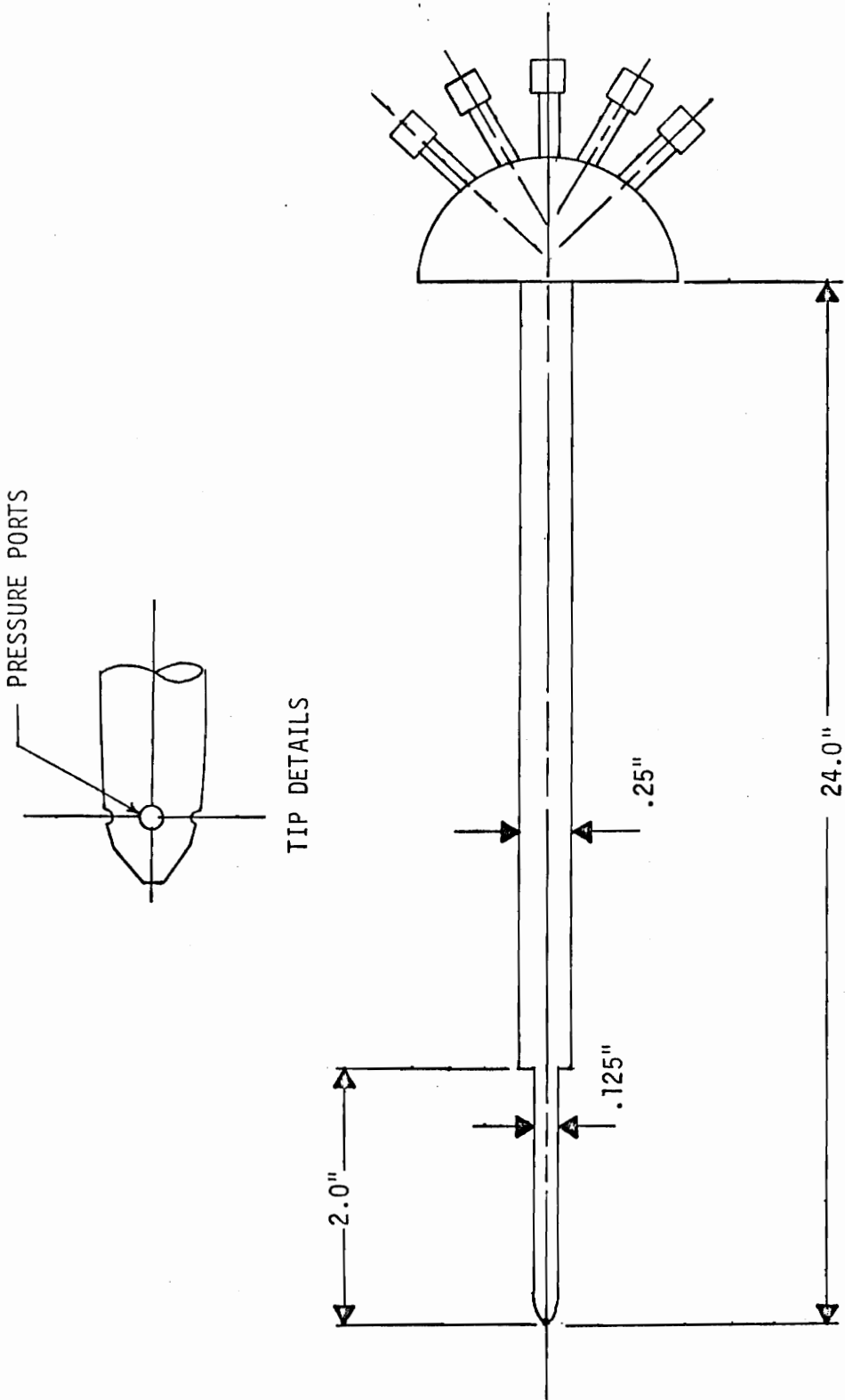
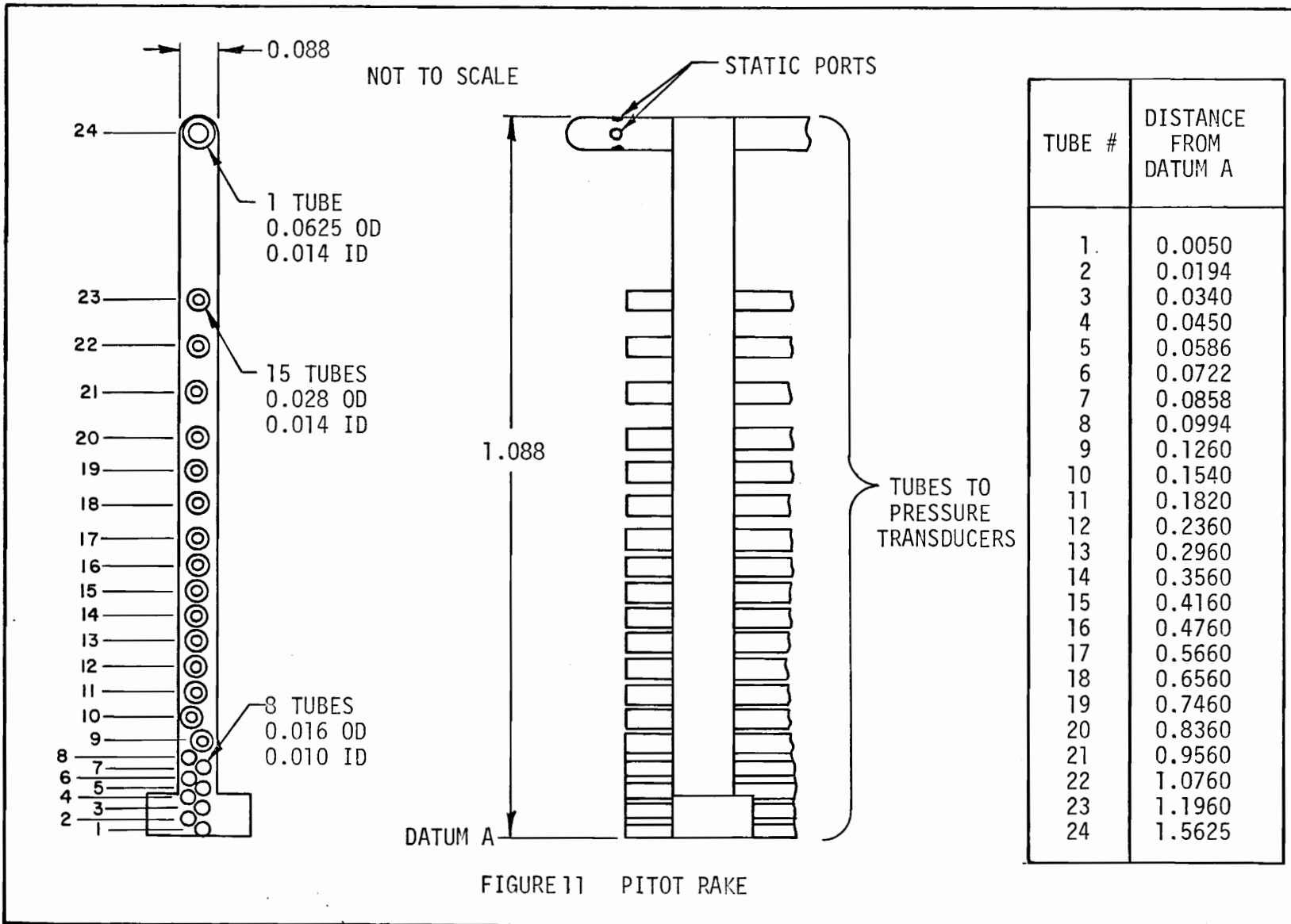


Fig. 10 Yawhead Probe



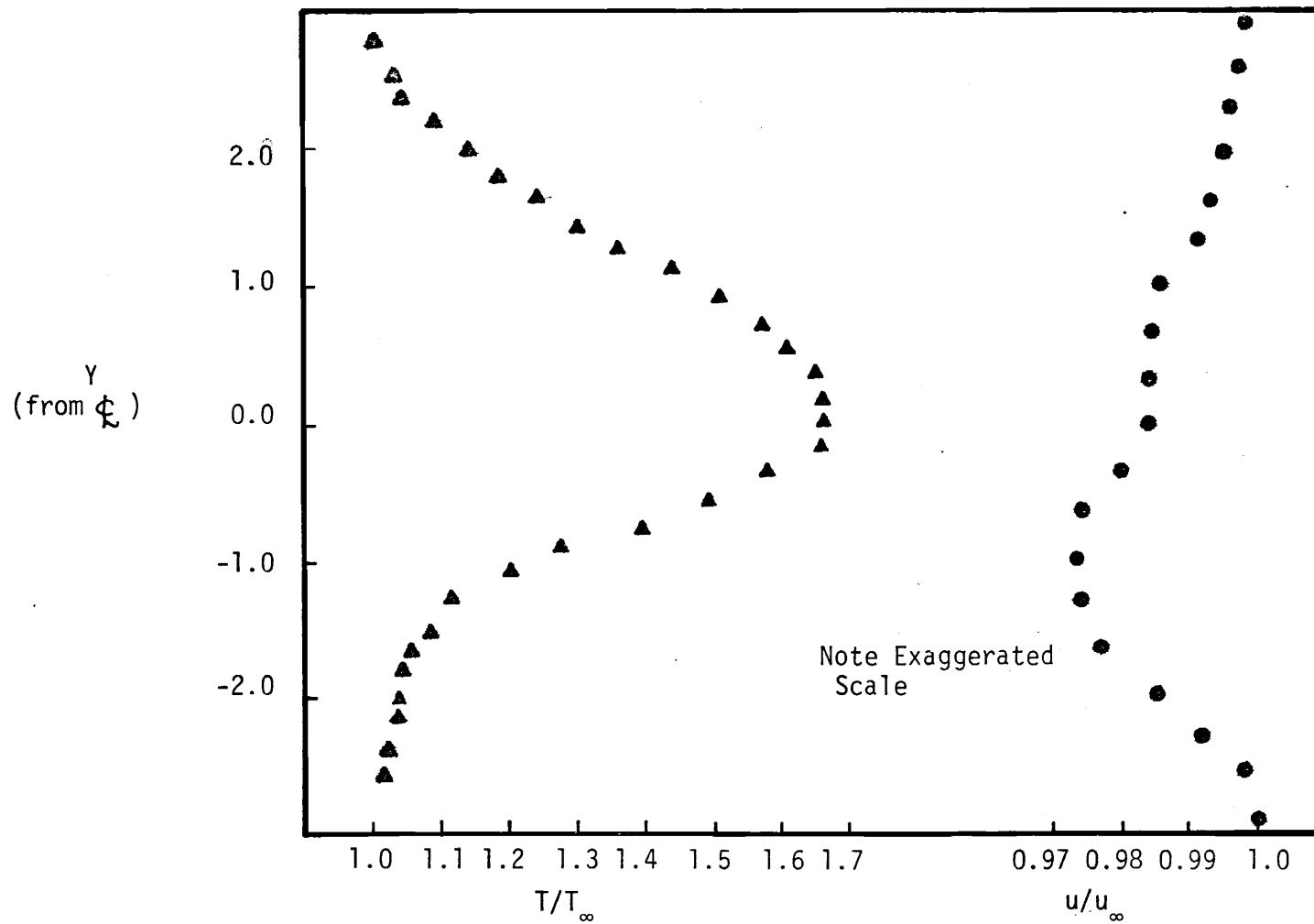


Fig. 12 Velocity and Temperature Profiles Upstream of Body

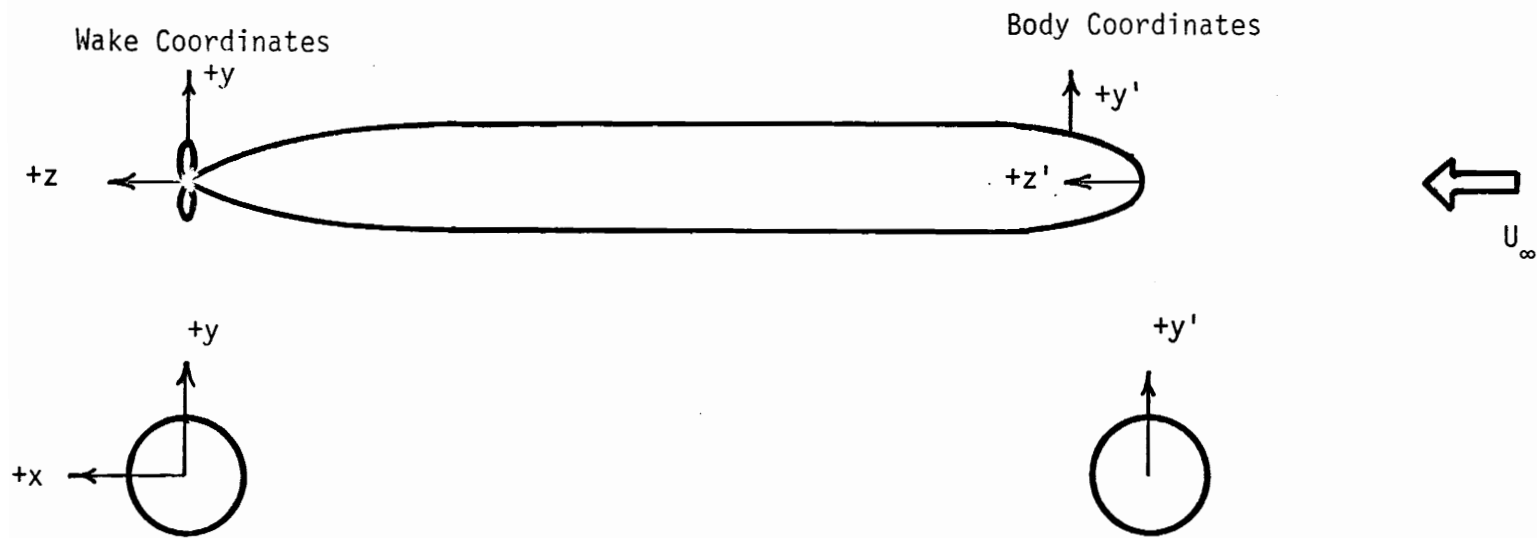


Fig. 13 Schematic of Coordinate Systems

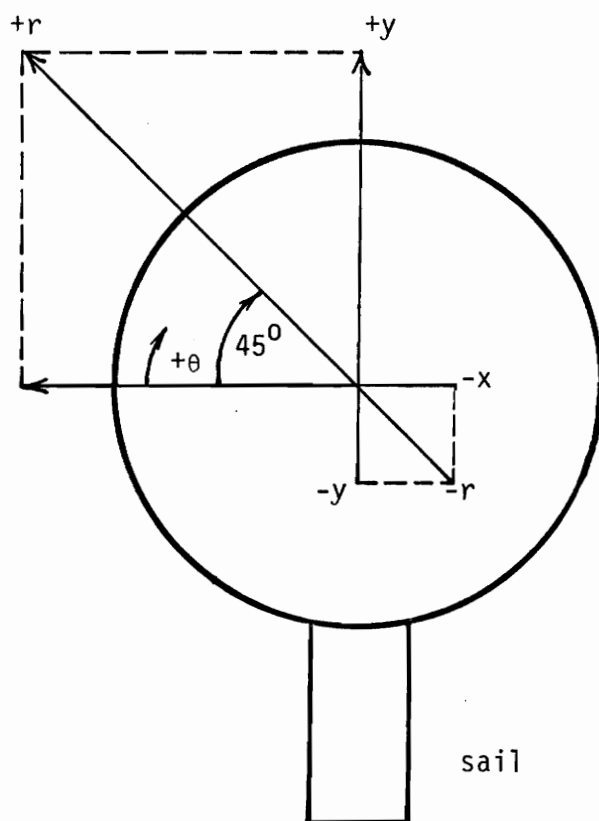


Fig. 14 Wake Traverse Paths

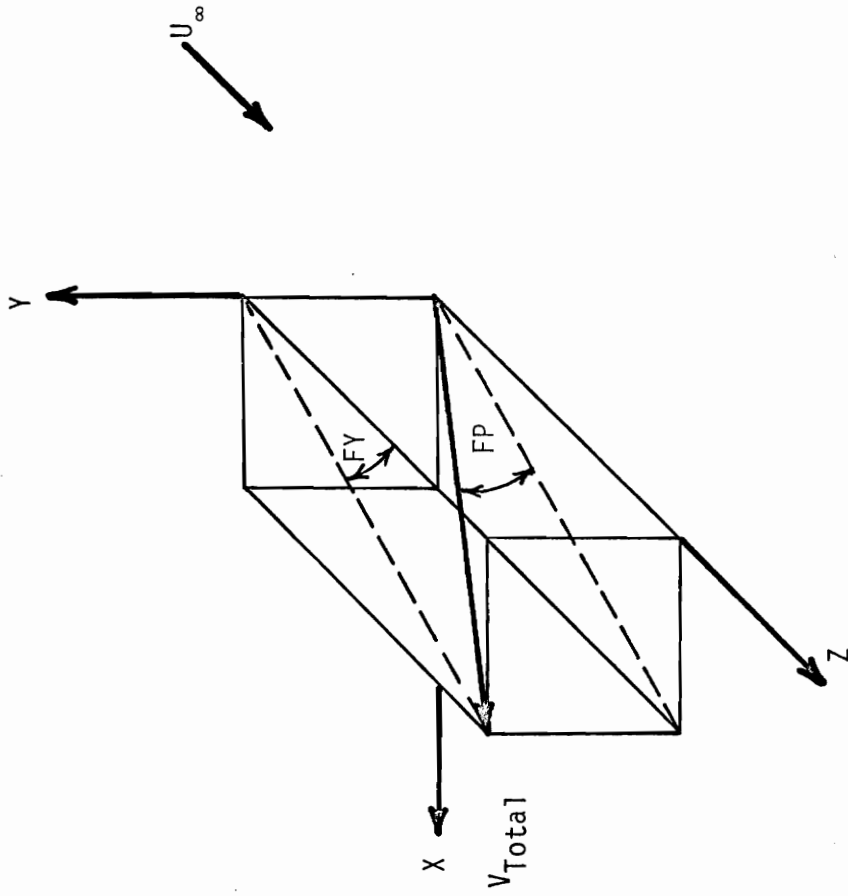


Fig. 15 Wake Coordinate System

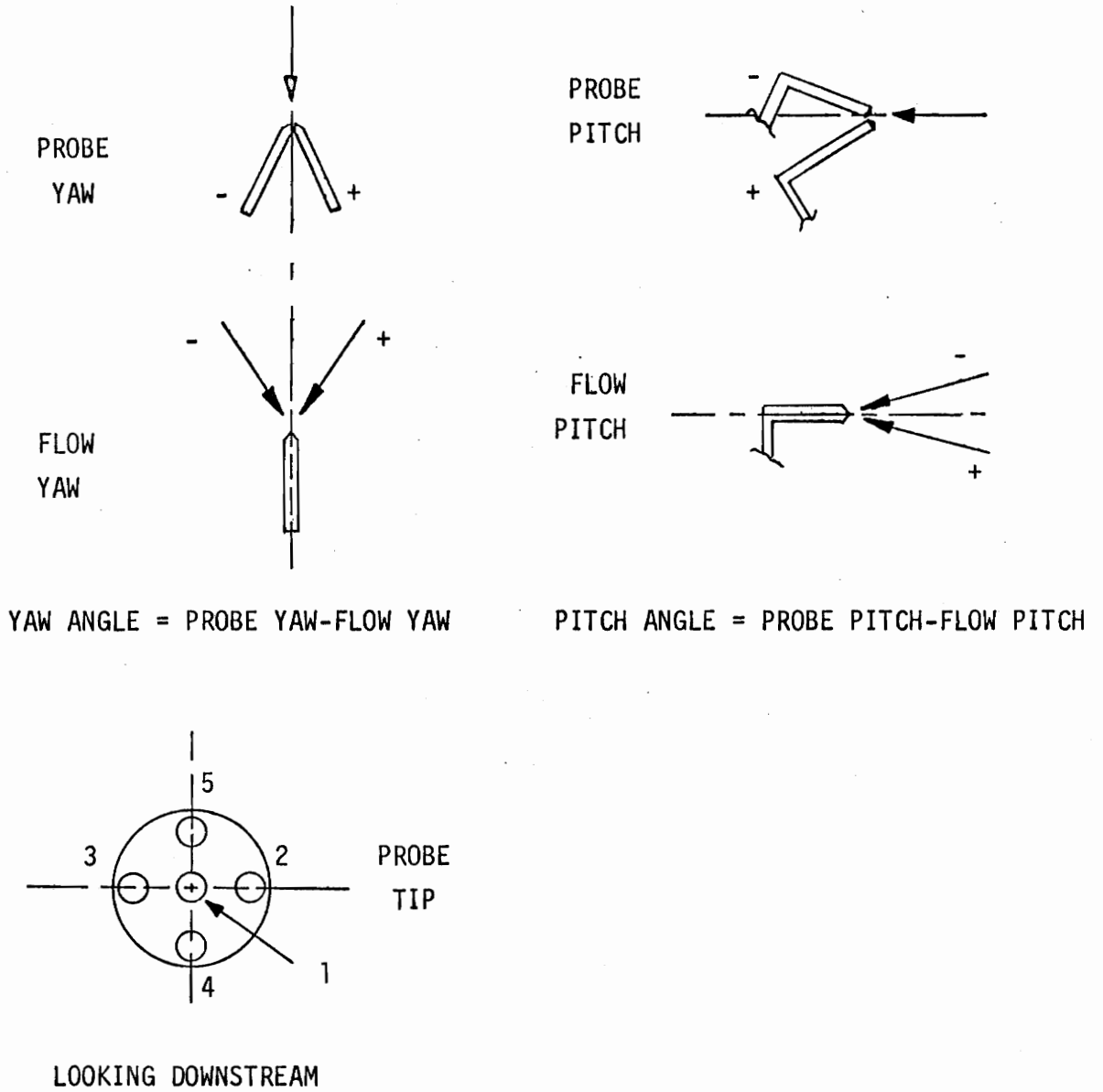


Fig. 16 Sign Conventions

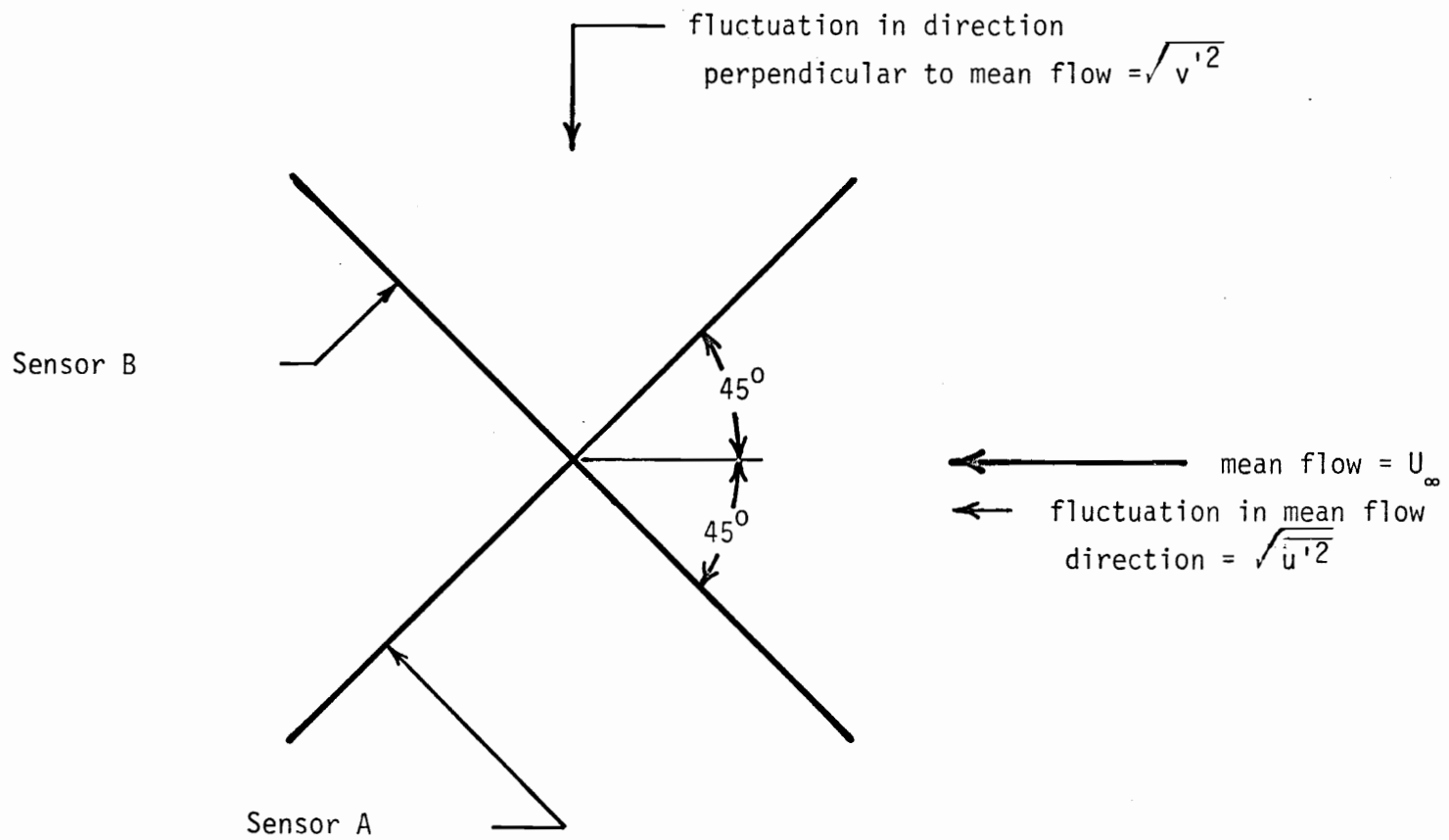


Fig. 17 Cross-wire Probe

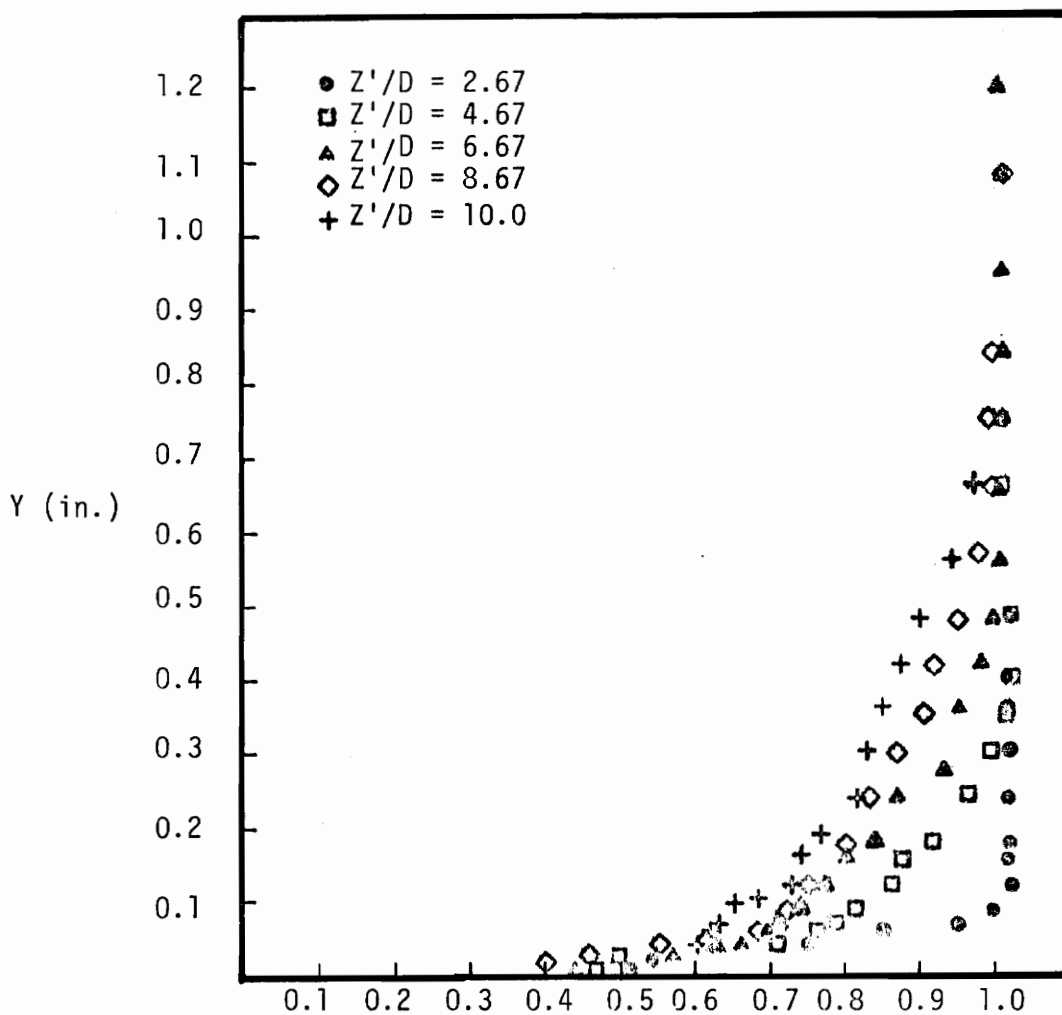


Fig. 18 Boundary Layer Velocity Profiles
at Various Stations on the Body

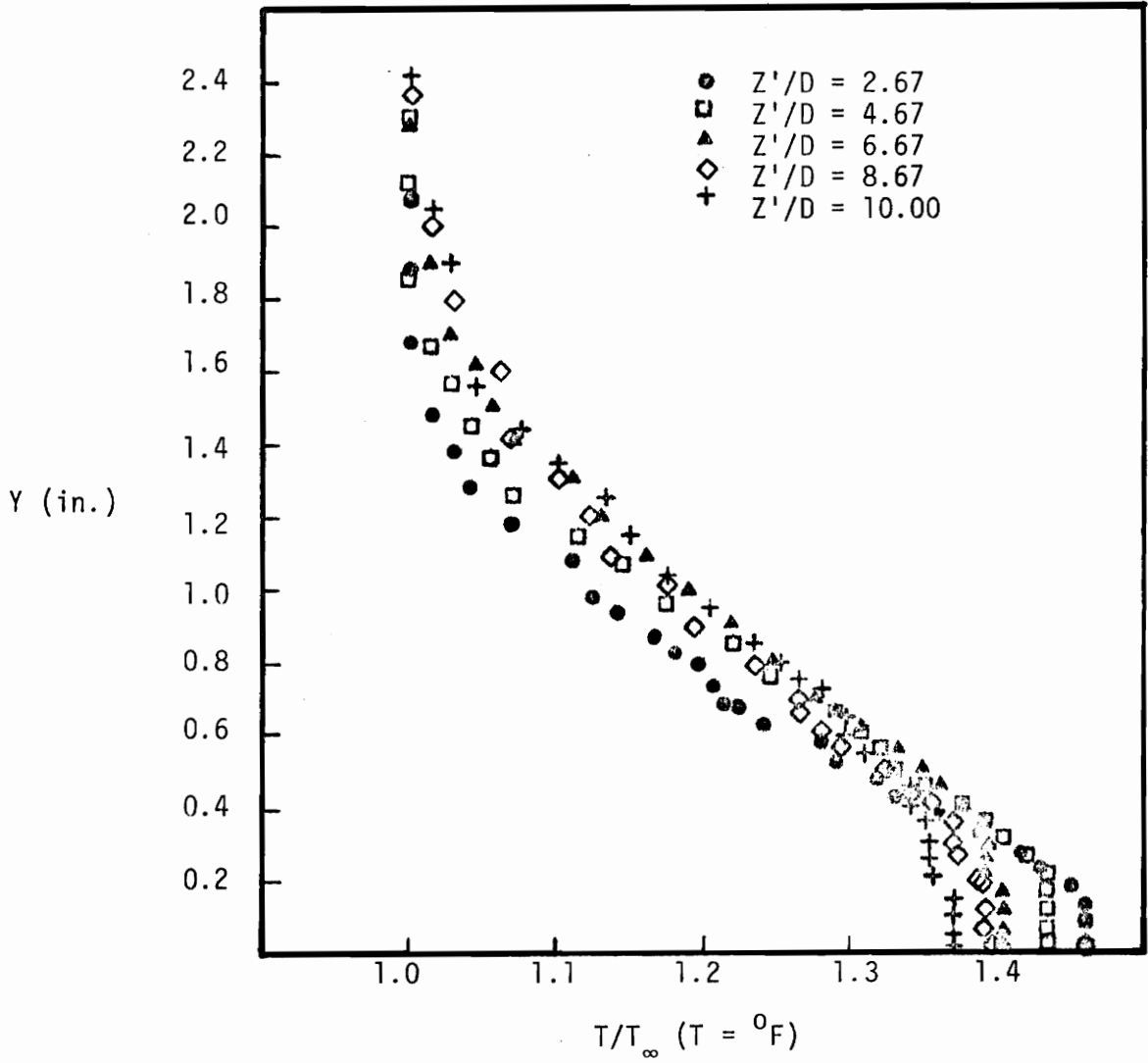


Fig. 19 Temperature Profiles at Various Stations on the Body

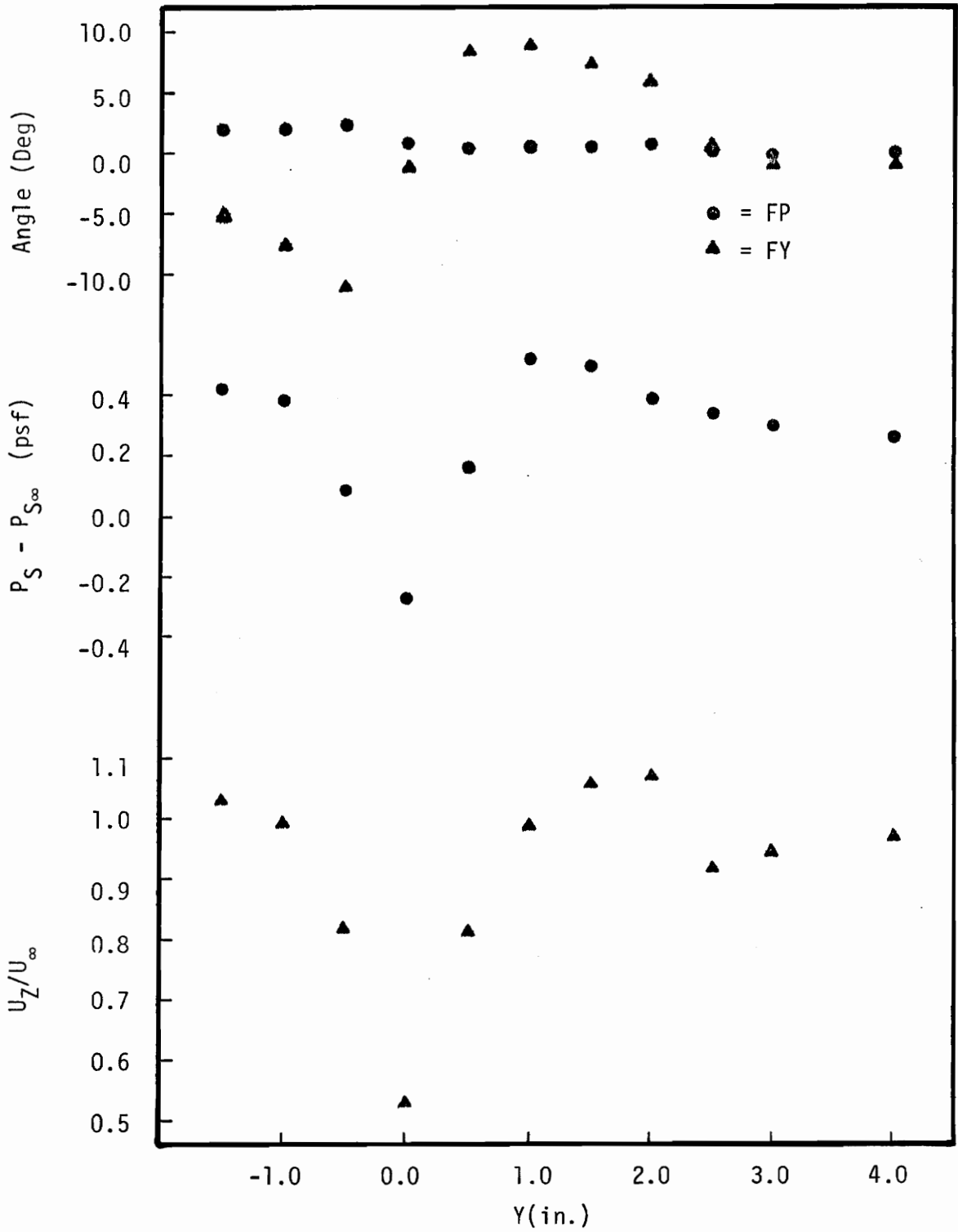


Figure 20

Flow Angularity, Mean Static Pressure, Mean Axial Velocity
at $Z/D = 0.33$, $X = 0$, $\theta = 90^\circ$

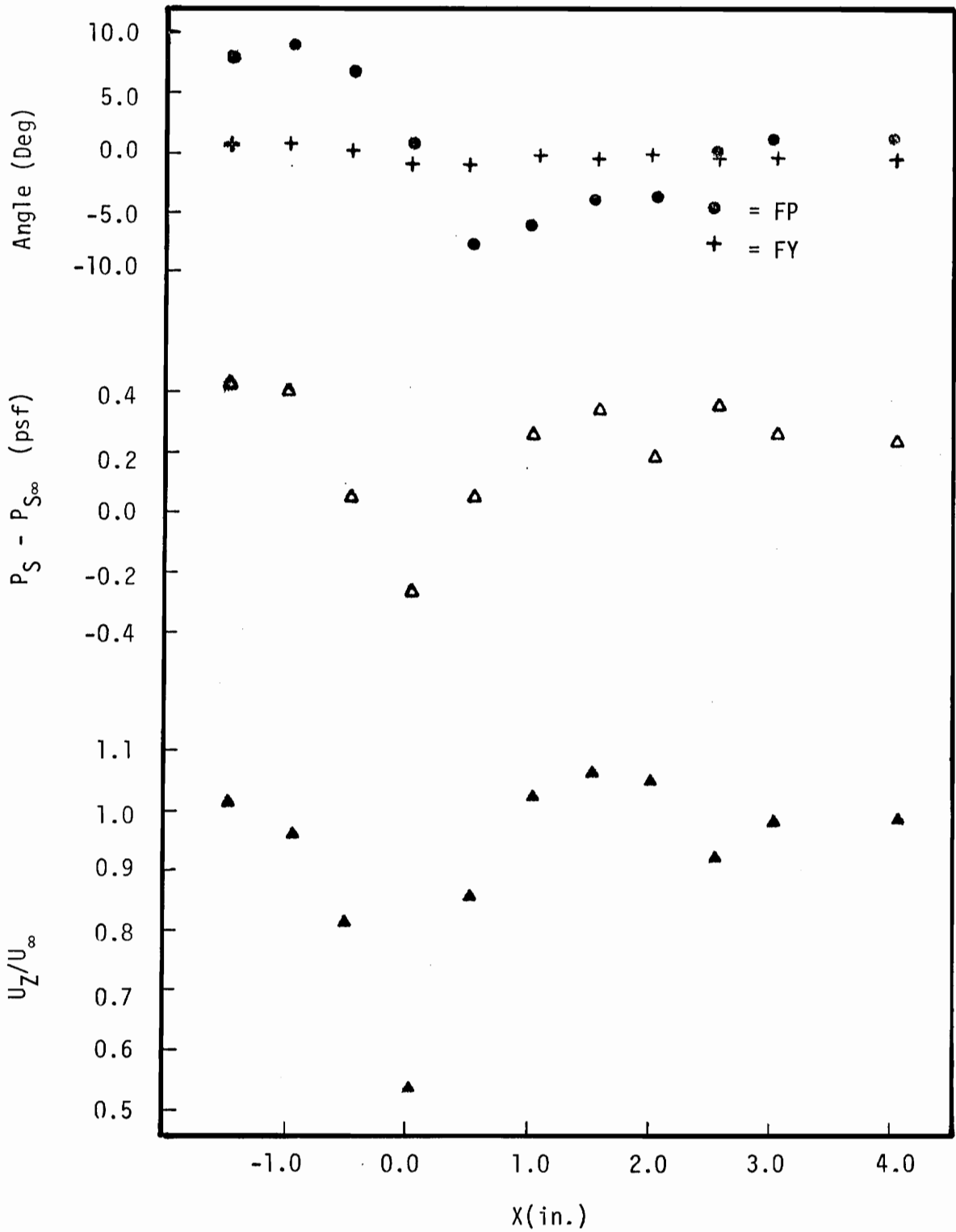


Figure 21

Flow Angularity, Mean Static Pressure, Mean Axial Velocity
at $Z/D = 0.33$, $Y = 0$, $\theta = 90^\circ$

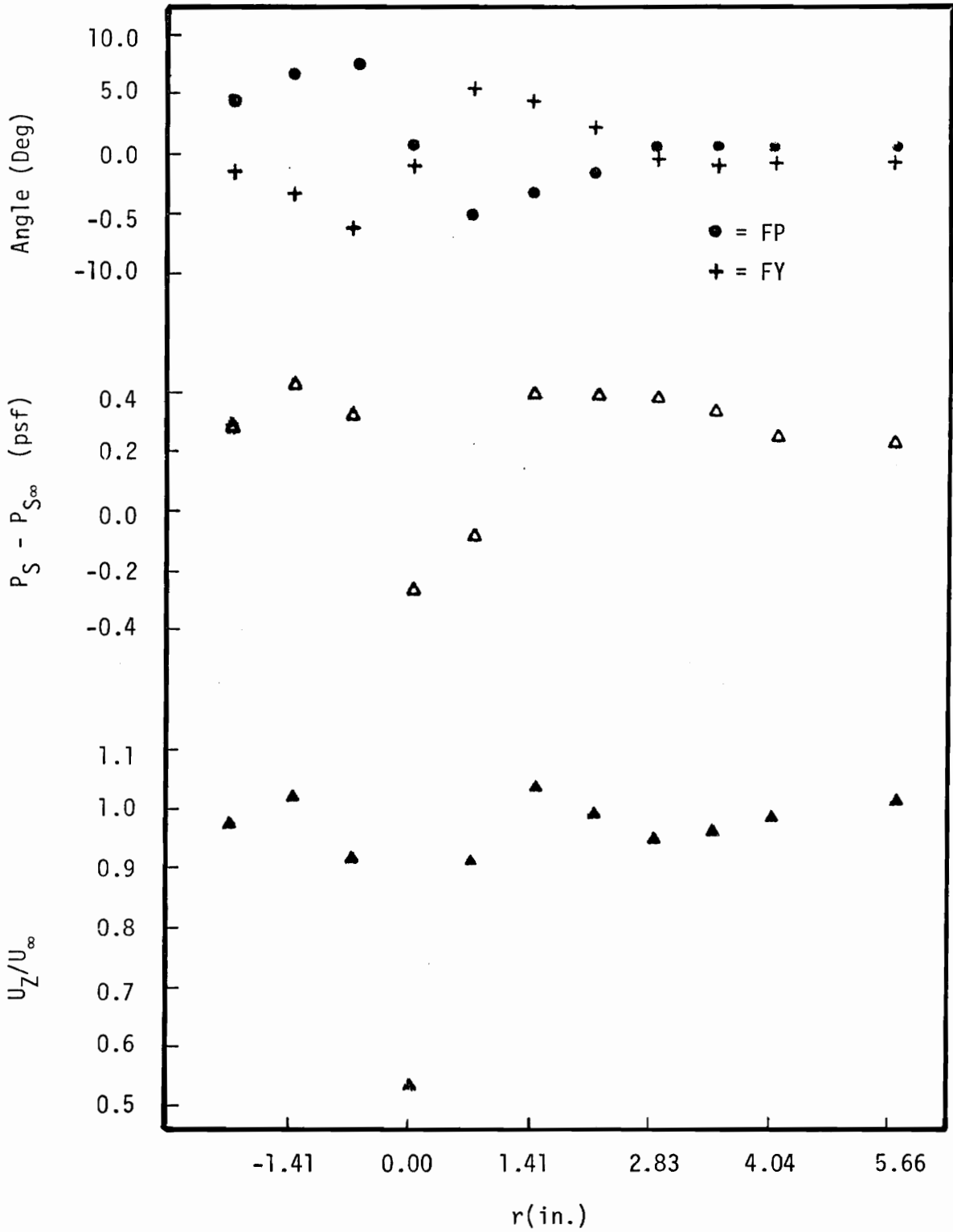


Figure 22

Flow Angularity, Mean Static Pressure, Mean Axial Velocity
at $Z/D = 0.33$, $X = Y$, $\theta = 45^\circ$

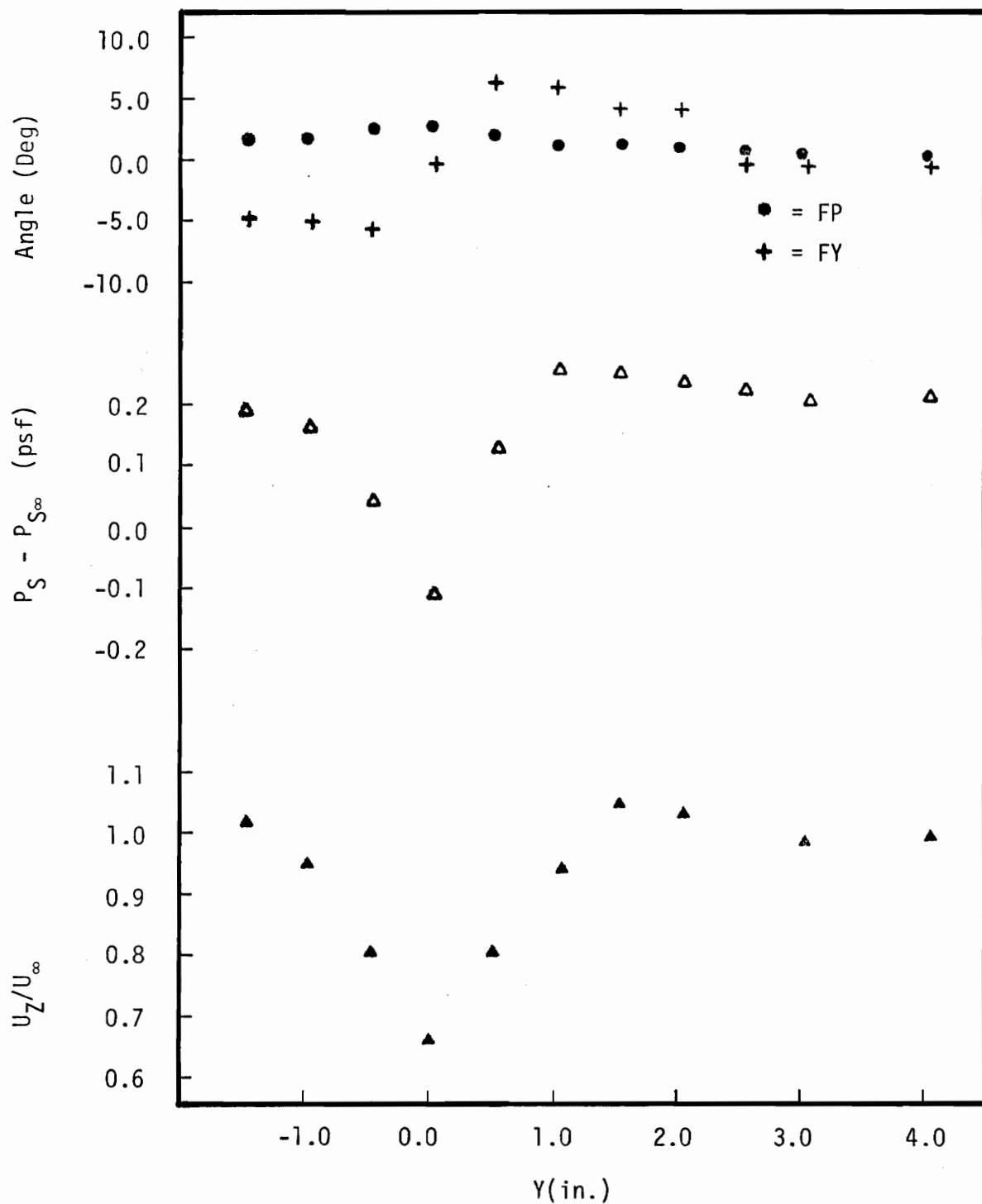


Figure 23

Flow Angularity, Mean Static Pressure, Mean Axial Velocity
at $Z/D = 1.0$, $X = 0$, $\theta = 90^\circ$

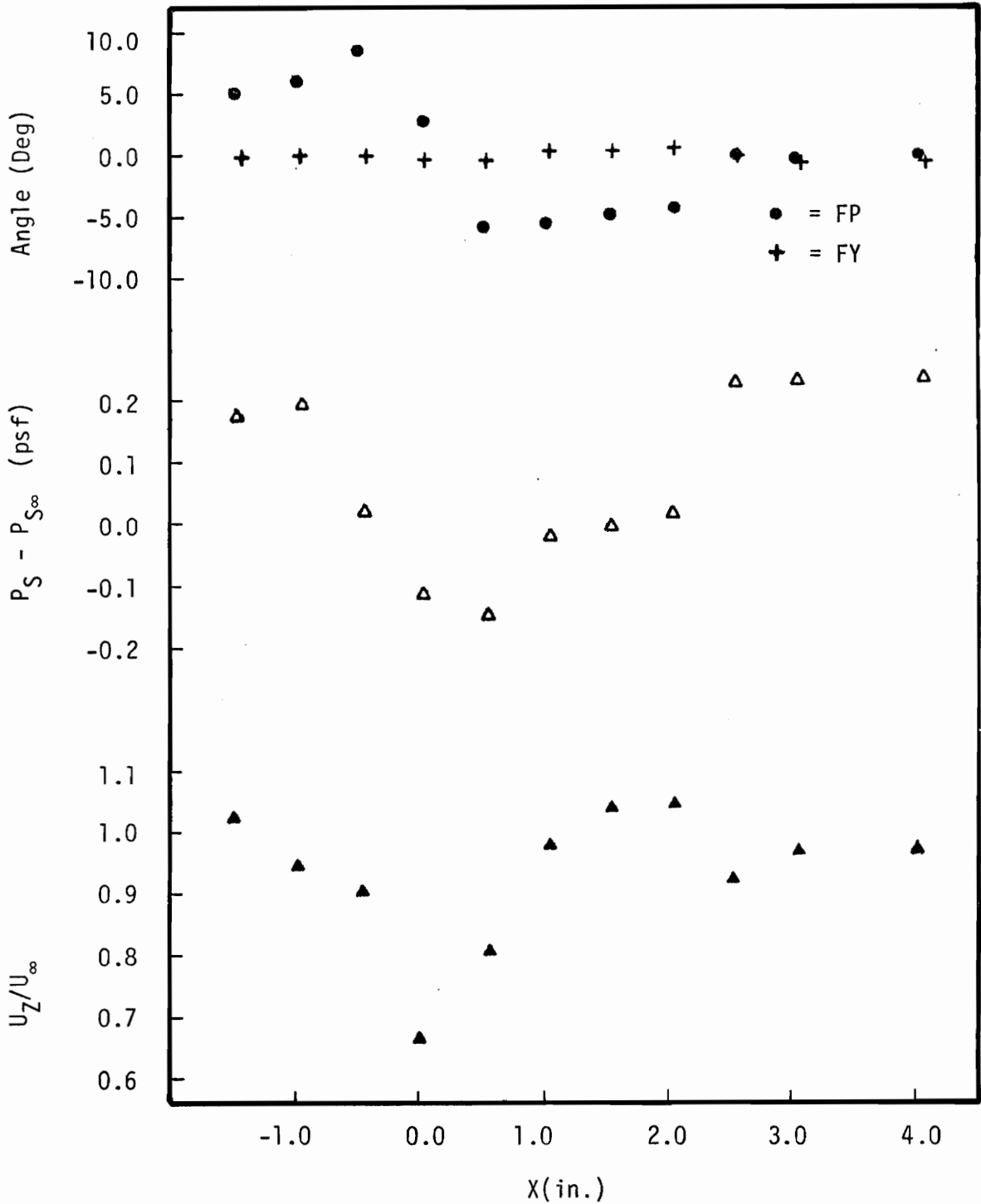


Figure 24

Flow Angularity, Mean Static Pressure, Mean Axial Velocity
at $Z/D = 1.0$, $Y = 0$, $\theta = 0^\circ$

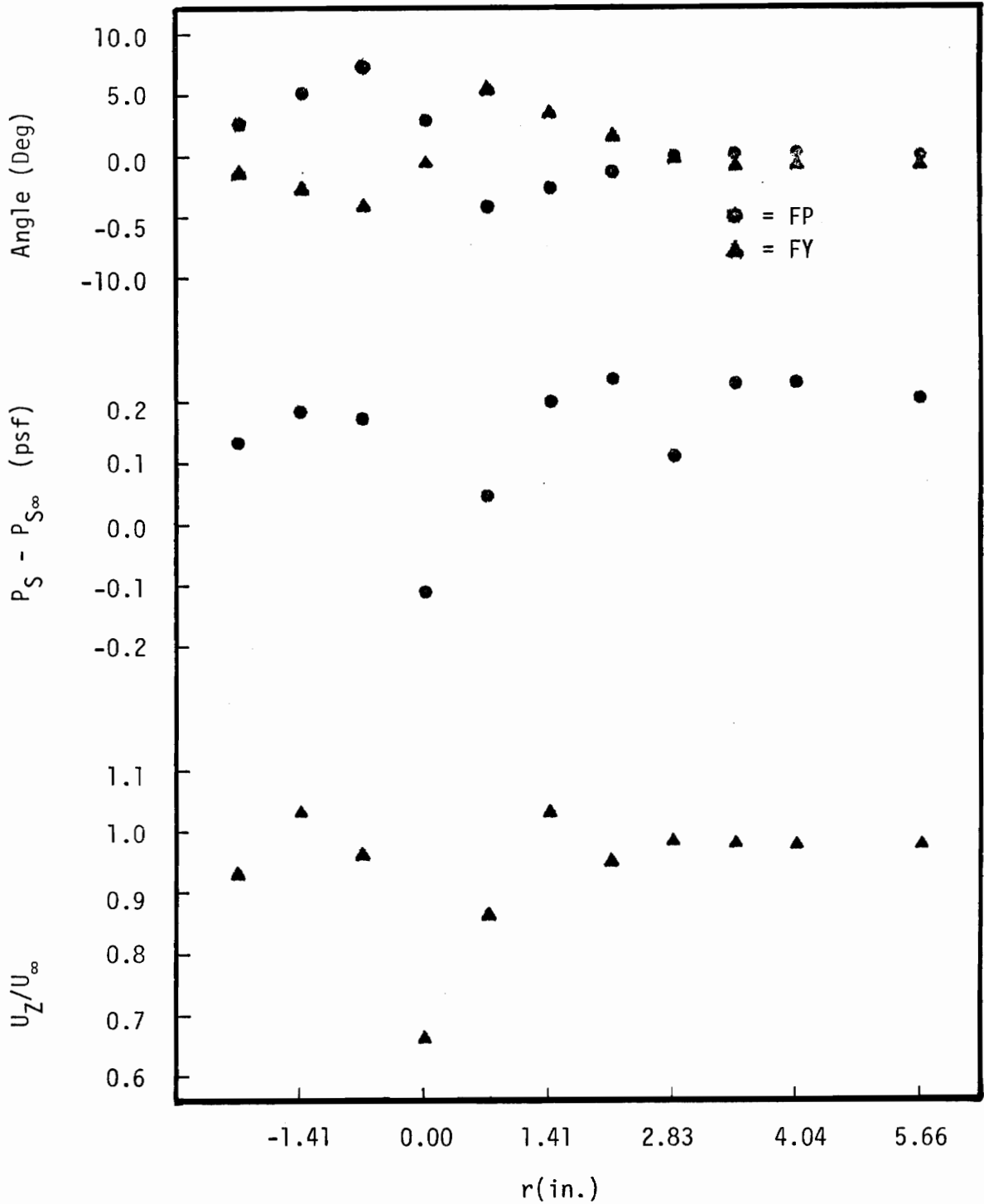


Figure 25

Flow Angularity, Mean Static Pressure, Mean Axial Velocity
at $Z/D = 1.0$, $X = Y$, $\theta = 45^\circ$

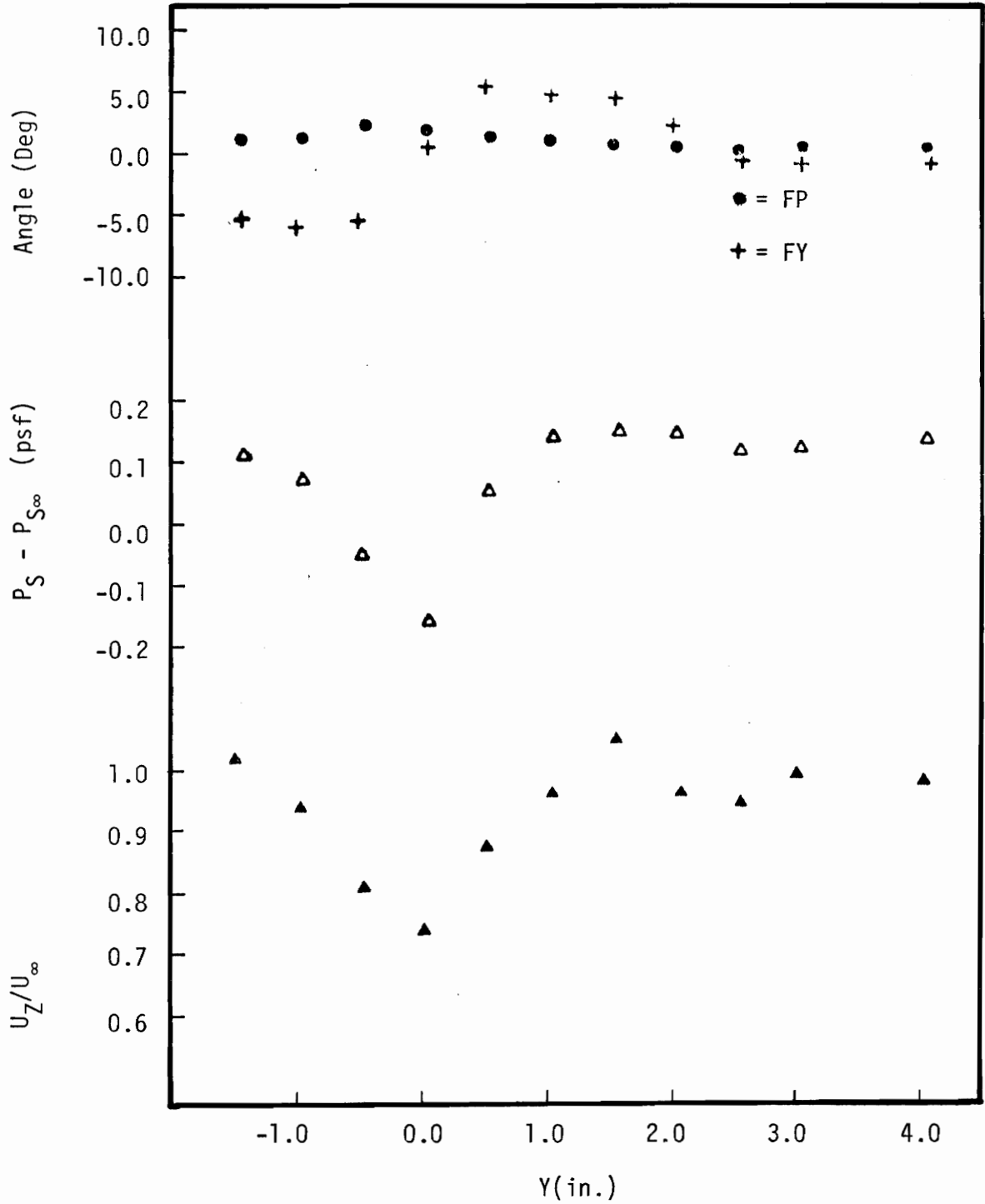


Figure 26

Flow Angularity, Mean Static Pressure, Mean Axial Velocity
at $Z/D = 2.0$, $X = 0$, $\theta = 90^\circ$

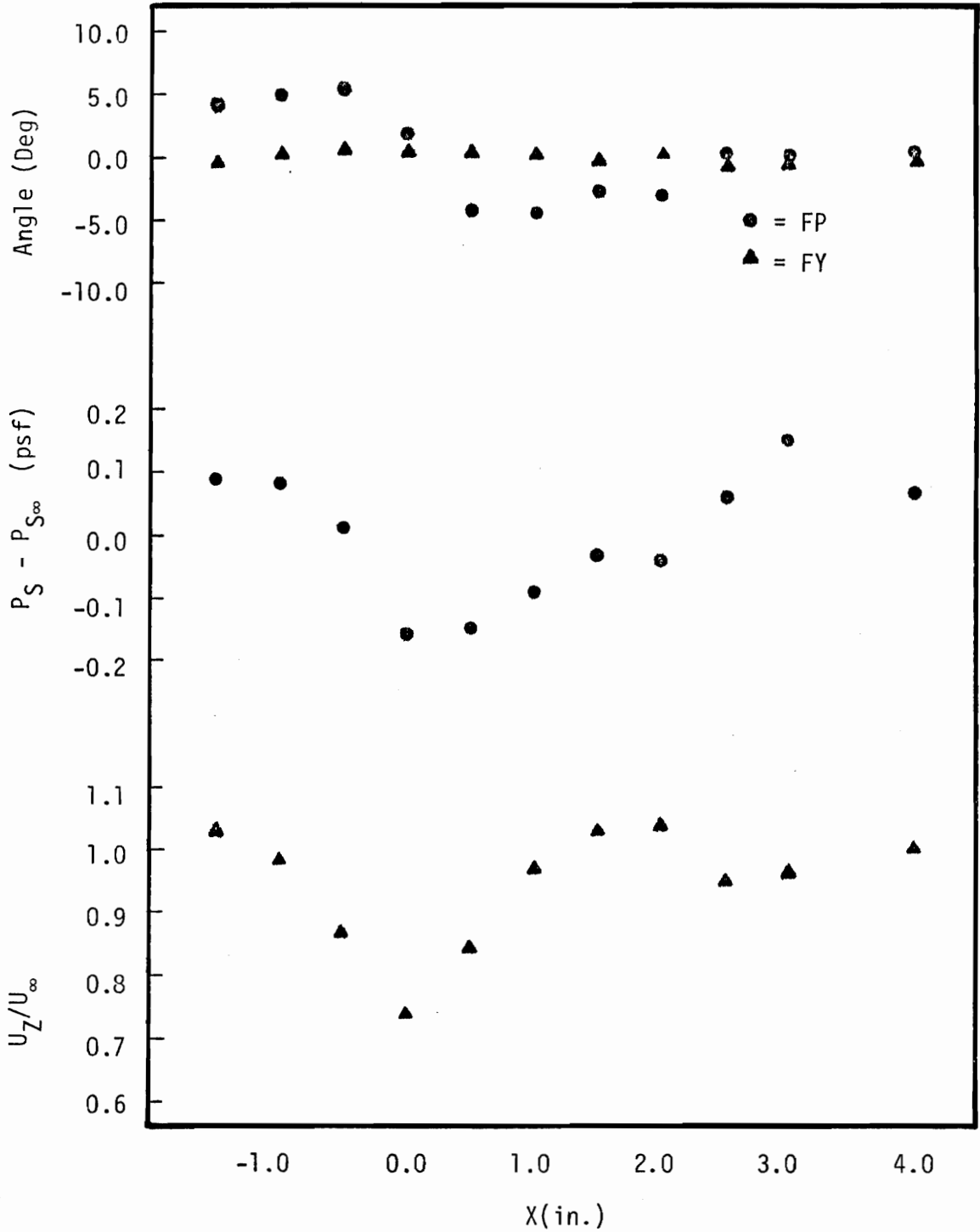


Figure 27

Flow Angularity, Mean Static Pressure, Mean Axial Velocity
at $Z/D = 2.0$, $Y = 0$, $\theta = 0^\circ$

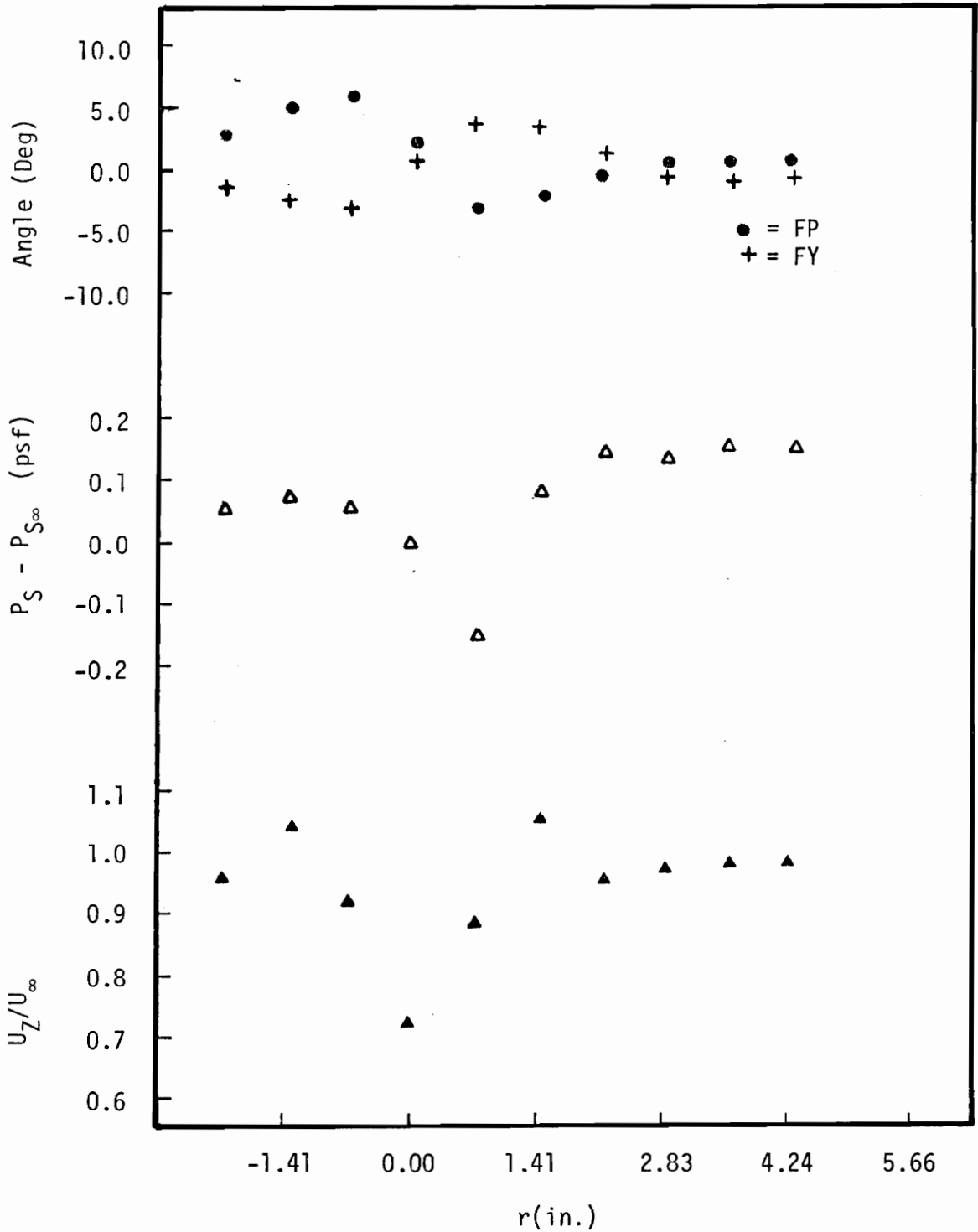


Figure 28

Flow Angularity, Mean Static Pressure, Mean Axial Velocity
at $Z/D = 2.0$, $Y = X$, $\theta = 45^\circ$

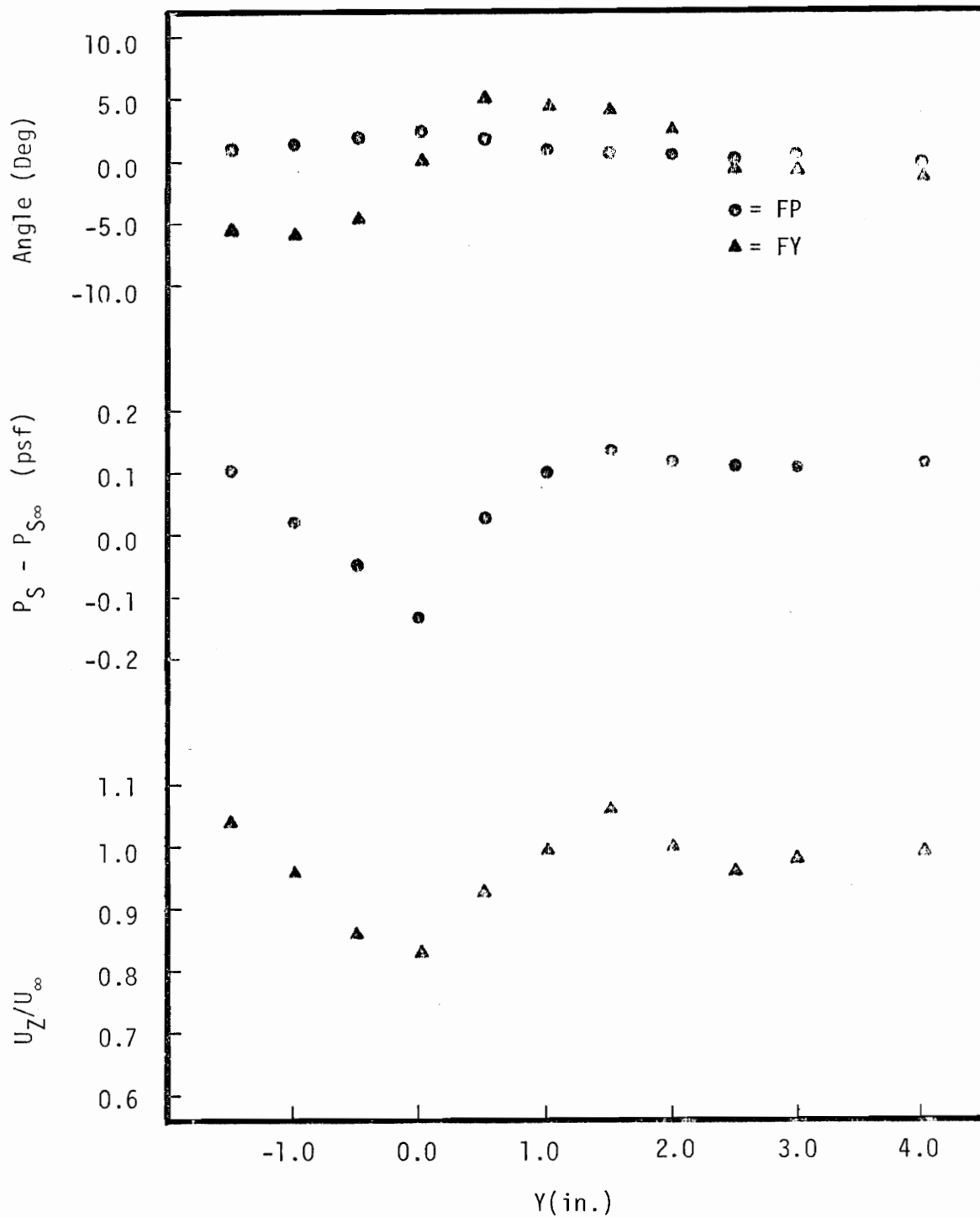


Figure 29

Flow Angularity, Mean Static Pressure, Mean Axial Velocity
at $Z/D = 3.0$, $X = 0$, $\theta = 90^\circ$

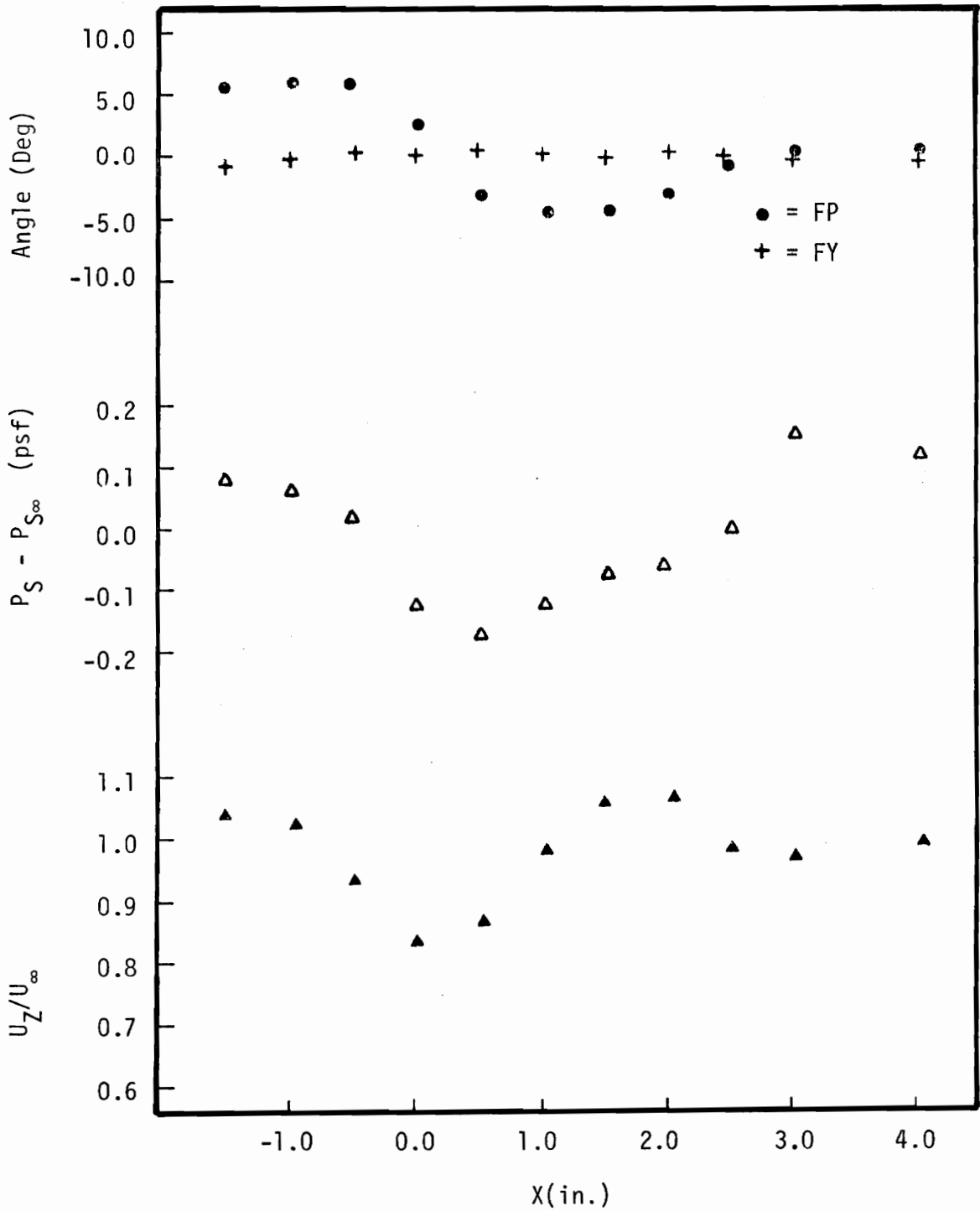


Figure 30

Flow Angularity, Mean Static Pressure, Mean Axial Velocity
at $Z/D = 3.0$, $Y = 0$, $\theta = 0^\circ$

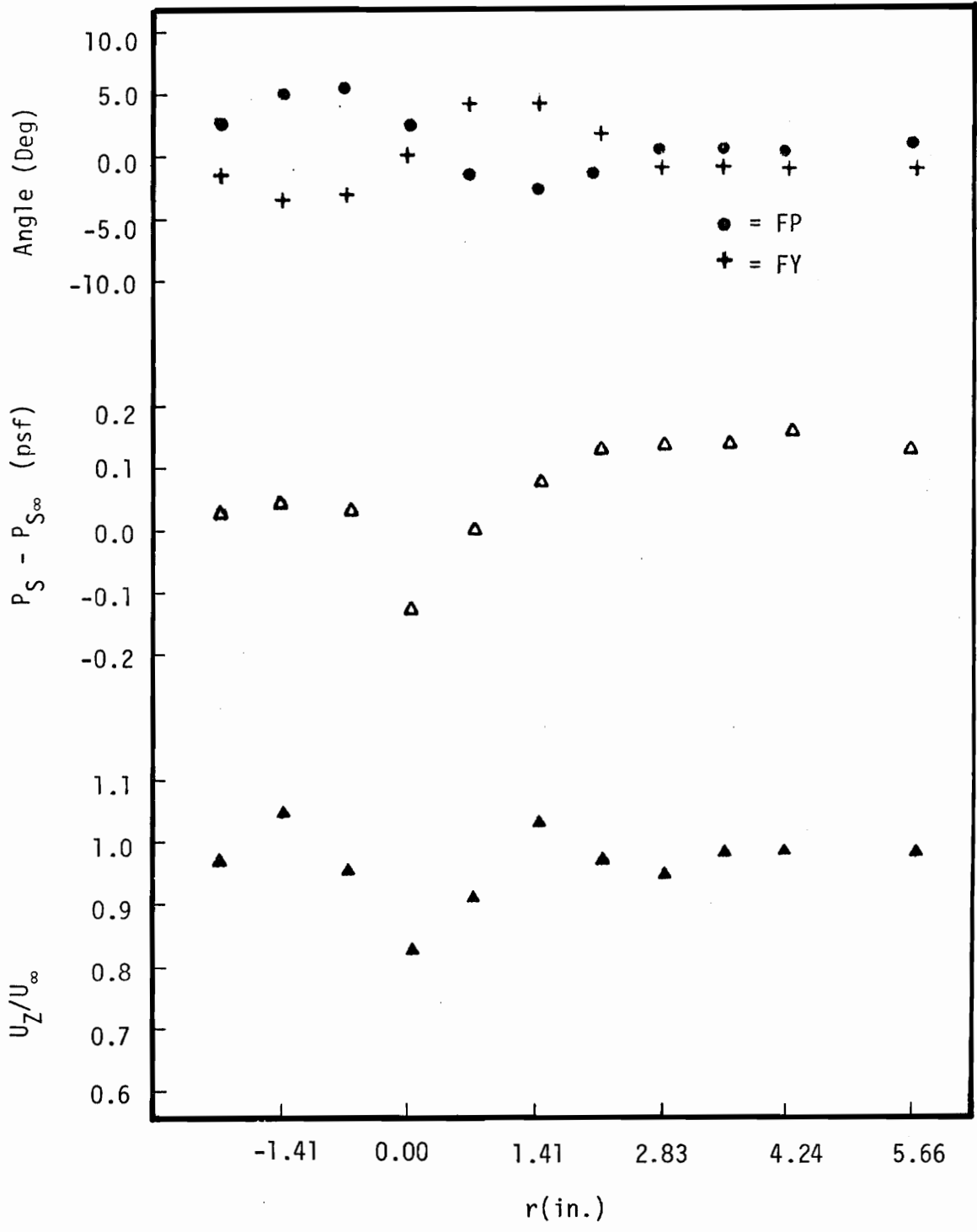


Figure 31

Flow Angularity, Mean Static Pressure, Mean Axial Velocity
at $Z/D = 3.0$, $Y = X$, $\theta = 45^\circ$

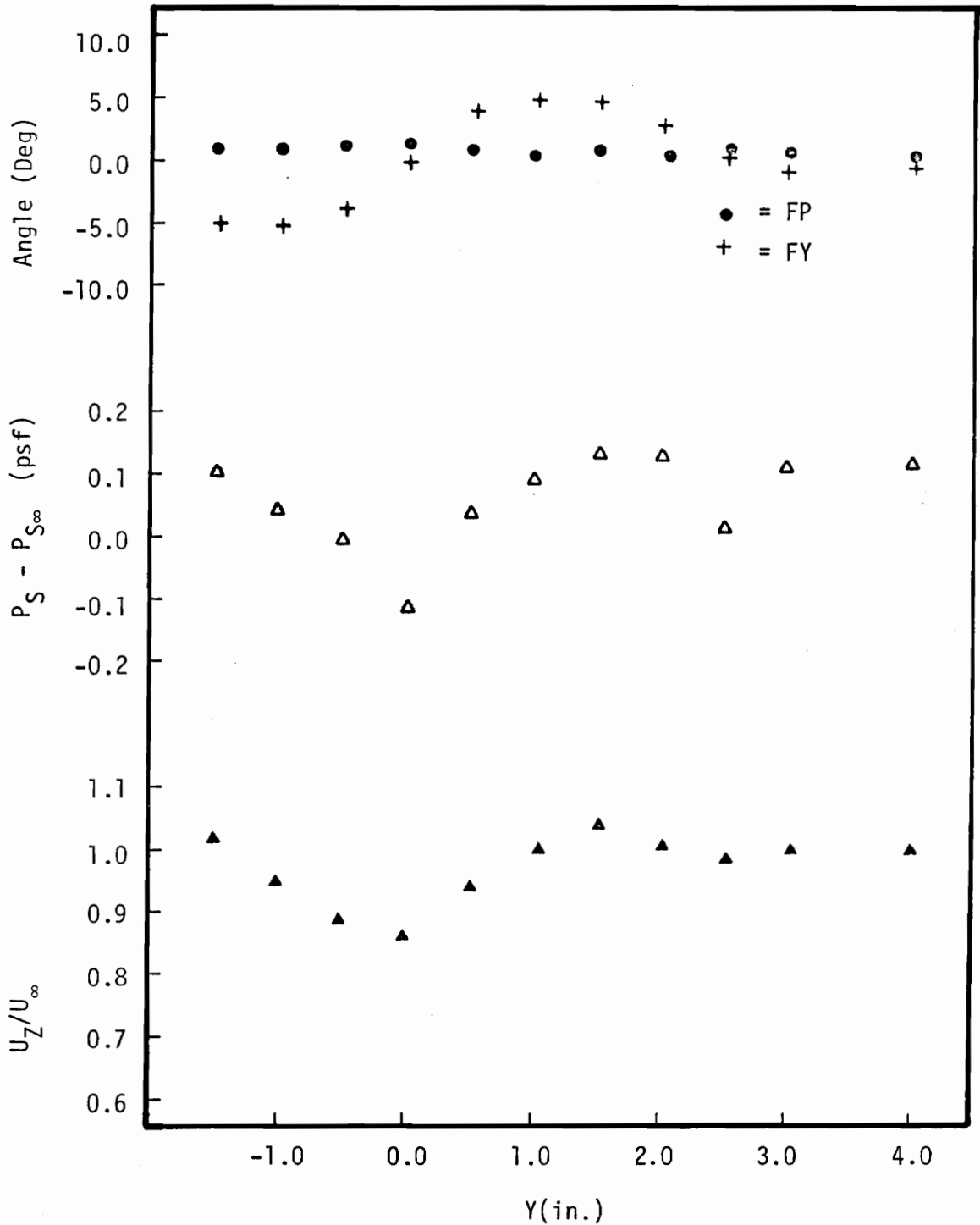


Figure 32

Flow Angularity, Mean Static Pressure, Mean Axial Velocity
at $Z/D = 4.0$, $X = 0$, $\theta = 90^\circ$

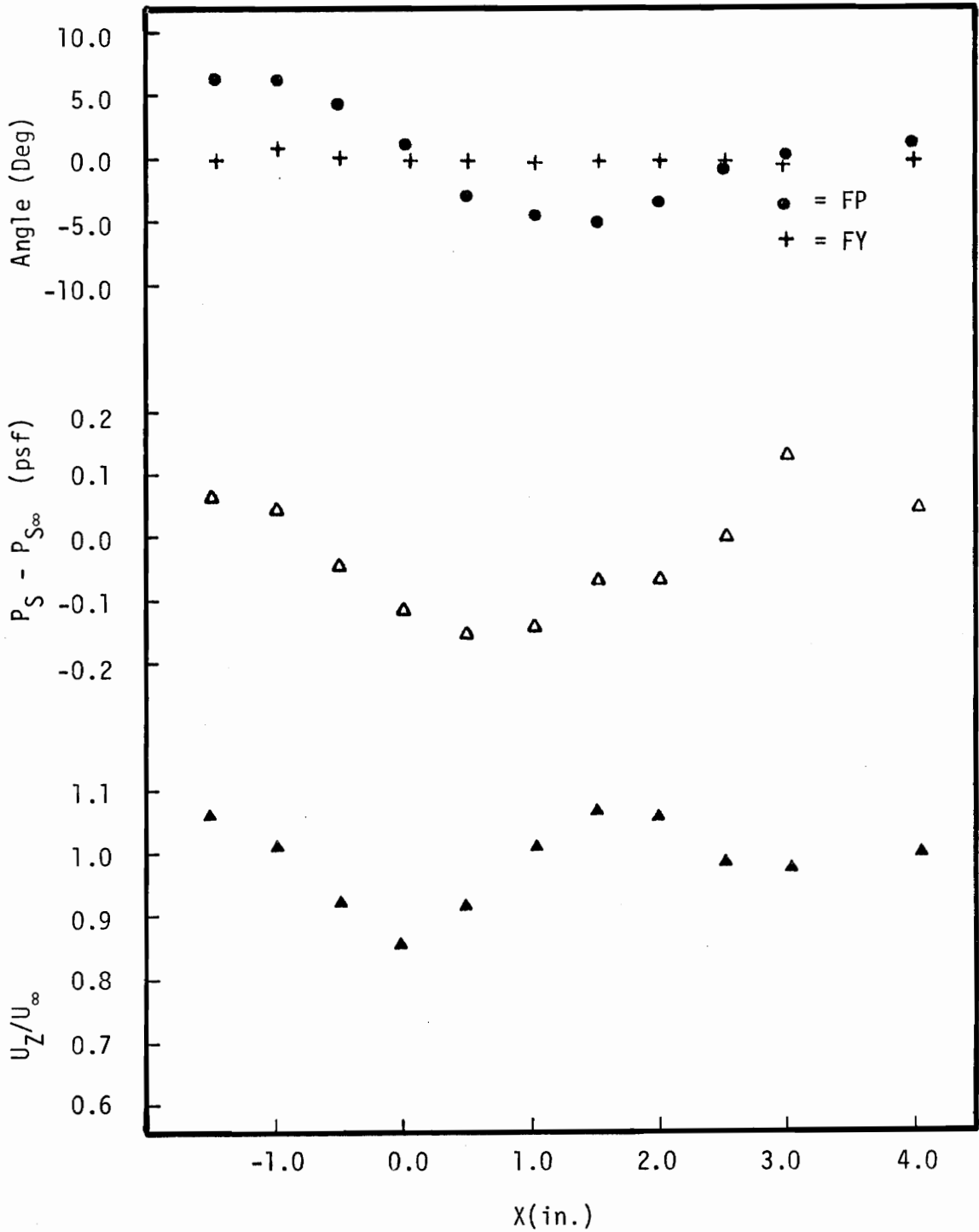


Figure 33

Flow Angularity, Mean Static Pressure, Mean Axial Velocity
at $Z/D = 4.0$, $Y = 0$, $\theta = 0^\circ$

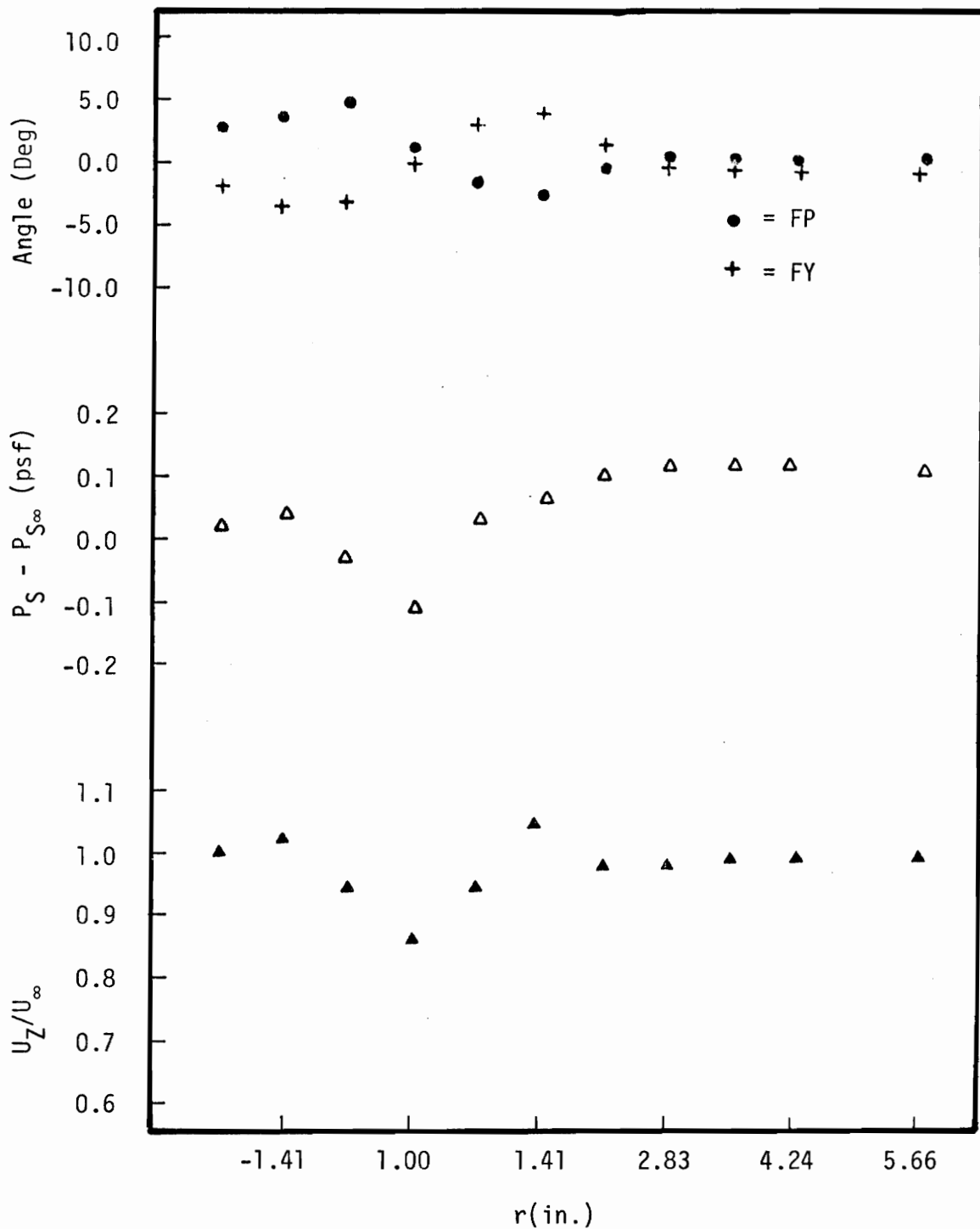


Figure 34

Flow Angularity, Mean Static Pressure, Mean Axial Velocity
at $Z/D = 4.0$, $Y = X$, $\theta = 45^\circ$

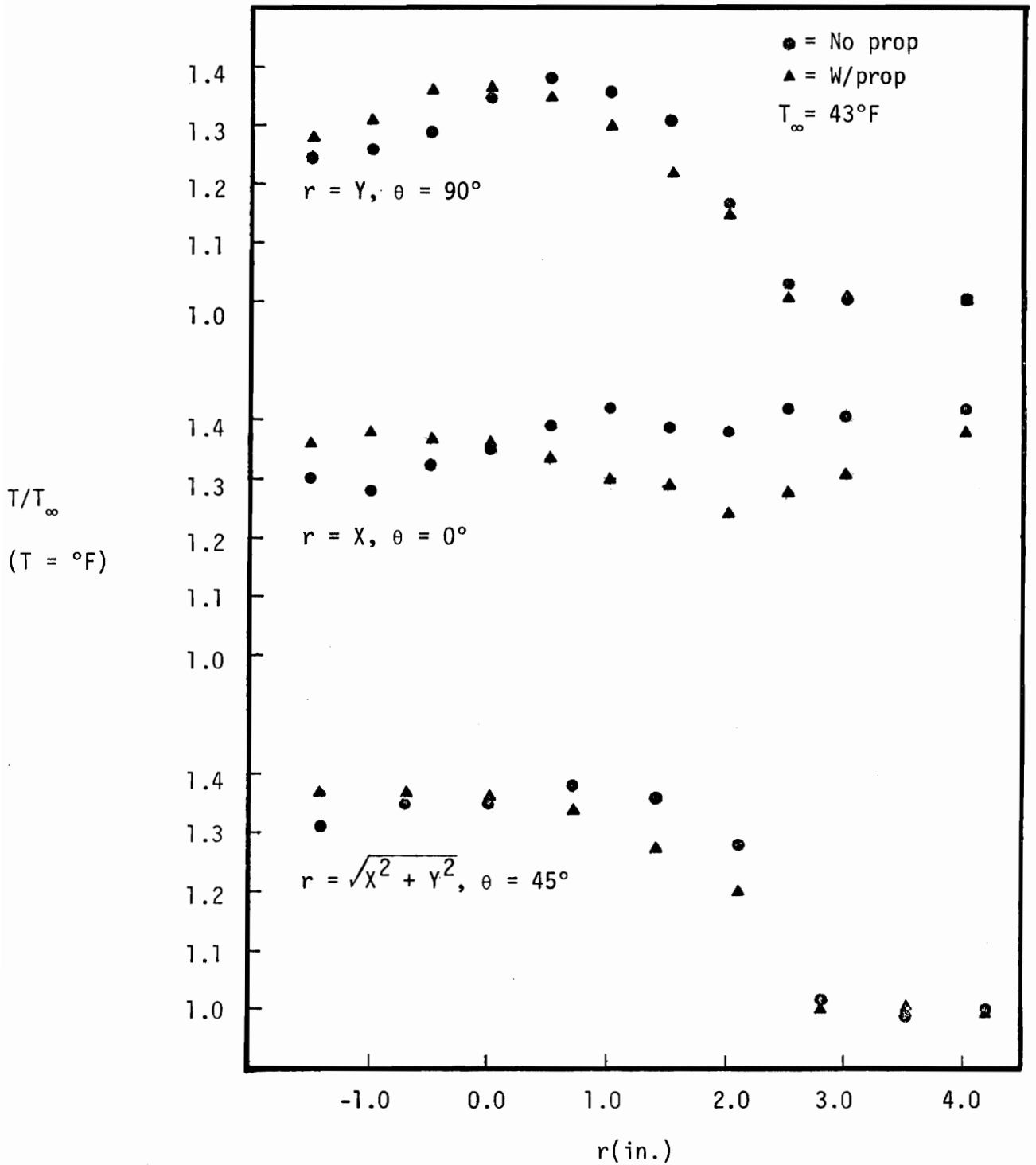


Figure 35

Temperature Distributions in the Wake at
 $Z/D = 0.33$

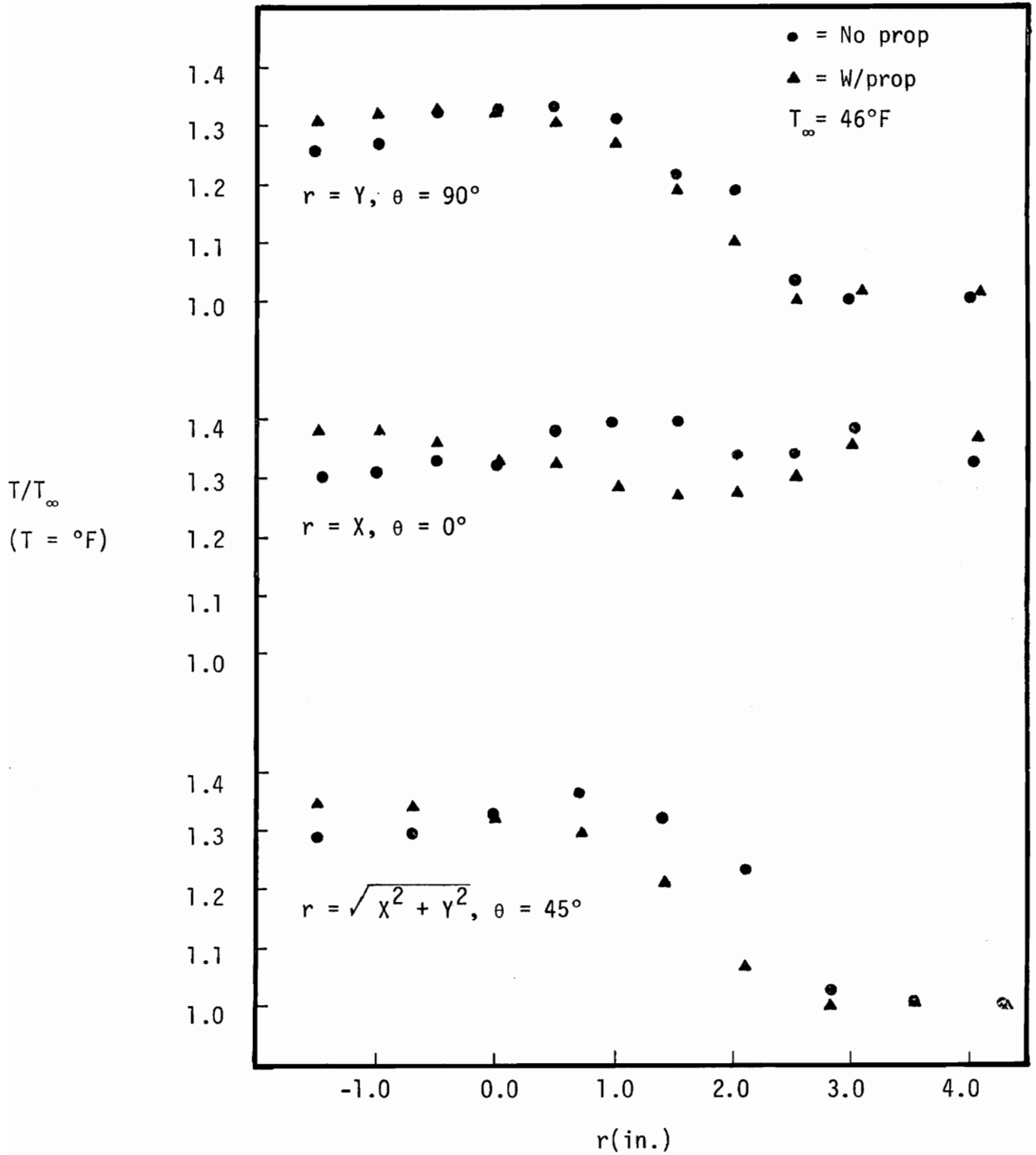


Figure 36

Temperature Distributions in the Wake
 $Z/D = 1.0$

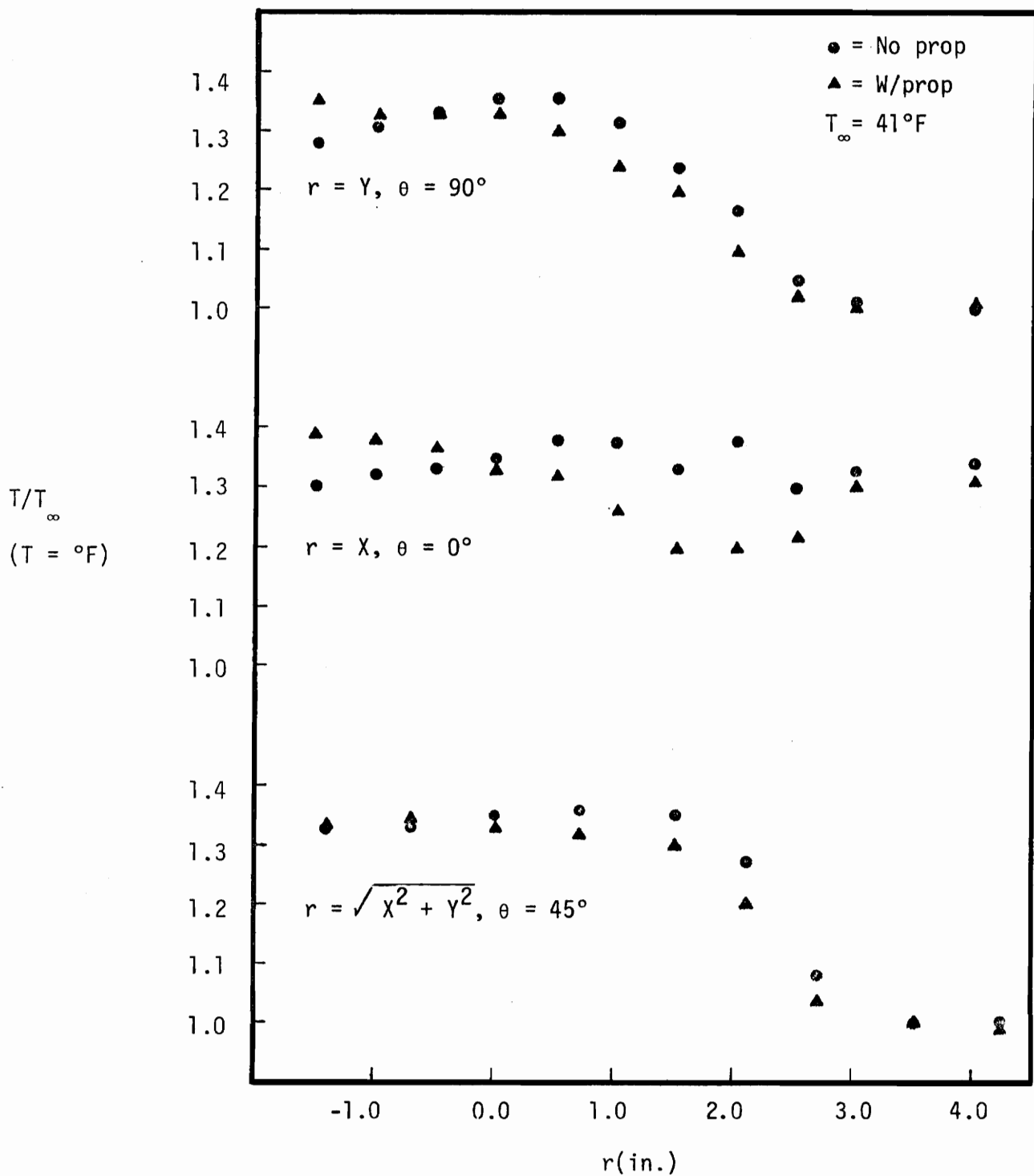


Figure 37

Temperature Distributions in the Wake at
 $Z/D = 2.0$

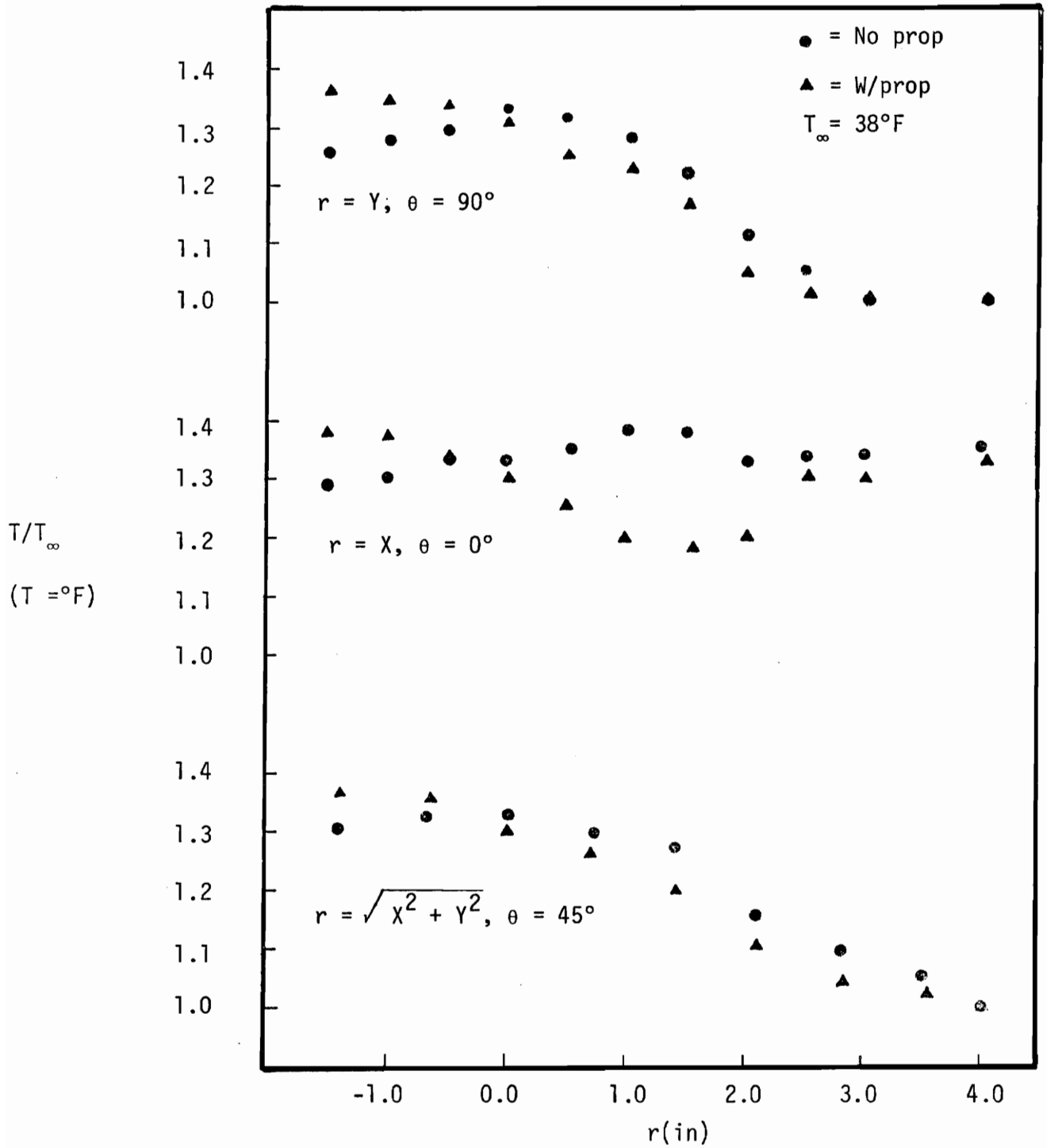


Figure 38

Temperature Distributions in the Wake at $Z/D = 3.0$

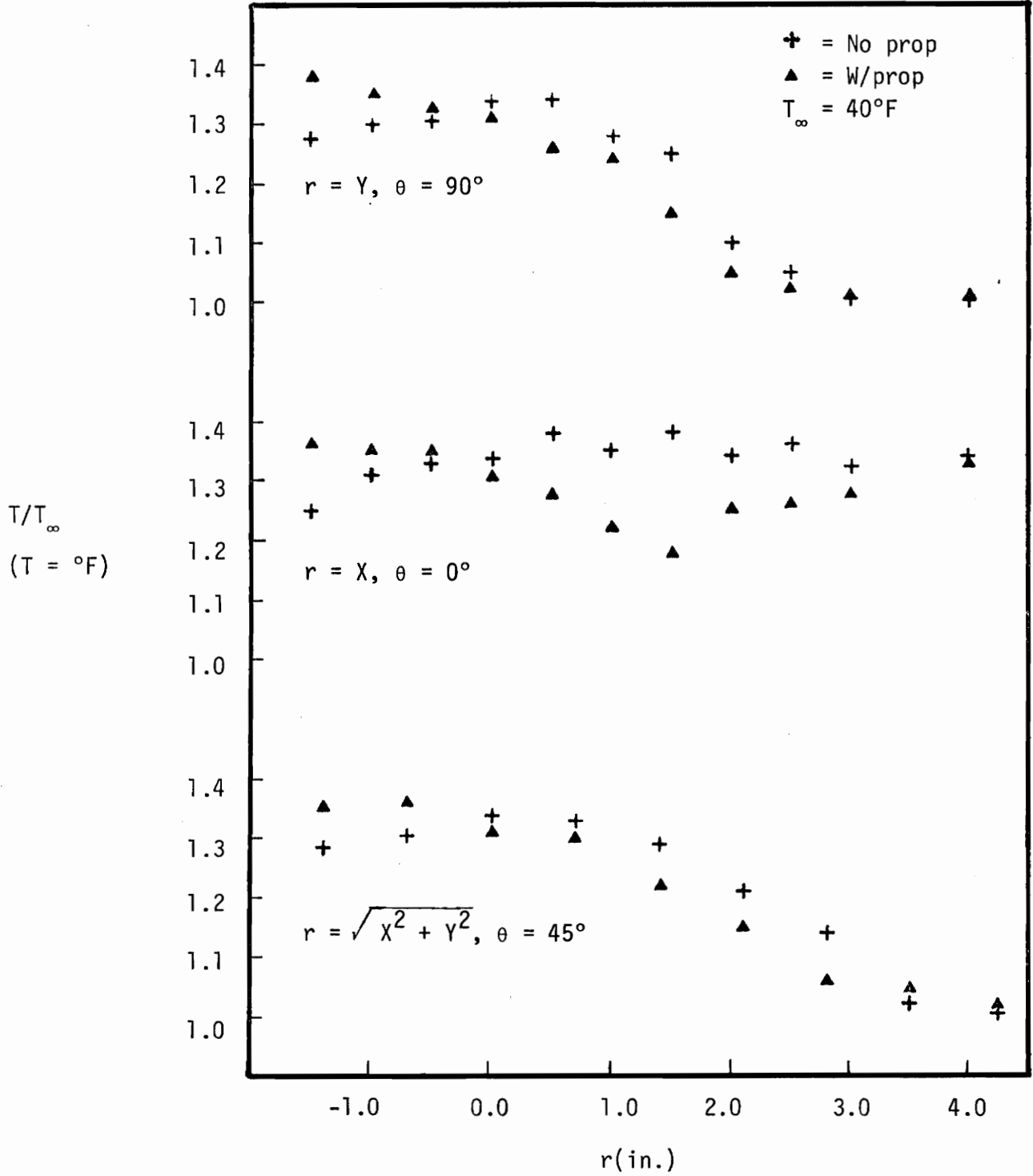


Figure 39

Temperature Distributions in the Wake at
Z/D = 4.0

$$\sqrt{\frac{u'^2}{U_\infty}}$$

$$\sqrt{\frac{v'^2}{U_\infty}}$$

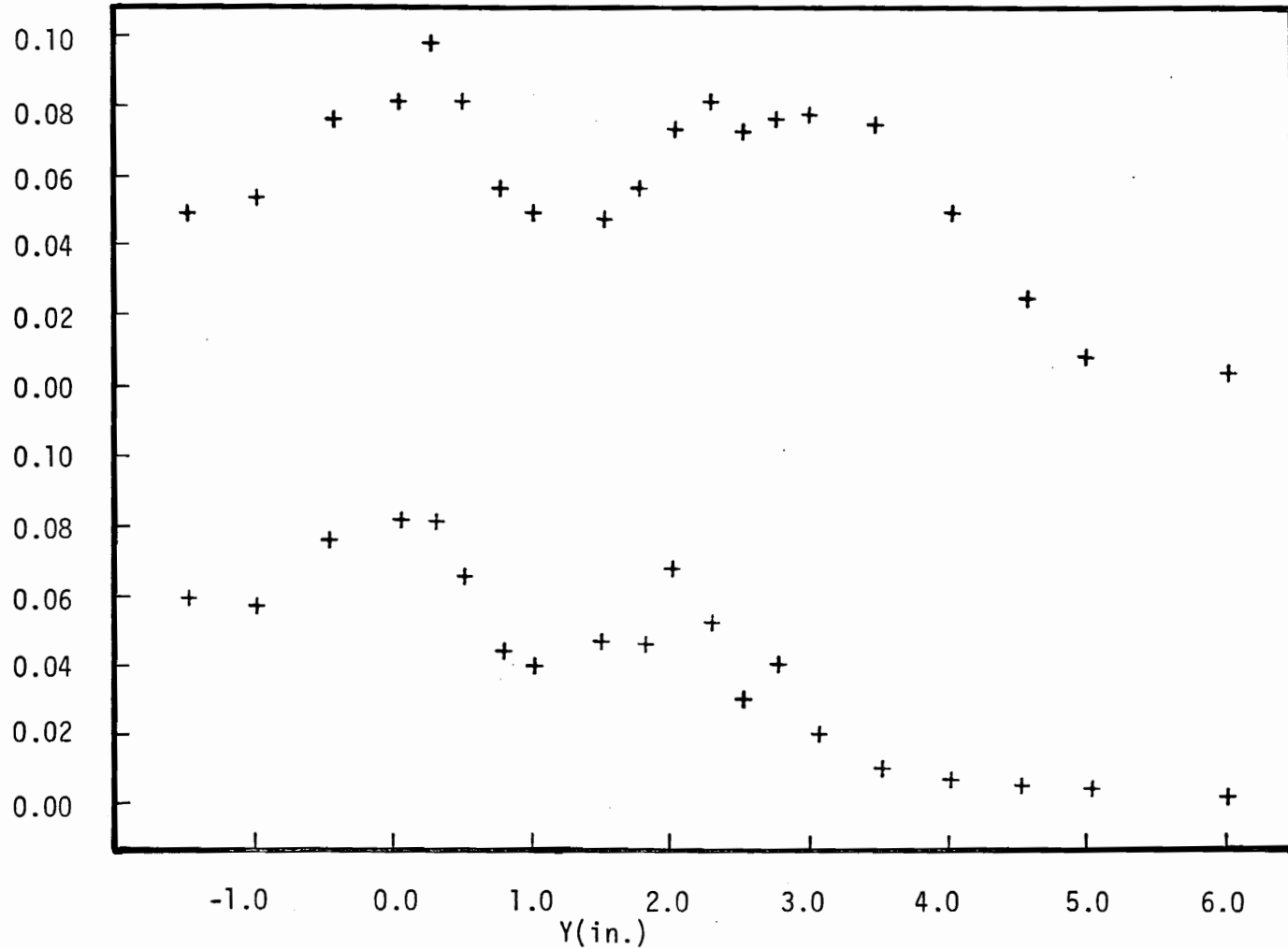


Figure 40

Axial and Radial Turbulence Intensity Distribution at $Z/D = 0.33$, $X = 0$,
 $\theta = 90^\circ$

$$\sqrt{\frac{u'^2}{U_\infty}}$$

$$\sqrt{\frac{v'^2}{U_\infty}}$$

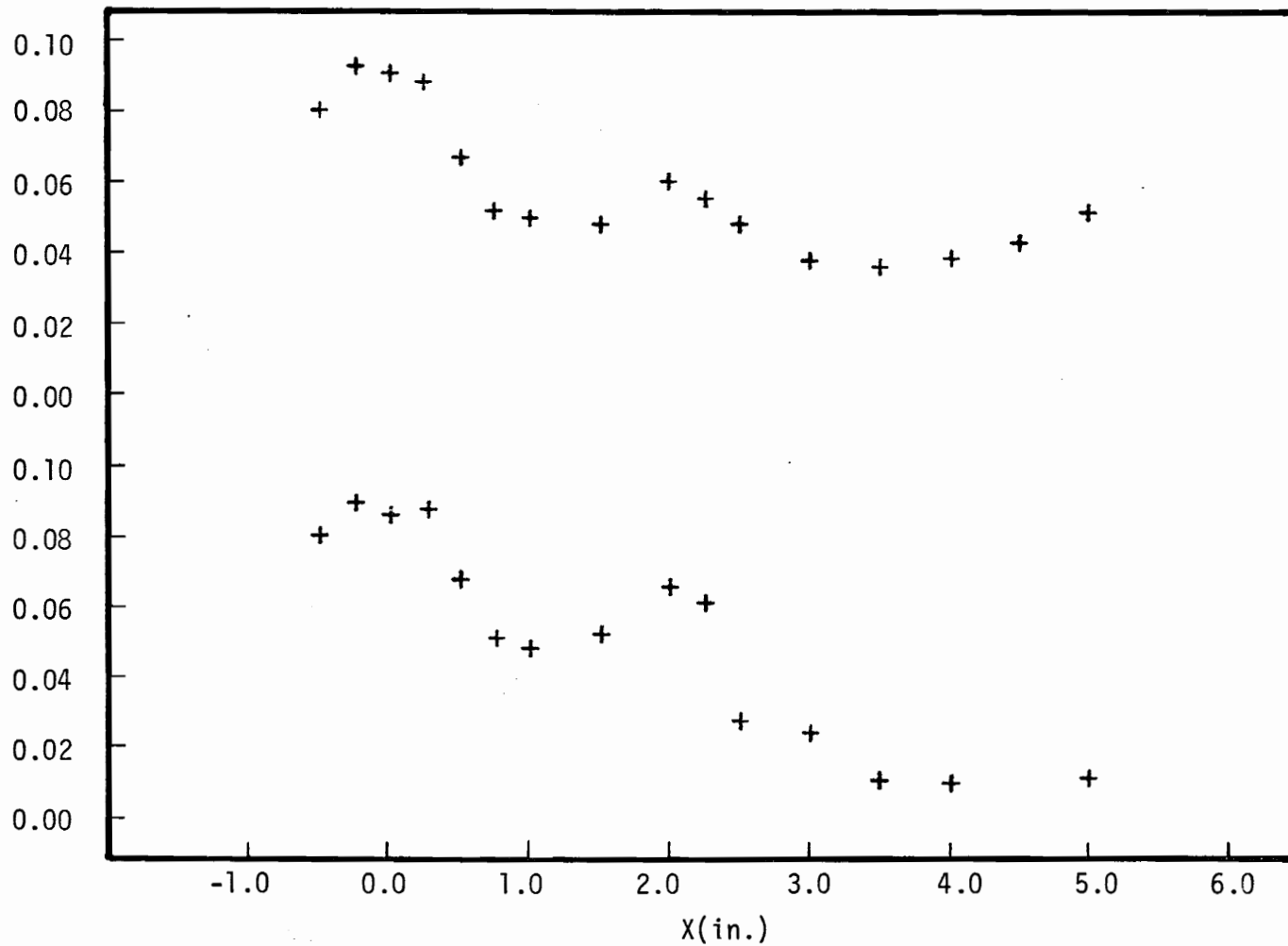


Figure 41

Axial and Radial Turbulence Intensity Distribution at
 $Z/D = 0.33, Y = 0, \theta = 0^\circ$

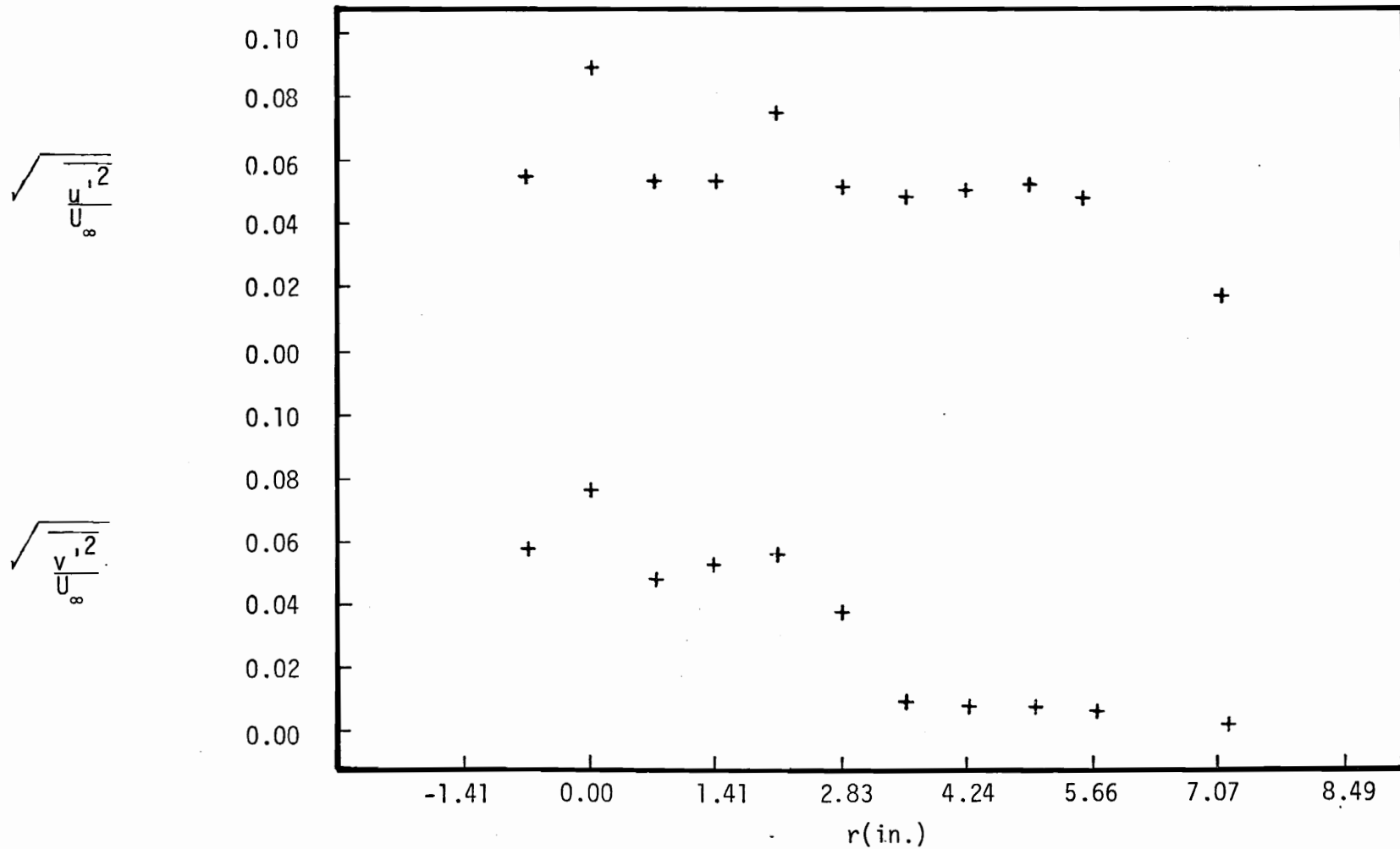


Figure 42

Axial and Radial Turbulence Intensity Distribution at
 $Z/D = 0.33, Y = X, \theta = 45^\circ$

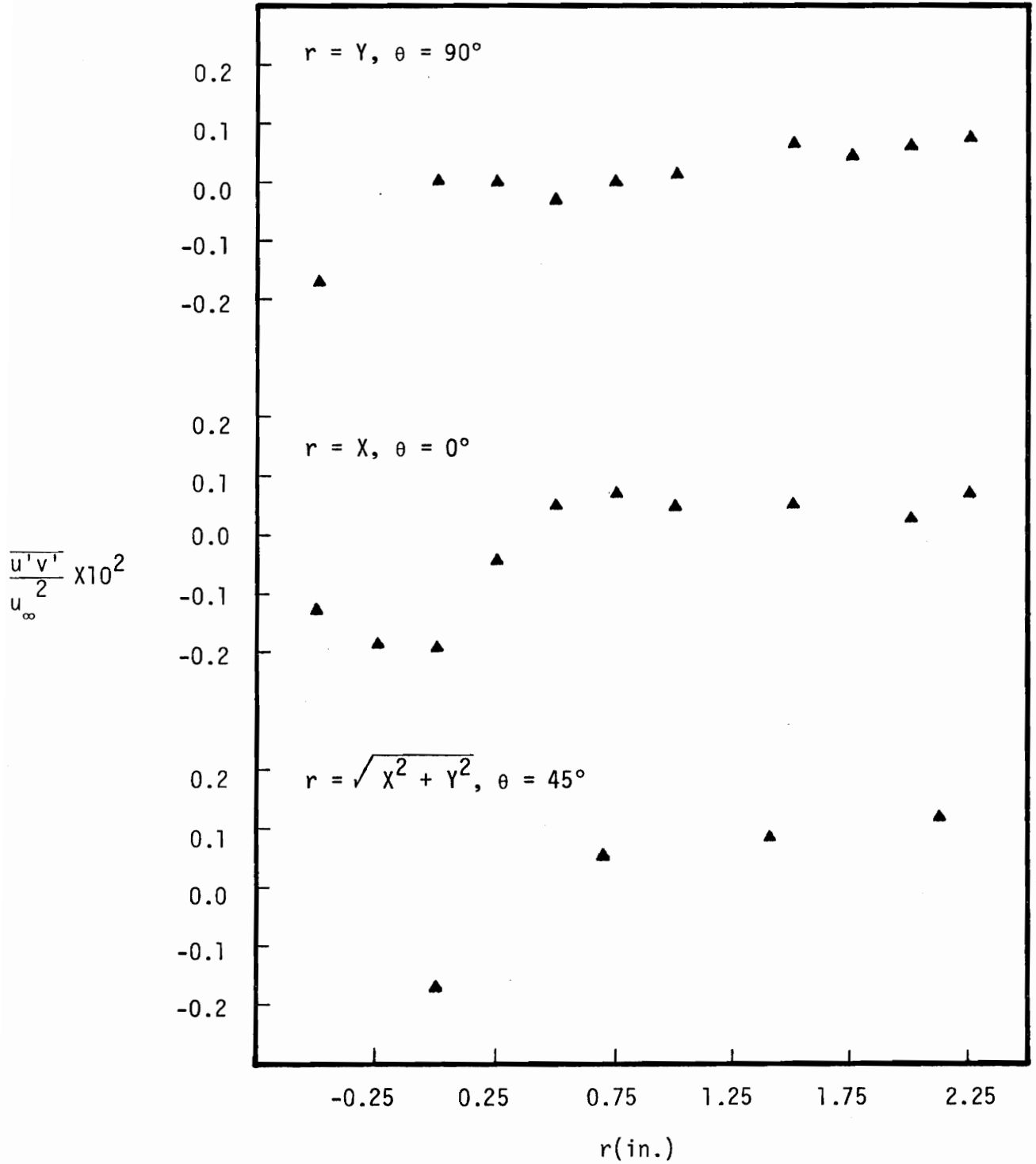


Figure 43

Radial Shear Stream Distribution
at $Z/D = 0.33$.

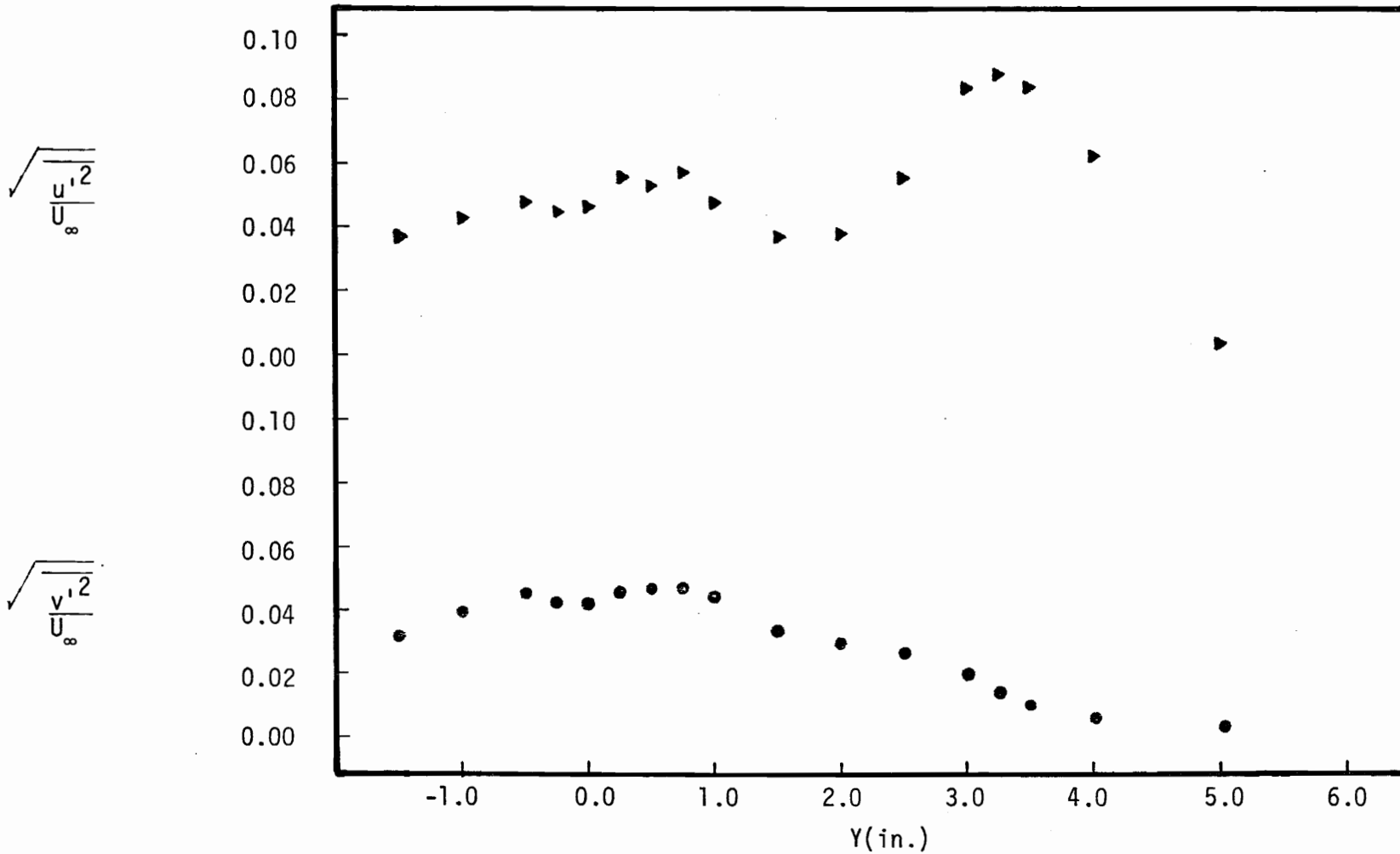


Figure 44

Axial and Radial Turbulence Intensity Distribution at
 $Z/D = 4.0, X = 0, \theta = 90^\circ$

$$\sqrt{\frac{u'^2}{U_\infty^2}}$$

$$\sqrt{\frac{v'^2}{U_\infty^2}}$$

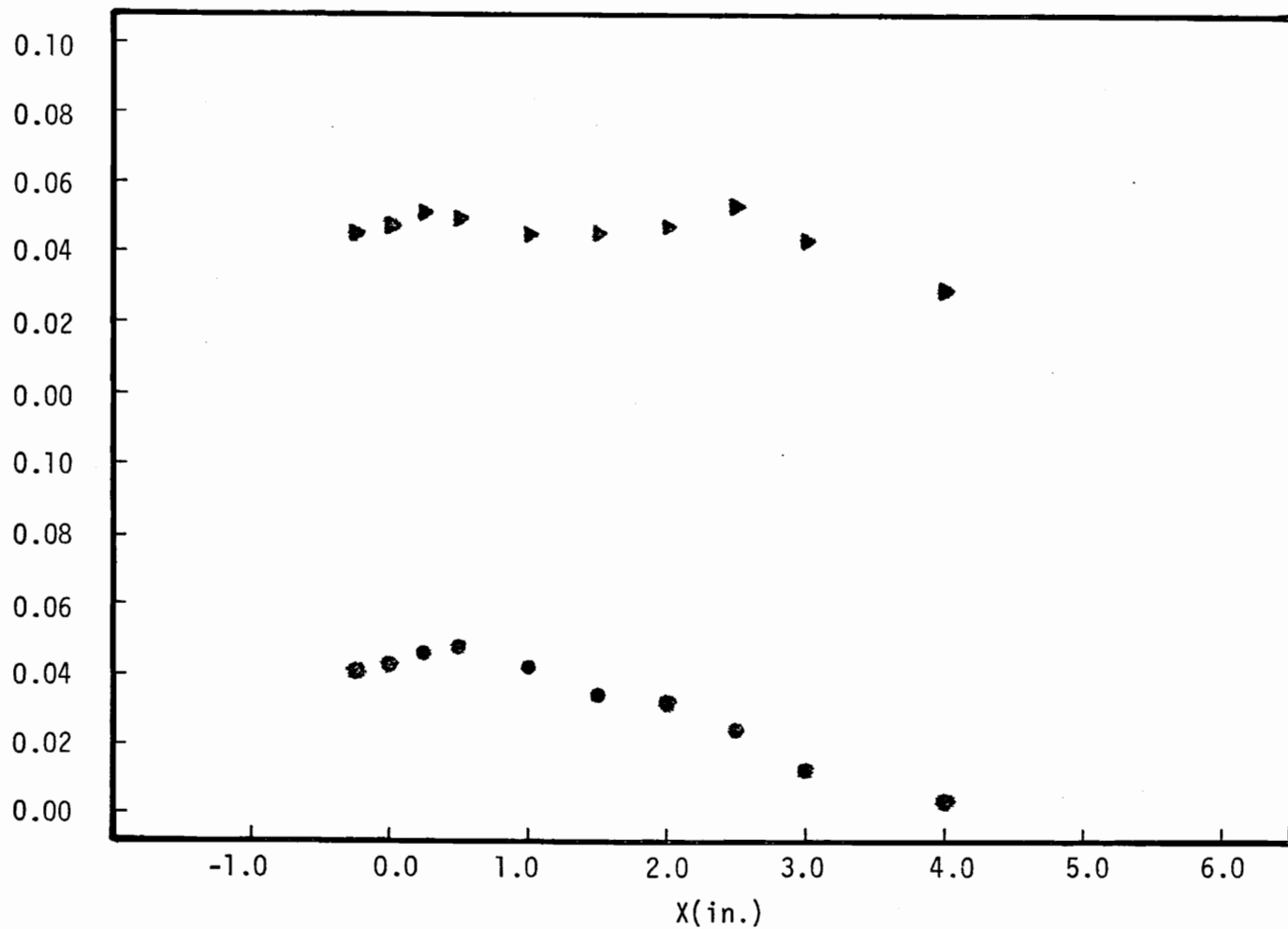


Figure 45

Axial and Radial Turbulence Intensity Distribution at
 $Z/D = 4.0, Y = 0, \theta = 0^\circ$

$$\frac{\sqrt{u'^2}}{U_\infty}$$

$$\frac{\sqrt{v'^2}}{U_\infty}$$

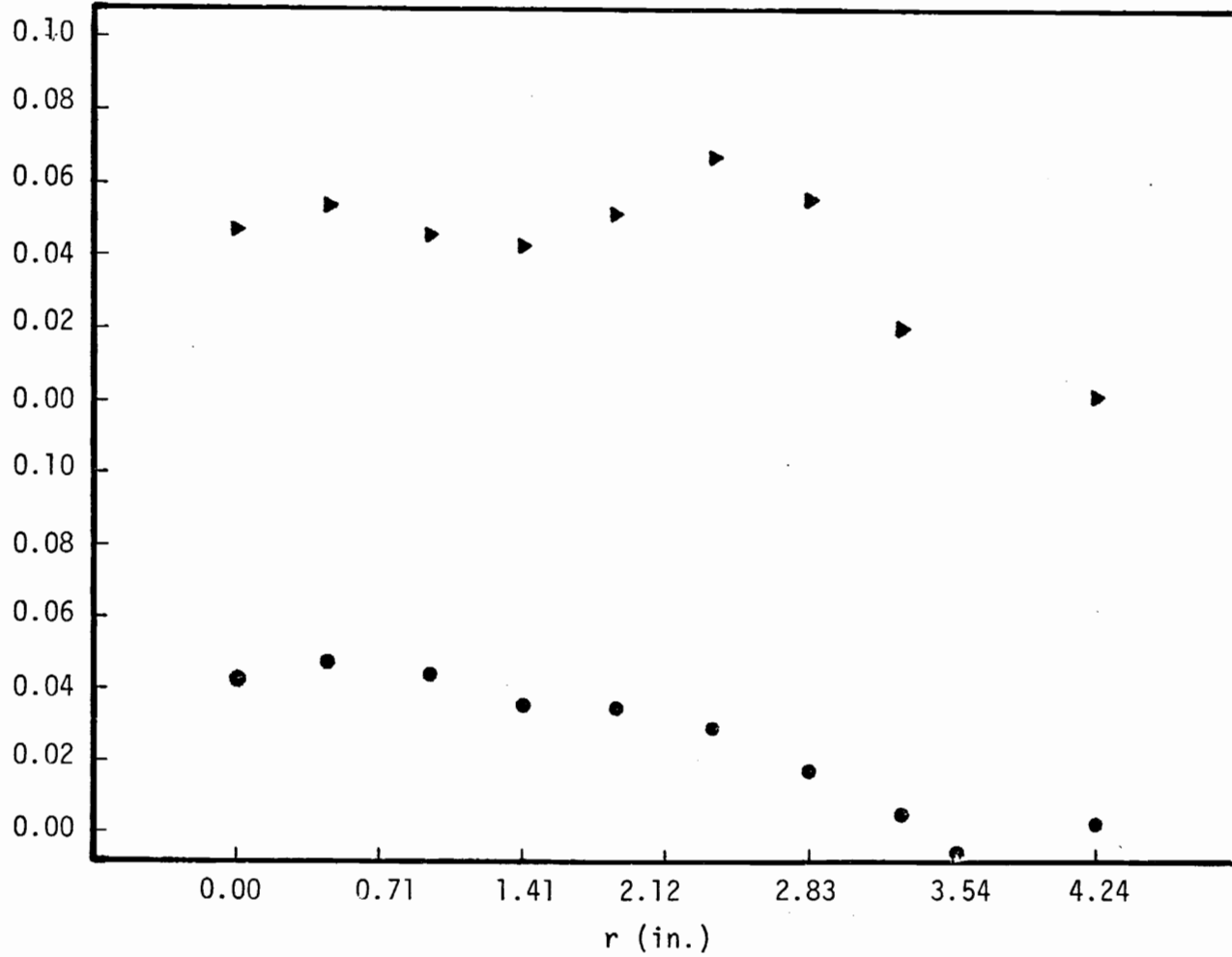


Fig. 46 Axial and Radial Turbulence Intensity Distribution at $Z/D = 4.0$,
 $y = x$, $\theta = 45^\circ$

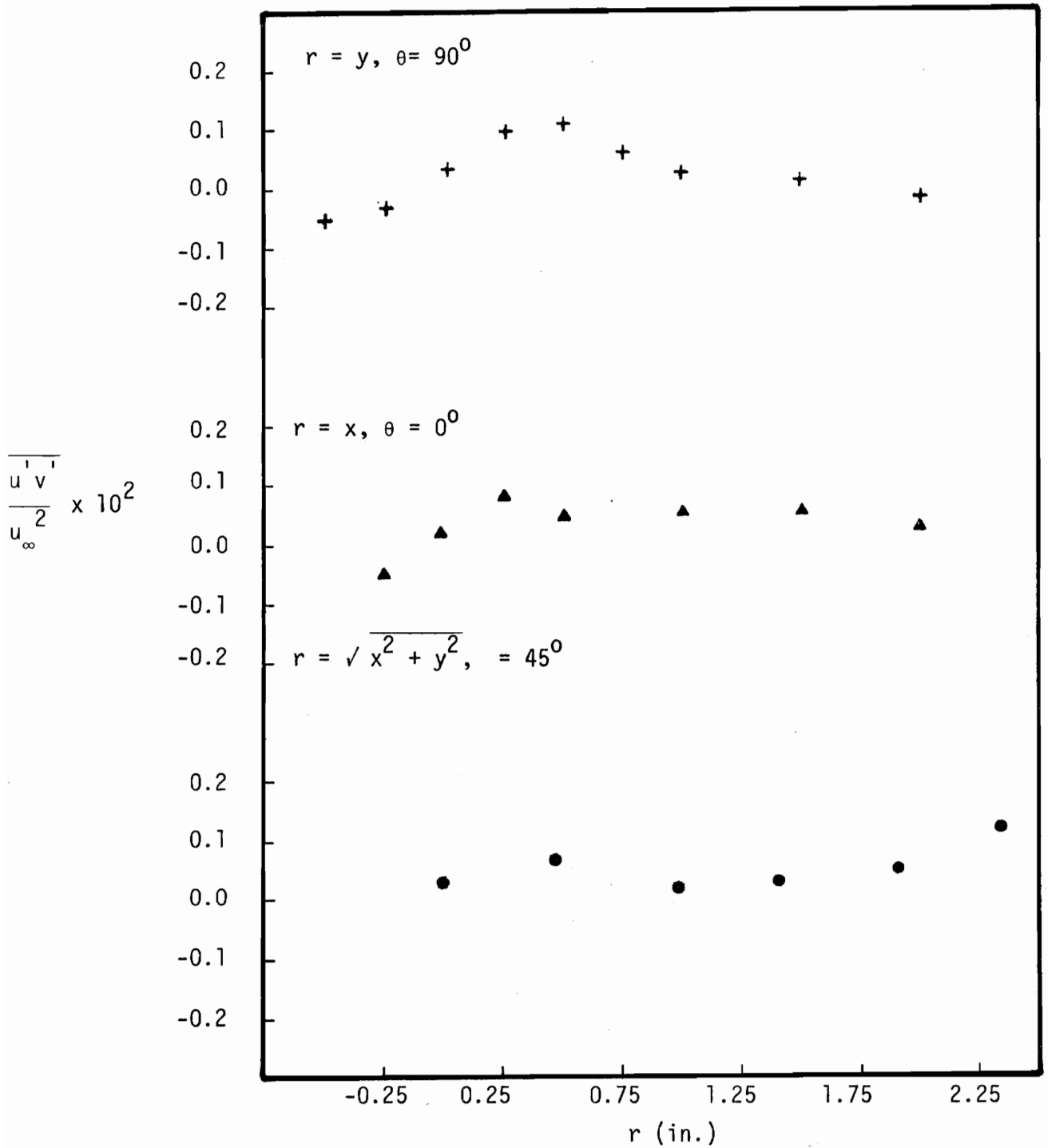


Fig. 47 Radial Shear Stress Distributions at $Z/D = 4.0$

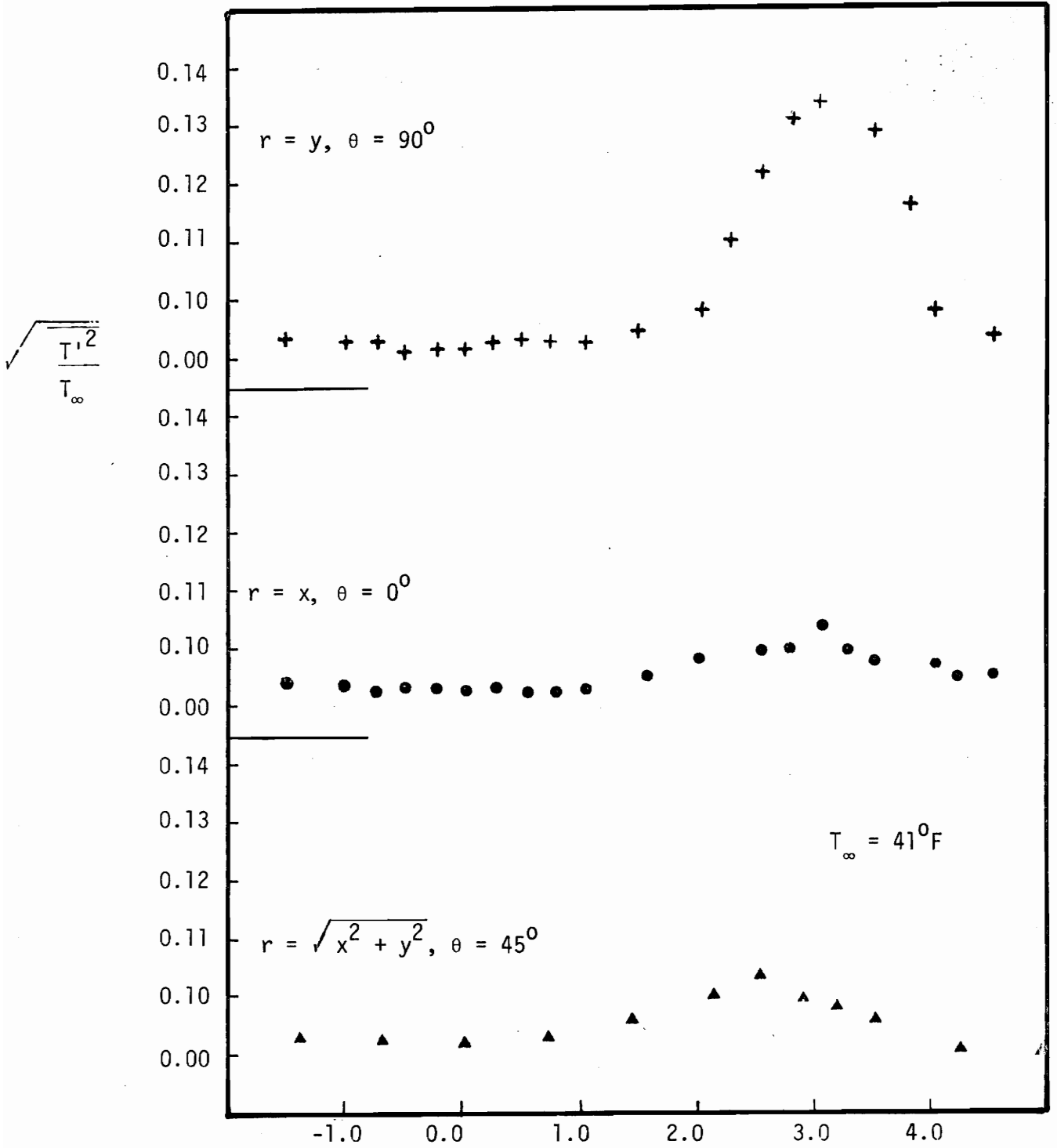


Fig. 48 Temperature Fluctuation Distribution at $Z/D = 0.33$

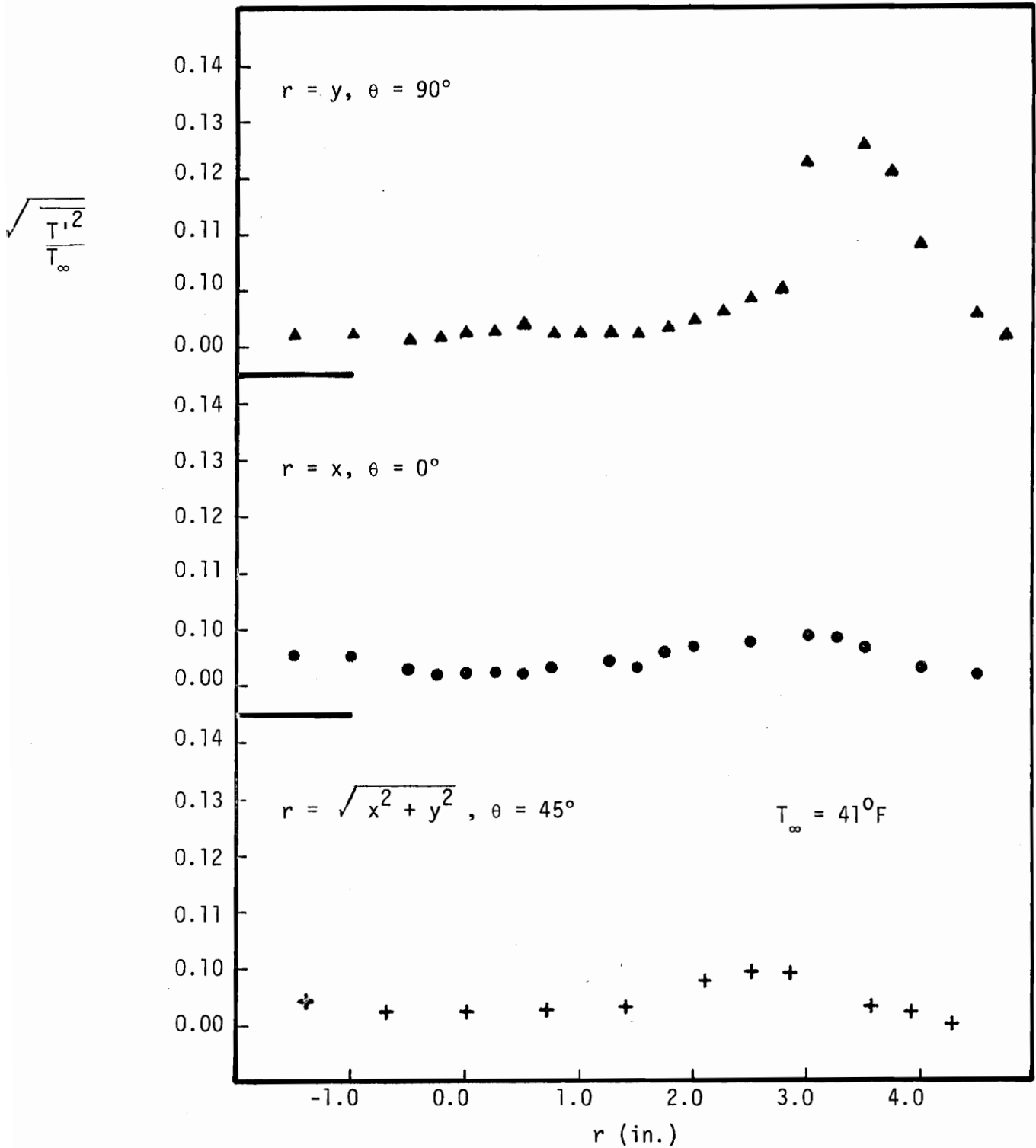


Fig. 49 Temperature Fluctuation Distribution at $Z/D = 4.0$

APPENDIX A

TABULATED DATA

TABLE A-1

Mean Velocity and Temperature Profiles on Body at $Z'/D = 2.67$
 Injection Temperature = $212^{\circ}\text{F} - 217^{\circ}\text{F}$
 Free Stream Properties: $T_{\infty} = 72^{\circ}\text{F}$, $P_{S\infty} = 27.91 \text{ in. Hg}$, $u_{\infty} = 69.33 \text{ ft/sec.}$

$Y'(\text{in.})$	u/u_{∞}	T/T_{∞} ($T = ^{\circ}\text{F}$)
0.0050	0.510	1.458
0.0194	0.543	1.458
0.0340	0.752	1.458
0.0450	0.763	1.458
0.0586	0.848	1.458
0.0722	0.955	1.458
0.0858	1.000	1.458
0.0994	1.010	1.458
0.1260	1.022	1.458
0.1540	1.023	1.444
0.1820	1.025	1.444
0.2360	1.026	1.431
0.2960	1.026	1.417
0.3560	1.025	1.375
0.4160	1.023	1.347
0.4760	1.021	1.319
0.5660	1.019	1.278
0.6560	1.015	1.222
0.7460	1.014	1.208
0.8360	1.012	1.181
0.9560	1.009	1.125
1.0760	1.006	1.097
1.1960	1.005	1.069
2.0800	1.000	1.000

TABLE A-2

Mean Velocity and Temperature Profiles on Body at $Z'/D = 4.67$
 Injection Temperature = $212^{\circ}\text{F} - 217^{\circ}\text{F}$
 Free Stream Properties: $T_{\infty} = 69^{\circ}\text{F}$, $P_{S_{\infty}} = 27.81$, $u_{\infty} = 69.26$ ft/sec

Y' (in.)	u/u_{∞}	T/T_{∞} ($T = ^{\circ}\text{F}$)
0.0050	0.476	1.435
0.0194	0.500	1.435
0.0340	0.707	1.435
0.0450	0.698	1.435
0.0586	0.764	1.435
0.0722	0.790	1.435
0.0858	0.808	1.435
0.1260	0.864	1.435
0.1540	0.876	1.435
0.1820	0.922	1.435
0.2360	0.965	1.420
0.2960	1.007	1.406
0.3560	1.025	1.391
0.4160	1.028	1.377
0.4760	1.026	1.348
0.5660	1.024	1.319
0.6560	1.022	1.290
0.7460	1.019	1.246
0.8360	1.017	1.217
0.9560	1.015	1.174
1.0760	1.012	1.130
1.1960	1.009	1.087
2.1100	1.000	1.000

TABLE A-3

Mean Velocity and Temperature Profiles on Body at $Z'/D = 6.67$
 Injection Temperature = $212^{\circ}\text{F} - 217^{\circ}\text{F}$
 Free Stream Properties: $T_{\infty} = 69^{\circ}\text{F}$, $P_{S\infty} = 27.91$, $u_{\infty} = 69.14$

Y' (in.)	u/u_{∞}	T/T_{∞} ($T = ^{\circ}\text{F}$)
0.0050	0.440	1.406
0.0194	0.570	1.406
0.0340	0.638	1.406
0.0450	0.650	1.406
0.0586	0.699	1.406
0.0722	0.704	1.406
0.0858	0.740	1.406
0.1260	0.777	1.406
0.1540	0.801	1.406
0.1820	0.838	1.391
0.2360	0.873	1.391
0.2960	0.927	1.391
0.3560	1.954	1.391
0.4160	0.979	1.377
0.4760	1.999	1.362
0.5660	1.009	1.333
0.6560	1.012	1.290
0.7460	1.013	1.275
0.8360	1.014	1.246
0.9560	1.013	1.203
1.0760	1.010	1.159
1.1960	1.008	1.130
2.0900	1.000	1.000

TABLE A-4

Mean Velocity and Temperature Profiles on Body at $Z'/D = 8.67$

Injection Temperature = $212^{\circ}\text{F} - 217^{\circ}\text{F}$

Free Stream Properties: $T_{\infty} = 68^{\circ}\text{F}$, $P_{S\infty} = 27.90$, $u_{\infty} = 69.08$ ft/sec

Y' (in.)	u/u_{∞}	T/T_{∞} ($T = ^{\circ}\text{F}$)
0.0050	0.400	1.397
0.0194	0.450	1.397
0.0340	0.545	1.397
0.0450	0.620	1.397
0.0586	0.680	1.397
0.0722	0.700	1.397
0.0858	0.720	1.397
0.1260	1.751	1.397
0.1540	1.752	1.382
0.1820	0.795	1.382
0.2360	0.826	1.368
0.2960	0.871	1.368
0.3560	1.905	1.368
0.4160	1.926	1.353
0.4760	0.952	1.338
0.5660	0.976	1.294
0.6560	0.990	1.265
0.7460	0.996	1.250
0.8360	1.999	1.221
0.9560	1.004	1.176
1.0760	1.001	1.147
1.1960	1.000	1.118
2.3600	1.000	1.000

TABLE A-5

Mean Velocity and Temperature Profiles on Body at $Z'/D = 10.0$
 Injection Temperature = $212^{\circ}\text{F} - 217^{\circ}\text{F}$
 Free Stream Properties: $T_{\infty} = 68^{\circ}\text{F}$, $P_{S\infty} = 27.90$, $u_{\infty} = 69.08 \text{ ft/sec}$

$Y'(\text{in.})$	u/u_{∞}	T/T_{∞} ($T = ^{\circ}\text{F}$)
0.0050	0.380	1.368
0.0194	1.450	1.368
0.0340	0.500	1.368
0.0450	0.540	1.368
0.0586	0.617	1.368
0.0722	0.630	1.368
0.0858	0.647	1.368
0.1260	1.678	1.353
0.1540	1.740	1.353
0.1820	1.770	1.353
0.2360	0.816	1.353
0.2960	0.827	1.353
0.3560	1.846	1.353
0.4160	0.873	1.338
0.4760	1.906	1.324
0.5660	0.940	1.309
0.6560	0.970	1.294
0.7460	1.997	1.265
0.8360	1.012	1.235
0.9560	1.013	1.206
1.0760	1.010	1.162
1.1960	1.009	1.147
2.4000	1.000	1.000

TABLE A-6

Mean Velocity and Temperature Profiles in the Wake at $Z/D = 0.33$
 Injection Temperature = $182^{\circ}\text{F} - 191^{\circ}\text{F}$, $Q = 1.0$ in. H_2O

$x(\text{in.})$	$Y(\text{in.})$	$P_{S\infty}(\text{in.Hg})$	$FP(\text{Deg})$	$FY(\text{Deg})$	U_Z/U_{∞}	$P_S - P_{S\infty}(\text{psf})$	$T(^{\circ}\text{F}, \text{No prop})$	$T(^{\circ}\text{F}, \text{W/prop})$
0.0	-1.5	28.01	2.19	- 5.34	1.03	0.43	53.5	55.0
0.0	-1.0	28.01	2.29	- 7.54	0.99	0.39	54.0	56.5
0.0	-0.5	28.01	2.36	-11.32	0.82	0.09	55.5	58.5
0.0	0.0	28.01	0.89	- 1.16	0.53	-0.27	58.0	58.5
0.0	0.5	28.02	0.37	8.59	0.82	0.16	59.5	58.0
0.0	1.0	28.02	0.62	8.84	0.99	0.52	58.5	56.0
0.0	1.5	28.02	0.62	7.46	1.06	0.49	56.5	52.5
0.0	2.0	28.02	0.99	6.24	1.07	0.39	50.5	49.5
0.0	2.5	28.01	0.34	0.89	0.92	0.35	44.5	43.5
0.0	3.0	28.01	0.05	- 0.69	0.94	0.30	43.0	43.0
0.0	4.0	28.00	0.07	- 1.04	0.97	0.26	43.0	43.0
-1.5	0.0	28.00	8.10	0.89	1.02	0.40	56.0	58.5
-1.0	0.0	28.00	9.14	0.19	0.96	0.41	55.0	59.5
-0.5	0.0	27.99	10.10	- 0.09	0.81	0.05	57.0	59.0
0.5	0.0	27.99	-7.96	- 1.69	0.86	0.05	60.0	57.5
1.0	0.0	27.97	-6.33	- 0.99	1.02	0.26	61.0	56.0
1.5	0.0	27.97	-4.19	- 0.84	1.07	0.33	60.0	55.5
2.0	0.0	27.95	-3.84	- 0.51	1.05	0.17	59.5	53.5
2.5	0.0	27.95	0.22	- 0.79	0.92	0.35	61.0	55.0
3.0	0.0	27.94	1.28	- 0.66	0.98	0.31	60.5	57.0
4.0	0.0	27.91	1.11	- 0.81	0.98	0.24	61.0	61.0
-1.5	-1.5	28.00	4.06	- 1.64	0.97	0.27	56.0	57.0
-1.0	-1.0	27.99	6.43	- 3.81	1.02	1.44	56.5	59.0
-0.5	-0.5	27.99	7.56	- 6.51	0.91	0.32	58.0	59.0
0.5	0.5	27.98	-5.66	5.16	0.91	0.11	59.5	57.5

TABLE A-6 (Continued)

x(in.)	Y(in.)	$P_{S\infty}$ (in.Hg)	FP(Deg)	FY(Deg)	U_Z/U_∞	$P_S - P_{S\infty}$ (psf)	T(°F, No prop)	T(°F, W/prop)
1.0	1.0	27.98	-3.50	4.11	1.03	0.40	58.5	54.5
1.5	1.5	27.97	-1.85	2.19	0.99	0.37	55.0	51.5
2.0	2.0	27.97	0.30	- 0.46	0.94	0.37	43.5	43.0
2.5	2.5	27.94	0.27	- 0.76	0.96	0.33	43.0	43.0
3.0	3.0	27.94	0.20	- 0.76	0.98	0.26	43.0	43.0
4.0	4.0	27.92	0.69	- 1.54	1.01	0.23	43.0	43.0

TABLE A-7

Mean Velocity and Temperature Profiles in the Wake at $Z/D = 1.0$
 Injection Temperature = $193^{\circ}\text{F} - 196^{\circ}\text{F}$, $Q = 1.0 \text{ in. H}_2\text{O}$

x(in.)	Y(in.)	$P_{S\infty}$ (in.Hg)	FP(Deg)	FY(Deg)	U_Z/U_{∞}	$P_S - P_{S\infty}$ (psf)	T($^{\circ}\text{F}$, No prop)	T($^{\circ}\text{F}$, W/prop)
0.0	-1.5	27.64	1.45	-5.06	1.01	0.18	58.0	60.0
0.0	-1.0	27.63	1.63	-5.39	0.95	0.16	58.0	60.5
0.0	-0.5	27.63	2.39	-5.96	0.80	0.04	60.5	61.0
0.0	0.0	27.63	2.71	-0.56	0.66	-0.11	61.0	61.0
0.0	0.5	27.61	1.97	6.01	0.80	0.12	61.0	60.0
0.0	1.0	27.61	1.13	5.49	0.94	0.25	60.5	58.0
0.0	1.5	27.61	1.33	4.09	1.04	0.25	56.0	54.5
0.0	2.0	27.60	0.99	3.74	1.03	1.23	54.5	50.5
0.0	2.5	27.60	0.62	-0.69	0.92	0.22	47.5	46.0
0.0	3.0	27.60	0.12	-0.51	0.98	0.21	46.0	46.0
-1.5	0.0	27.59	4.75	-0.34	1.02	0.17	60.0	63.5
-1.0	0.0	27.59	6.21	-0.06	0.95	0.20	60.0	63.5
-0.5	0.0	27.58	8.79	-0.11	0.90	0.02	61.0	62.5
0.5	0.0	27.58	-5.81	-0.09	0.80	-0.15	63.5	60.5
1.0	0.0	27.58	-5.74	0.34	0.98	-0.02	64.5	59.0
1.5	0.0	27.58	-4.36	0.24	1.04	0.00	64.0	58.5
2.0	0.0	27.58	-4.31	0.49	1.04	0.03	61.5	58.5
2.5	0.0	27.57	-0.17	-0.49	0.92	0.23	61.5	60.0
3.0	0.0	27.56	-0.62	-0.74	0.97	0.24	63.5	62.5
4.0	0.0	27.56	0.12	-0.89	0.97	0.24	61.0	62.5
-1.5	-1.5	27.55	2.56	-1.49	0.93	0.13	58.0	60.0
-1.0	-1.0	27.55	5.37	-2.91	1.03	0.19	59.0	61.0
-0.5	-0.5	27.55	7.19	-3.79	0.96	0.17	60.0	61.5
0.5	0.5	27.55	-4.36	5.64	0.86	0.05	62.5	59.5

TABLE A-7 (Continued)

x(in.)	Y(in.)	$P_{S\infty}$ (in.Hg)	FP(Deg)	FY(Deg)	U_Z/U_∞	$P_S - P_{S\infty}$ (psf)	T(°F, No prop)	T(°F, W/prop)
1.0	1.0	27.55	-2.59	3.49	1.03	0.20	61.0	55.5
1.5	1.5	27.55	-1.45	1.74	0.95	0.24	56.5	49.0
2.0	2.0	27.55	-0.44	-0.09	0.98	0.11	48.0	46.0
2.5	2.5	27.56	0.34	-0.69	0.97	0.24	46.0	46.0
3.0	3.0	27.56	0.17	-0.89	0.98	0.23	46.0	46.0
4.0	4.0	27.56	0.25	-0.91	0.98	0.21	46.0	46.0

TABLE A-8

Mean Velocity and Temperature Profiles in the Wake at $Z/D = 2.0$
 Injection Temperature = $189^{\circ}\text{F} - 195^{\circ}\text{F}$, $Q = 1.0 \text{ in. H}_2\text{O}$

x(in.)	Y(in.)	$P_{S_{\infty}}$ (in.Hg)	FP(Deg)	FY(Deg)	U_Z/U_{∞}	$P_S - P_{S_{\infty}}$ (psf)	T($^{\circ}\text{F}$, No prop)	T($^{\circ}\text{F}$, W/prop)
0.0	-1.5	27.49	1.28	-5.01	1.02	0.11	52.5	55.5
0.0	-1.0	27.49	1.70	-5.94	0.94	0.07	53.5	54.5
0.0	-0.5	27.49	2.29	-5.16	0.81	-0.05	54.5	54.5
0.0	0.0	27.49	1.90	0.49	0.74	-0.16	55.5	54.5
0.0	0.5	27.48	1.23	5.41	0.87	0.06	55.5	53.5
0.0	1.0	27.48	1.06	4.74	0.96	0.14	54.0	51.0
0.0	1.5	27.48	0.76	4.39	1.05	0.15	51.0	49.0
0.0	2.0	27.47	0.62	2.01	0.96	0.15	48.0	45.0
0.0	2.5	27.47	0.22	-0.31	0.95	0.12	43.0	42.0
0.0	3.0	27.47	0.32	-0.99	0.99	0.13	41.5	41.0
0.0	4.0	27.46	0.27	-0.91	0.98	0.14	41.0	41.0
-1.5	0.0	27.48	5.10	-0.39	1.03	0.08	53.5	57.0
-1.0	0.0	27.47	6.01	0.21	0.98	0.08	54.0	56.5
-0.5	0.0	27.47	6.35	0.76	0.87	0.01	54.5	56.0
0.5	0.0	27.47	-4.16	0.46	0.84	-0.15	56.5	54.0
1.0	0.0	27.47	-4.68	0.11	0.97	-0.09	56.5	51.5
1.5	0.0	27.48	-2.78	-0.04	1.03	-0.03	45.4	49.0
2.0	0.0	27.48	-3.03	0.24	1.04	-0.04	56.5	49.0
2.5	0.0	27.48	0.34	-0.31	0.95	0.06	53.5	50.0
3.0	0.0	27.48	0.25	-0.34	0.97	0.15	54.5	53.5
4.0	0.0	27.48	0.76	-0.06	1.00	0.07	55.0	54.5
-1.5	-1.5	27.48	2.81	-1.66	0.96	0.06	53.5	54.5
-1.0	-1.0	27.48	4.98	-2.96	1.04	0.08	52.5	54.5
-0.5	-0.5	27.48	5.74	-3.41	0.91	0.05	54.5	55.0
0.5	0.5	27.48	-3.42	3.69	0.88	-0.01	56.0	54.0

TABLE A-8 (Continued)

x(in.)	Y(in.)	$P_{S\infty}$ (in.Hg)	FP(Deg)	FY(Deg)	U_Z/U_∞	$P_S - P_{S\infty}$ (psf)	T(°F, No prop)	T(°F, W/prop)
1.0	1.0	27.49	-2.12	3.11	1.05	0.08	55.5	53.5
1.5	1.5	27.49	-0.54	0.84	0.95	0.14	52.0	49.0
2.0	2.0	27.49	0.52	-0.66	0.97	0.14	44.5	42.0
2.5	2.5	27.50	0.54	-1.09	0.98	0.16	41.0	41.0
3.0	3.0	27.50	0.67	-10.1	0.98	0.15	41.0	41.0

TABLE A-9

Mean Velocity and Temperature Profiles in the Wake at Z/D = 3.0
 Injection Temperature - 186°F - 191°F, Q = 1.0 in. H₂O

x(in.)	Y(in.)	P _{S∞} (in.Hg)	FP(Deg)	FY(Deg)	U _Z /U _∞	P _S - P _{S∞} (psf)	T(°F, No prop)	T(°F, W/prop)
0.0	-1.5	27.71	1.06	-5.69	1.04	0.10	47.5	51.5
0.0	-1.0	27.71	1.45	-6.06	0.96	0.02	48.5	51.0
0.0	-0.5	27.72	1.72	-4.89	0.86	-0.05	49.5	50.5
0.0	0.0	27.72	2.29	0.29	0.83	-0.13	50.5	49.5
0.0	0.5	27.72	1.90	4.99	0.93	0.03	50.0	47.5
0.0	1.0	27.73	0.99	4.69	0.99	0.10	48.5	46.5
0.0	1.5	27.73	0.69	4.29	1.06	0.14	46.5	44.5
0.0	2.0	27.73	0.67	2.69	1.00	0.12	42.0	40.0
0.0	2.5	27.73	0.17	-0.39	0.96	0.11	40.0	38.5
0.0	3.0	27.73	0.42	-1.04	0.98	0.12	38.0	38.0
0.0	4.0	27.73	0.20	-1.19	0.99	0.12	38.0	38.0
-1.5	0.0	27.73	5.42	-0.69	1.04	0.08	48.5	52.5
-1.0	0.0	27.74	5.66	-0.11	1.02	0.07	49.5	52.0
-0.5	0.0	27.74	5.91	0.39	0.93	0.02	50.5	51.0
0.5	0.0	27.74	-3.37	0.14	0.87	-0.18	51.5	47.5
1.0	0.0	27.74	-4.80	-0.24	0.98	-0.13	52.5	45.5
1.5	0.0	27.74	-4.46	-0.11	1.06	-0.08	52.0	45.0
2.0	0.0	27.74	-3.35	0.19	1.06	-0.06	50.5	45.5
2.5	0.0	27.74	-0.96	-0.24	0.98	-0.00	51.0	49.5
3.0	0.0	27.74	0.07	-0.59	0.97	0.15	51.0	49.5
4.0	0.0	27.74	0.34	-0.44	0.99	0.12	51.5	50.5
-1.5	-1.5	27.75	2.32	-1.49	0.97	0.03	49.0	50.0
-1.0	-1.0	27.75	5.02	-3.66	1.05	0.05	49.5	52.0
-0.5	-0.5	27.75	5.07	-3.29	0.95	0.03	50.5	51.5
0.5	0.5	27.75	-1.97	4.26	0.91	0.00	49.5	48.0

TABLE A-9 (Continued)

x(in.)	Y(in.)	$P_{S\infty}$ (in.Hg)	FP(Deg)	FY(Deg)	U_Z/U_∞	$P_S - P_{S\infty}$ (psf)	T(°F, No prop)	T(°F, W/prop)
1.0	1.0	27.75	-2.66	4.14	1.03	0.08	48.5	45.5
1.5	1.5	27.75	-1.33	1.59	0.97	0.13	44.0	42.0
2.0	2.0	27.75	0.07	-0.94	0.95	0.14	42.0	40.0
2.5	2.5	27.75	0.17	-1.04	0.99	0.14	39.5	39.0
3.0	3.0	27.75	0.07	-1.09	0.98	0.16	38.0	38.0
4.0	4.0	27.75	0.74	-1.31	0.98	0.13	38.0	38.0

TABLE A-10

Mean Velocity and Temperature Profiles in the Wake at $Z/D = 4.0$
 Injection Temperature = $188^{\circ}\text{F} - 193^{\circ}\text{F}$, $Q = 1.0 \text{ in. H}_2\text{O}$

$x(\text{in.})$	$Y(\text{in.})$	$P_{S_{\infty}}(\text{in. Hg})$	FP(Deg)	FY(Deg)	U_Z/U_{∞}	$P_S - P_{S_{\infty}}(\text{psf})$	$T(^{\circ}\text{F}, \text{No prop})$	$T(^{\circ}\text{F}, \text{W/prop})$
0.0	-1.5	27.77	0.86	-5.54	1.02	0.10	51.0	55.0
0.0	-1.0	27.77	0.84	-5.31	0.95	0.05	52.0	54.0
0.0	-0.5	27.77	1.11	-3.99	0.89	-0.01	52.0	53.0
0.0	0.0	27.78	1.03	-0.01	0.86	-0.12	53.5	52.5
0.0	0.5	27.78	0.69	3.96	0.93	0.03	53.5	50.5
0.0	1.0	27.79	0.71	4.79	0.99	0.09	51.0	49.5
0.0	1.5	27.79	0.47	4.16	1.04	0.13	50.0	46.0
0.0	2.0	27.79	0.54	2.44	1.00	0.12	44.0	42.0
0.0	2.5	27.79	0.42	-0.04	0.98	0.01	42.0	41.0
0.0	3.0	27.79	0.37	-0.94	0.99	0.11	41.0	40.0
0.0	4.0	27.79	0.25	-1.11	0.99	0.11	40.0	40.0
-1.5	0.0	27.80	6.55	-0.76	1.06	0.08	50.0	54.5
-1.0	0.0	27.81	6.28	-0.39	1.01	0.05	52.5	54.0
-0.5	0.0	27.81	4.38	0.14	0.92	-0.05	53.0	54.0
0.5	0.0	27.81	-3.00	-0.14	0.92	-0.15	55.0	51.0
1.0	0.0	27.82	-4.78	-0.16	1.01	-0.14	54.0	49.0
1.5	0.0	27.82	-4.98	0.14	1.07	-0.07	55.0	47.0
2.0	0.0	27.82	-3.33	-0.09	1.05	-0.07	53.5	50.0
2.5	0.0	27.82	-0.42	-0.16	0.98	0.00	54.5	50.5
3.0	0.0	27.82	0.17	-0.34	0.97	0.13	53.0	51.0
4.0	0.0	27.83	0.54	-0.14	1.00	0.05	53.5	53.0
-1.5	-1.5	27.85	2.71	-1.99	0.99	0.02	50.5	53.0
-1.0	-1.0	27.85	4.70	-3.84	1.03	0.05	51.0	54.0
-0.5	-0.5	27.85	4.26	-3.44	0.94	-0.03	52.0	54.5
0.5	0.5	27.84	-2.12	2.96	0.94	0.03	53.0	52.0
1.0	1.0	27.84	-2.93	3.84	1.05	0.06	51.5	49.0

TABLE A-10 (Continued)

x(in.)	Y(in.)	$P_{S\infty}$ (in.Hg)	FP(Deg)	FY(Deg)	U_Z/U_∞	$P_S - P_{S\infty}$ (psf)	T(°F, No prop)	T(°F, W/prop)
1.5	1.5	27.84	-0.74	1.14	0.98	0.11	48.5	46.0
2.0	2.0	27.83	0.30	-0.56	0.98	0.12	45.5	42.0
2.5	2.5	27.83	0.34	-0.99	0.99	0.11	41.0	41.5
3.0	3.0	27.83	0.34	-1.09	0.99	0.12	41.0	41.0

TABLE A-11

Axial and Radial Turbulence Intensities and Radial Shear Stress
 in the Wake at Z/D = 0.33
 Injection Temperature - 192°F - 201°F, Q = 1.0 in. H₂O

x(in.)	Y(in.)	P _{S∞} (in.Hg)	T(°F)	$\frac{\sqrt{u'^2}}{U_\infty}$	$\frac{\sqrt{v'^2}}{U_\infty}$	$\left(\frac{u'v'}{U_\infty^2}\right) \times 10^2$
0.00	-1.50	28.24	65.0	0.050	0.059	-0.096
0.00	-1.00	28.24	66.0	0.054	0.056	-0.092
0.00	-0.50	28.24	68.0	0.076	0.076	-0.170
0.00	0.00	28.24	70.0	0.081	0.083	0.005
0.00	0.25	28.24	70.0	0.098	0.081	0.000
0.00	0.50	28.24	70.0	0.081	0.066	-0.033
0.00	0.75	28.24	71.0	0.056	0.046	-0.005
0.00	1.00	28.24	69.0	0.049	0.041	0.013
0.00	1.50	28.24	65.0	0.048	0.048	0.062
0.00	1.75	28.24	64.0	0.056	0.046	0.044
0.00	2.00	28.24	62.0	0.073	0.068	0.062
0.00	2.25	28.25	60.0	0.081	0.053	0.074
0.00	2.50	28.25	56.0	0.073	0.031	-----
0.00	2.75	28.25	52.0	0.077	0.040	-----
0.00	3.00	28.25	50.0	0.077	0.021	-----
0.00	3.50	28.25	49.0	0.075	0.010	-----
0.00	4.00	28.25	49.0	0.051	0.007	-----
0.00	4.50	28.26	49.0	0.025	0.005	-----
0.00	5.00	28.26	49.0	0.010	0.004	-----
0.00	6.00	28.26	49.0	0.003	0.003	0.000
-0.50	0.00	28.25	69.0	0.080	0.080	-0.127
-0.75	0.00	28.25	70.0	0.093	0.089	-0.186

TABLE A-11 (Continued)

x(in.)	Y(in.)	$P_{S\infty}$ (in.Hg)	T(°F)	$\frac{\sqrt{u'^2}}{U_\infty}$	$\frac{\sqrt{v'^2}}{U_\infty}$	$\left(\frac{u'v'}{U_\infty^2}\right) \times 10^2$
0.00	0.00	28.25	69.0	0.091	0.086	-0.190
0.25	0.00	28.24	69.0	0.087	0.087	-0.046
0.50	0.00	28.24	68.0	0.067	0.065	0.048
0.75	0.00	28.24	67.0	0.052	0.051	0.070
1.00	0.00	28.24	65.0	0.049	0.047	0.047
1.50	0.00	28.24	64.0	0.048	0.052	0.055
2.00	0.00	28.24	66.0	0.060	0.066	0.029
2.25	0.00	28.24	68.0	0.056	0.061	0.072
2.50	0.00	28.24	69.0	0.048	0.028	-----
3.00	0.00	28.24	70.0	0.038	0.025	-0.008
3.50	0.00	28.24	71.0	0.037	0.011	-----
4.00	0.00	28.24	71.0	0.039	0.010	-----
4.50	0.00	28.24	72.0	0.044	0.011	-----
5.00	0.00	28.24	72.0	0.052	0.011	-----
6.70	0.00	28.24	71.0	0.061	0.013	-----
-0.50	-0.50	28.23	72.0	0.056	0.057	-0.095
0.00	0.00	28.23	72.0	0.088	0.075	-0.164
0.50	0.50	28.23	70.0	0.052	0.047	0.056
1.00	1.00	28.23	67.0	0.053	0.051	0.089
1.50	1.50	28.23	62.0	0.073	0.056	0.114
2.00	2.00	28.23	54.0	0.051	0.038	0.003
2.50	2.50	28.23	53.0	0.048	0.009	-----
3.00	3.00	28.22	52.0	0.051	0.008	-----
3.50	3.50	28.22	52.0	0.052	0.007	-----
4.00	4.00	28.22	52.0	0.048	0.006	-----
5.00	5.00	28.22	52.0	0.015	0.001	-----

TABLE A-12

Axial and Radial Turbulence Intensities and Radial Stress
 in the Wake at Z/D = 4.0
 Injection Temperature - 180°F - 184°F, Q = 1.0 in. H₂O

x(in.)	Y(in.)	P _{S∞} (in.Hg)	T(°F)	$\frac{\sqrt{u'^2}}{U_\infty}$	$\frac{\sqrt{v'^2}}{U_\infty}$	$\left(\frac{u'v'}{U_\infty^2}\right) \times 10^2$
0.00	-1.50	27.84	57.0	0.037	0.032	-0.036
0.00	-1.00	27.83	56.0	0.043	0.041	-0.046
0.00	-0.50	27.83	55.0	0.048	0.045	0.055
0.00	-0.25	27.83	54.0	0.045	0.042	0.029
0.00	0.00	27.83	54.0	0.046	0.042	0.039
0.00	0.25	27.83	53.0	0.056	0.046	0.095
0.00	0.50	27.82	52.0	0.052	0.048	0.107
0.00	0.75	27.82	50.0	0.057	0.048	0.063
0.00	1.00	27.82	49.0	0.048	0.044	0.030
0.00	1.50	27.82	47.0	0.037	0.034	0.017
0.00	2.00	27.82	44.0	0.038	0.030	0.011
0.00	2.50	27.81	42.0	0.055	0.016	0.040
0.00	3.00	27.81	42.0	0.085	0.019	-----
0.00	3.25	27.80	42.0	0.088	0.014	-----
0.00	3.50	27.80	41.0	0.085	0.010	-----
0.00	4.00	27.80	41.0	0.063	0.007	-----
0.00	5.00	27.80	41.0	0.004	0.003	-----
-0.25	0.00	27.79	55.0	0.049	0.042	-0.053
0.00	0.00	27.78	54.0	0.050	0.044	0.020
0.25	0.00	27.78	53.0	0.053	0.048	0.075
0.50	0.00	27.78	53.0	0.052	0.050	0.044

TABLE A-12 (Continued)

x(in.)	Y(in.)	$P_{S\infty}$ (in.Hg)	T(°F)	$\frac{\sqrt{u'^2}}{U_\infty}$	$\frac{\sqrt{v'^2}}{U_\infty}$	$\left(\frac{u'v'}{U_\infty^2}\right) \times 10^2$
1.00	0.00	27.78	50.0	0.047	0.044	0.051
1.50	0.00	27.78	49.0	0.048	0.036	0.054
2.00	0.00	27.78	50.0	0.049	0.033	0.029
2.50	0.00	27.78	53.0	0.055	0.025	0.052
3.00	0.00	27.78	53.0	0.045	0.015	0.019
4.00	0.00	27.78	54.0	0.031	0.004	0.004
0.00	0.00	27.77	54.0	0.048	0.043	0.031
0.33	0.33	27.77	54.0	0.054	0.047	0.061
0.67	0.67	27.76	53.0	0.046	0.045	0.023
1.00	1.00	27.76	49.0	0.043	0.036	0.031
1.33	1.33	27.76	49.0	0.053	0.035	0.046
1.67	1.67	27.76	45.0	0.067	0.029	0.125
2.00	2.00	27.76	43.0	0.056	0.018	-----
2.33	2.33	27.76	42.0	0.021	0.006	-----
3.00	3.00	27.76	42.0	0.002	0.003	-----

TABLE A-13

Temperature Fluctuations in the Wake at $Z/D = 0.33$
 Injection Temperature = $172^{\circ}\text{F} - 178^{\circ}\text{F}$, $Q = 1.0 \text{ in. H}_2\text{O}$, $T_{\infty} = 41^{\circ}\text{F}$

$x(\text{in.})$	$Y(\text{in.})$	$P_{S_{\infty}}(\text{in.})$	$\frac{\sqrt{T'^2}}{T_{\infty}}$
0.00	-1.50	27.57	0.038
0.00	-1.00	27.57	0.031
0.00	-0.75	27.57	0.022
0.00	-0.50	27.57	0.011
0.00	-0.25	27.57	0.014
0.00	0.00	27.57	0.017
0.00	0.25	27.58	0.026
0.00	0.50	27.58	0.032
0.00	0.75	27.58	0.024
0.00	1.00	27.58	0.030
0.00	1.50	27.58	0.047
0.00	2.00	27.58	0.081
0.00	2.25	27.58	0.110
0.00	2.50	27.59	0.122
0.00	2.75	27.59	0.130
0.00	3.00	27.59	0.134
0.00	3.25	27.59	0.138
0.00	3.50	27.59	0.128
0.00	3.75	27.59	0.116
0.00	4.00	27.59	0.083
0.00	4.50	27.58	0.030
0.00	5.00	27.58	0.004
0.00	5.50	27.58	0.001
0.00	6.00	27.58	0.001
-1.50	0.00	27.57	0.032
-1.00	0.00	27.57	0.021
-0.85	0.00	27.57	0.019
-0.50	0.00	27.57	0.025
-0.25	0.00	27.57	0.025
0.00	0.00	27.57	0.018
0.25	0.00	27.57	0.020
0.50	0.00	27.57	0.018
0.75	0.00	27.57	0.020
1.00	0.00	27.57	0.026
1.50	0.00	27.57	0.043
2.00	0.00	27.57	0.076
2.50	0.00	27.57	0.091
2.75	0.00	27.57	0.100
3.00	0.00	27.57	0.103
3.25	0.00	27.58	0.096

TABLE A-13 (Continued)

x(in.)	Y(in.)	$P_{S_{\infty}}$ (in.)	$\frac{\sqrt{T_1^2}}{T_{\infty}}$
3.50	0.00	27.58	0.089
3.75	0.00	27.58	0.085
4.00	0.00	27.58	0.066
4.25	0.00	27.58	0.057
4.50	0.00	27.58	0.048
5.00	0.00	27.58	0.053
5.50	0.00	27.58	0.044
-1.50	-1.50	27.58	0.053
-1.00	-1.00	27.58	0.044
-0.50	-0.50	27.58	0.031
0.00	0.00	27.58	0.021
0.50	0.50	27.58	0.031
1.00	1.00	27.58	0.061
1.50	1.50	27.58	0.116
1.75	1.75	27.58	0.124
2.00	2.00	27.58	0.109
2.25	2.25	27.58	0.095
2.50	2.50	27.58	0.071
3.00	3.00	27.58	0.013
3.50	3.50	27.58	0.001

TABLE A-14

Temperature Fluctuations in the Wake at $Z/D = 0.33$
 Injection Temperature = $169^{\circ}\text{F} - 174^{\circ}\text{F}$, $Q = 1.0 \text{ in. H}_2\text{O}$, $T_{\infty} = 41^{\circ}\text{F}$

$x(\text{in.})$	$Y(\text{in.})$	$P_{S_{\infty}}(\text{in.})$	$\frac{\sqrt{T'^2}}{T_{\infty}}$
0.00	-1.50	27.54	0.024
0.00	-1.00	27.54	0.022
0.00	-0.50	27.55	0.019
0.00	-0.25	27.54	0.023
0.00	0.00	27.54	0.028
0.00	0.25	27.55	0.032
0.00	0.50	27.55	0.031
0.00	0.75	27.55	0.028
0.00	1.00	27.55	0.027
0.00	1.25	27.55	0.028
0.00	1.50	27.55	0.029
0.00	1.75	27.54	0.034
0.00	2.00	27.54	0.041
0.00	2.25	27.55	0.065
0.00	2.50	27.56	0.086
0.00	2.75	27.55	0.101
0.00	3.00	27.55	0.123
0.00	3.50	27.56	0.136
0.00	3.75	27.55	0.121
0.00	4.00	27.55	0.108
0.00	4.50	27.55	0.059
0.00	4.75	27.56	0.024
0.00	5.00	27.56	0.002
0.00	6.00	27.56	0.001
-1.50	0.00	27.57	0.050
-1.00	0.00	27.57	0.044
-0.50	0.00	27.57	0.029
-0.25	0.00	27.57	0.025
0.00	0.00	27.57	0.025
0.25	0.00	27.57	0.025
0.50	0.00	27.57	0.026
0.75	0.00	27.57	0.032
1.25	0.00	27.57	0.040
1.50	0.00	27.57	0.027
1.75	0.00	27.57	0.055
2.00	0.00	27.57	0.064
2.50	0.00	27.57	0.079
3.00	0.00	27.58	0.086
3.25	0.00	27.58	0.088
3.50	0.00	27.58	0.072

TABLE A-14 (Continued)

x(in.)	Y(in.)	$P_{S_{\infty}}$ (in.)	$\frac{\sqrt{T_1^2}}{T_{\infty}}$
4.00	0.00	27.58	0.042
4.50	0.00	27.58	0.022
5.00	0.00	27.58	0.028
-1.50	-1.50	27.58	0.050
-1.00	-1.00	27.58	0.042
-0.50	-0.50	27.58	0.020
0.00	0.00	27.58	0.026
0.50	0.50	27.58	0.026
1.00	1.00	27.58	0.033
1.50	1.50	27.58	0.081
1.75	1.75	27.57	0.094
2.00	2.00	27.57	0.086
2.50	2.50	27.57	0.037
2.75	2.75	27.57	0.022
3.00	3.00	27.57	0.001

VITA

The author was born in Rainelle, West Virginia, on June 6, 1946. He later received his public education in Portsmouth, Virginia, graduating from Woodrow Wilson High School in 1965. In September, 1965, the author enrolled in Old Dominion University in Norfolk, Virginia, and received the Bachelor of Science of Engineering degree in June, 1970. The author enrolled in the graduate school of V.P.I. in September, 1970, and received the Master of Science degree in Aerospace Engineering in June, 1972. The author received an honorable discharge from the United States Marine Corps Reserve in June, 1971, having entered that service in 1963.

Thomas J. Swear, Jr.

THE FLOW ABOUT A SLENDER PROPELLER-DRIVEN
BODY IN A TEMPERATURE-STRATIFIED FLUID

by

Thomas Franklin Swean, Jr.

ABSTRACT

An experimental study of the turbulent wake produced by a stern-propellor-driven body moving in a temperature-stratified fluid is presented. The velocity and thermal boundary layers on the body upstream of the propellor are also examined. Mean flow velocities, static pressure, flow angularity and mean temperature distributions are reported at five downstream stations, $Z/D = 0.33, 1.0, 2.0, 3.0,$ and 4.0 . Turbulence data, including temperature fluctuations are reported at $Z/D = 0.33$ and $Z/D = 4.0$. The measurements were taken using thermocouples and pitot tubes of various size, a yawhead probe, a cross-wire hot-wire, and a straight-wire hot-wire as appropriate. For measuring the temperature fluctuations, the straight hot-wire probe was operated in the low-overheat mode to maximize temperature sensitivity. The testing was conducted in the Virginia Tech 6' X 6' subsonic wind tunnel at free-stream $Re_D \approx 2.04 \times 10^5$. The temperature variation provides a means of tracing the wake development in the near-body region. The principal effect of the propellor is to induce a more or less rigid rotation immediately downstream of the body. The fluid is apparently mixed much less than was anticipated. Temperature fluctuation is mild across the wake except in the vicinity of the propellor tips where it

becomes relatively large. The high temperature fluctuation often occurred in regions of low mean temperature gradients which indicates that current modeling techniques should be re-examined.